Interaction and Synchronization of Spiral Waves in a Reaction-Diffusion System

A thesis submitted to Indian Institute of Technology Guwahati for the degree of Doctor of Philosophy

Hrishikesh Kalita

Roll No: 186122011

Supervisor: Prof. Sumana Dutta

Department of Chemistry

Indian Institute of Technology Guwahati

Guwahati-781039, Assam, India

Dedicated to my late uncle Nagendra Chandra Kalita,
my sister Kritika, and my dear friends Hirak and Nazir

Declaration

I do hereby declare that the research work embodied in this thesis entitled "Interaction and Synchronization of Spiral Waves in a Reaction-Diffusion System" has been carried out by me under the supervision of Prof. Sumana Dutta, Professor, Department of Chemistry, Indian Institute of Technology Guwahati, Assam - 781039, India. The research works have been carried out from August 2018 to July 2023.

In keeping with the general practice of reporting scientific observations, due acknowledgments have been made wherever the work described is based on the findings of other investigations.

Place: IIT Guwahati
date:

Hrishikesh Kalita
Roll No: 186122011

INDIAN INSTITUTE OF TECHNOLOGY GUWAHATI
Prof. Sumana Dutta
Professor
Department of Chemistry
Indian Institute of Technology Guwahati
Guwahati, 781039, Assam, India
Phone no: +91-361-258-2322(O)
Email: sumana@iitg.ac.in

To Whom It May Concern

This is to certify that the research work presented in this thesis entitled "Interaction and Synchronization of Spiral Waves in a Reaction-Diffusion System" is an authentic record of the results obtained from the research work carried out by Hrishikesh Kalita (Roll No. 186122011) under my supervision in the Department of Chemistry, Indian Institute of Technology Guwahati, India. This work is original and has not been submitted elsewhere for a degree or award.

Place: IIT Guwahati
date:

Prof. Sumana Dutta
(Thesis Supervisor)

Acknowledgment

I would like to first convey my profound gratitude to Prof. Sumana Dutta for her constant guidance, support, and encouragement throughout my Ph.D. I am very fortunate to have such a mentor. She has been a great help to me throughout my Ph.D. I want to express my heartfelt thanks to her. I want to thank Prof. Ashish Kumar Gupta, Prof. Aditya Narayan Panda, and Dr. Pankaj Kumar Mishra, who make up my doctoral committee, for their remarks and especially their challenging questions, which made me conduct additional studies and get a deeper insight.

I am glad to have friendly and helpful seniors like Dr. Nirmali Prabha Das and Dr. Dhriti Mahanta. I am thankful for their guidance, suggestions, and academic and technical help throughout my Ph.D. I am grateful to my lab mates for maintaining a cordial, cooperative, and efficient lab atmosphere. I especially want to thank my labmate Parvej Khan for his academic and technical support.

I want to acknowledge my family and close relatives. I am forever lucky to have such a support system behind me. I have also had the good fortune to come across several outstanding teachers who have contributed to building the foundation for my life. I would first like to thank my late uncle Nagendra Chandra Kalita for his constant mentoring and teaching at my primary and secondary school levels. He also inspires me to read books. In this regard, I'm also very grateful to my cousin sister Mousumi Malakar, from whom I picked up the habit of reading books. I am thankful to the teachers at Srimanta Sankardev Vidyalaya, where I laid the groundwork for my early schooling. I attribute my foundation in mathematics to my father Bikarna Ranjan Kalita and my foundation in fundamental science to my science teacher Binod Hazarika. I also want to thank the teachers in the Department of Chemistry, Nowgong College, for helping me build my foundation in chemistry. Being taught by academics from NITM and IITG make me feel incredibly fortunate. A special thanks to Dr. Amit Kumar Paul for encouraging my questioning mindset and cultivating a love for teaching.

I want to express my gratitude to Hirak Jyoti Baishya, who has been with me constantly throughout this journey. His insights into life, most importantly, his authentic nature, and his simple and realistic viewpoint towards life have been a great help to me on my way to self-exploration and reality.

I acknowledge my friend Mrinmoy Roy, Nazir Uddin, Parvej Khan, Hirak Jyoti Baishya, Suman Ghosh, Jitendra Nath, and Nabajyoti Kalita. Scooty rides with Mrinmoy to explore nature and his distinct analysis of economics and politics, chemistry study with Nabajyoti during Ph.D. coursework and our philosophical discussions, fun with Nazir and his sense of humor, discussions and debates with Parvej on our Ph.D. topics, politics, and social issues, playing games and exploring places with Suman, the joyous personality of Jitendra and exploring human nature with Hirak, have all made my time at IITG extremely memorable. I am blessed to have established such beautiful relationships with you all.

I want to acknowledge IIT Guwahati for providing me with such an excellent

platform for my Ph.D., the social environment, and the natural beauty, which made my stay pleasant and my learning such a wonderful experience.

All the people that taught us things in life cannot be acknowledged in just a single piece of paper, and also, our mind cannot always recognize the values added to our lives by people. Valuable life lessons and experiences can be gained from many people, be they good or bad. Hence, I'd like to acknowledge every person that impacted my life, as I wouldn't be where I am today without even one of them.

Finally, I want to acknowledge this outstanding balance, the equilibrium, without which nothing would have become possible.

Abstract

Over the past few decades, spirals have attracted a lot of interest. From a spinning galaxy to a swarm of honeybees, rotating spirals are widespread in nature. Their widespread presence in nature has made the study of spiral waves relevant across various disciplines. In physical systems like fluid flows, liquid crystals, galactic formations, etc., in biological systems like the heart, chicken retina, neocortex, slime mould, etc., in chemical systems like the Belousov-Zhabotinsky (BZ) reaction system, the Briggs-Rauscher reaction, some simple precipitation processes, the oxidation of CO on platinum surfaces, etc., scientists have observed and studied spiral waves. Despite these studies, the ambiguity of spiral waves has prevented scientists from developing a comprehensive hypothesis.

The disruption of the heart's regular rhythm by spiral wave activity can lead to the development of heart disorders such as atrial and ventricular tachycardia and cardiac fibrillation. It also has a role to play in epilepsy. Therefore, spiral wave dynamics are of great interest to the scientific community, particularly its interaction dynamics and control. Even though we have some literature available on spiral wave interaction and control, there are many aspects yet to be explored.

Our study mainly addresses the issue of spiral wave interaction. When two spiral waves are close to one another, they interact either by annihilating or pushing one another away. These spiral waves may become pinned when they encounter unexcitable heterogeneity. The anchoring of spiral waves with inert, heterogeneous anomalies is observed in the heart, which has a deteriorating effect. The essential characteristics of a spiral wave, such as its rotating frequency, time period, etc., are modified by pinning. Finally, we have explored the interaction of two pinned spiral waves that were pinned to heterogeneities of different sizes. This study demonstrates how synchronisation results from such an interaction.

The BZ-reaction and cardiac tissue appear to be comparable in a number of important ways. The heart is an anisotropic medium that is highly discontinuous and inhomogeneous, in contrast to the BZ-reaction. However, the behavioural parallels between the two systems are so striking that BZ has become one of the best mimic systems to study spiral wave activity among scientists. We carried out our studies using thin layers of the ferroin-catalyzed BZ- reaction embedded in gel layers with malonic acid as the organic substrate. We employed the two-variable Barkley model of reaction diffusion equations for the theoretical analysis.

Chapter 1 broadly describes the field of non-linear dynamics, its history, and the primary purpose and goal of our work. We discussed some of the key branches of non-linear dynamics where our interests lie, starting with a fundamental definition of non-linear dynamics. The historical evolution of non-linear dynamics was then discussed. Then, we discussed chemical oscillators, particularly the BZ-reaction, as well as the theory that accounts for these kinds of chemical oscillating reactions and the self-organized patterns observed in them. Finally, we discussed our primary motivation and objective: spiral wave interaction dynamics.

Chapter 2 on methodology has two sections: theoretical and experimental. In the theoretical section, we discussed reaction diffusion systems. We talked about two systems that are widely used to study the BZ-reaction patterns: the Barkley and Oregonator models. Additionally, we defined the criteria for obtaining the spiral wave's tip in such models. In the experimental section, we thoroughly covered the BZ system's reaction mechanism, how to create spiral waves in the system, how to detect tips, etc. The final section of this chapter included a demonstration of the experimental setup.

Chapter 3 illustrates the interaction of several spiral rotors. Here, we conduct numerical simulations based on a reaction-diffusion model as well as experiments using the Belousov-Zhabotinsky reaction system. Depending on their relative chirality, phase angle, and distance separating them, the cores of two spirals may repel, attract, or remain immobile when they are very close to one another. We witnessed the attraction and annihilation of rotors placed in close proximity to one another. Otherwise, they push each other apart until they reach a critical distance, after which no more interaction seems to be possible. We have established a connection between the features of the spiral wave and this critical distance, which we shall refer to as the critical distance of interaction (d_c) throughout our publications. The relationship is $d_c = \lambda$ - d_s, where λ is the wavelength d_s is the core diameter. A system with up to eight rotors showed spontaneous symmetry-breaking instability, which we also noticed in experiments. The correctness of the numerical results has been effectively shown by our Belousov-Zhabotinsky reaction experiments. We might be able to comprehend the nature of such excitation waves and their interaction in heart tissue and cell membranes if we have a complete understanding of the dynamics of many spiral rotors placed in proximity in an excitable system.

In Chapter 4, we sought to investigate how the initial phase angle discrepancy affected the interactive behaviour. Our method is theoretical in this scenario. Our system consists of examples of two spiral waves that had a variety of initial phase angle deviations. When the initial phase angle is different the critical distance changes, and $d_c = \lambda$ - d_s. For a counter-rotating spiral pair, the critical distance (d_c), the distance at which all interaction ends, increases with an increase in phase angle difference, whereas for a co-rotating spiral pair, the tendency is entirely the reverse. A low phase angle difference between two counter-rotating spirals results in attraction when there is little space between them. As their distance grows, their attraction turns into repulsion, and when it reaches a particular limiting value, the critical distance (d_c), all contact between them ends. For counter-rotating spirals with a large phase angle difference, they only exhibit repulsion when very close together. At any phase angle difference, co-rotating spirals only exhibit repulsion when they are too close to each other, and no attractive interaction was observed. The system was initially asymmetrical. While interacting, this asymmetry often remains in the tip trajectory, although there extreme situations are observed as well. In some extreme circumstances this asymmetry blows up, such as one spiral drift, and there are times when phase resetting creates entirely symmetric states, such as symmetric annihilating states.

In chapter 5, we demonstrate that two counter-rotating spiral rotors pinned to circular heterogeneities can synchronize in frequency and phase, through experiments with the Belousov-Zhabotinsky reaction. Depending on how differently their respective characteristic frequencies are spaced, the phase synchronization takes on different forms. Across the tests, we detect in-phase and out-of-phase

synchronization, lag synchronization, and phase resetting. It is discovered that the distance between the two spirals, as well as the respective sizes of the pinning obstacles affect how long it takes for the two spirals to synchronize. On the basis of numerical simulations of an excitable reaction-diffusion model, our experimental findings are replicated and further explained.

List of Publications

1. Interaction of multiple spiral rotors in a reaction-diffusion system, H. Kalita and Sumana Dutta, Phys. Rev. E. **105**, 054213 (2022).

2. Rotational synchronization of pinned spiral waves, H. Kalita, P. Khan, and Sumana Dutta, Phys. Rev. E. **106**, 034201 (2022).

Contents

List of Figures

List of Tables

Chapter 1

Introduction

1.1 Non-linear dynamics

Dynamics is the study of how things change with time, or their time evolution [1]. Non-linear dynamics deals with systems in which the governing equations are not linear with respect to the system variables. Explaining the formation of complex structures is the main aim of non-linear dynamics [2]. Most of the phenomena in nature are non-linear, but this discipline is not well established like other disciplines of science. Its underlining principles and wide applicability have made it evolve in an interdisciplinary way rather than as a separate discipline. Initially, it had its foundation mainly in physics and applied mathematics [3]. In the last few decades, its application has spread in an exponential way to all branches of science and technology and even in the social sciences.

1.2 Self-organization

Self-organization has been a fascinating subject for non-linear scientists. Self - organization is defined as the spontaneous formation of temporal, spatial, or spatiotemporal patterns or structures from its constituents. The human brain itself is an example of a complex but well-organized system. From a microscopic level animal cell to an easily visible animal coat pattern, from planetary systems to galaxies, from self-organizing networks [4] in computer science to dissipative structures of oscillatory chemical reactions [5], from spontaneous symmetry-breaking processes such as spontaneous magnetization and crystal growth in classical physics [6] to the Bose-Einstein condensation [7] in quantum physics, from market self-organization in economics [8] to human and animal society, self-organization is almost everywhere.

1.3 Collective dynamics

Collective dynamics refers to the coordinated dynamics of a group or collection as a whole. The species in a collection can show completely different dynamics than the ones they show when they are present individually. A flock of birds, sheep, fish, etc. [9]. are very common examples of collective dynamics. The underlining mechanism responsible for such collective dynamics varies from system to system. For flocking bird dynamics, airflow and gravity are the mechanisms, but in the case of fish and bacteria, it is hydrodynamics [10].

The interactions between individual units are mainly of three types: (a) repulsive; (b) attractive; and (c) a mixture of both repulsive and attractive [11]. The interaction can be quantified by mathematics, and they give it a new name: coupling. These interactions, or couplings, are mainly non-linear in nature. So, we need the tools of non-linear science to study collective dynamics.

Each individual unit is known as an autonomous unit in scientific terms. Typically, they are represented by a self-sustaining oscillator and mathematically modeled by an oscillatory function. The most commonly studied oscillatory units are circadian rhythms in living species, current in electrical systems, and chemical concentration in reactions [12]. These autonomous units can give rise to periodic, aperiodic, and chaotic behavior [13]. The most interesting thing for a non-linear scientist is to see the collective behavior of two or more such oscillators.

Collective dynamics can demonstrate a plethora of phenomena like pattern formation [14], partial synchronization [15], chimera [16], cluster sate [17], phase flip [18] etc.

1.4 Synchronization

In Greek, sync means same and Chronos means time. Synchronization means the operation or activity of two or more things at the same time or rate. Interaction or coupling between two or more oscillators can lead to the adjustment of their oscillating rhythms. This adjustment gives rise to synchronization. Very common examples of systems showing synchronized patterns are the flashing of fireflies, circadian rhythm, neuronal activity in the brain, pendulums, and electrical systems. Even at the microscopic level, synchronization was reported. Synchronized patterns were found in the beating frequency of the flagella. Recent academic research shows synchronization in complicated chemical systems like mercury beating hearts [19], electrochemical [20, 18], Belousov-Zhabotinsky reaction [21], and also in complicated physical systems like Josephson junction [22], mechanical oscillators (metronomes) [23], Lasers [24].

1.5 A Brief History of Non-Linear Dynamics

A system having three or more interacting particles is difficult to solve using Newtonian mechanics. Scientists have been trying for decades to solve this problem. In the late 1800s, Poincare came up with a completely different way of looking at the problem [3]. Instead of solving the problem as a whole, his main focus was to look for the points where it would remain stable, which led to the concept of fixed points in non-linear dynamics [3]. His insights also helped to develop chaos theory, for which he is known as the father of chaos [3]. 1920-1950 is the period when several non-linear oscillators found their place in physics and engineering, especially in developing radio, radar, and lasers [3]. One of the important discoveries around this time was the KAM theory. It deals with the complex behaviour of Hamiltonian mechanics, like solving more than two body problems. The discovery of the computer around the 1950s has made the development of non-linear dynamics many fold faster. With the help of the computer, Lorentz studied atmospheric convection by solving three sets of differential equations [25]. It was observed that this system could lead to chaos at certain parameter values and initial conditions [25]. Another very important discovery by Allen Turing, who is popularly known

as the father of modern computing, is the use of reaction-diffusion equations to explain biological pattern formation. Turing, in his masterpiece "The Chemical Basis of Morphogenesis", has suggested that chemical reactions inside living organisms form the basis of morphogenesis. In 1971, Ruelle and Taken proposed a mechanism for the generation of turbulence and related phenomena in dissipative systems [26]. With this discovery, chaos theory has gained more insights, and its range of application has become wider. Later, Mandelbrot's set, used for the understanding of fractals, drew the attention of the scientific community. Fractals are geometrical objects that are self-similar when the distance at which they are viewed is changed; e.g., in the case of a river and its tributaries, every tributary has its own tributaries, so that it has the same structural organization as the entire river except that it covers a smaller area. This concept inspired scientists in many disciplines, including cosmology, medicine, engineering, genetics, and artists and musicians too. Some of the practical uses of fractal mathematics are in the generation of computer graphics, in computer file compression systems, in the architecture of the networks that make up the internet, and even in diagnosing some diseases. In the meantime, Winfree's mathematical modelling of biological phenomena, especially circadian rhythm and cardiac rhythm, has made an immense contribution to the medical sciences and brought it under the umbrella of nonlinear dynamics [27].

1.6 Chemical Oscillators

Oscillations in chemical systems are an emerging area of non-linear science. During the early 1900s, it was believed that homogeneous oscillatory reactions were impossible. In 1921, Bray proposed the first homogeneous oscillatory chemical reaction of iodate, iodine, and hydrogen peroxide, where he found a periodic variation of oxygen and hydrogen concentrations [28]. Initially, the scientific community did not accept his work because they thought that it would violate the second law of thermodynamics. They explained the experimental observation of such oscillations as being caused by dust, bubbles, or some impurities [28]. Then came the Belousov reaction in 1951, which showed a periodic change of colour from colourless to yellow, whose frequency increases with temperature. His recipe consisted of $KBrO_3$, H_2SO_4, Ce^{3+}/Ce^{4+} couple as catalysts, and citric acid as a reductant [28, 29]. He also noted travelling wave fronts when left unstirred. His work too got rejected, like Bray's [28]. A few years later, Zhabotinsky, a PhD student, started working on Belousov's reaction by taking malonic acid in place of citric acid and ferroin, both as indicators and catalysts, in place of Cerium [28]. The colour change was more visible when ferroin was used as an indicator, as it showed red in reduced form and blue in oxidized form [28, 29]. With those modifications, he was able to propagate chemical waves, which established spatial self-organization in homogeneous systems [28, 29]. This is a well-established reaction today and is known as the Belousov-Zhabotinsky (BZ) reaction. Again, the same question came up: "What about the second law of thermodynamics?" which had yet to be answered. It was very difficult to calculate the entropy change of the universe during a chemical reaction. So, scientists tried to seek answers in a more fundamental function, i.e., Gibbs free energy [28]. Initially, they compared those oscillating reactions to those of the pendulum [28]. In a pendulum, every oscillation goes through the equilibrium point, so Gibbs free energy keeps oscillating between two values as the reactants are converted to products and back to reactants. Finally,

they realized that one cannot compare a chemical oscillation to that of a pendulum. When a chemical reaction oscillates, it never passes through its equilibrium points. Instead, these are far from equilibrium phenomena, which are governed by non- equilibrium thermodynamics [30]. It's not the reactants and products but the concentration of intermediates that keeps oscillating. Therefore, free energy keeps decreasing monotonically with time. Prigogine pointed out that an open system kept far from equilibrium could exhibit self-organization by dissipating energy into the surrounding environment to compensate for the entropy decrease of the system by making the total entropy change positive [30]. Field, Körös, and Noyes developed a mathematical model of the BZ reaction named the Oregonator that could maintain all the essential features of the reaction [31].

1.7 Chemical Waves and Patterns

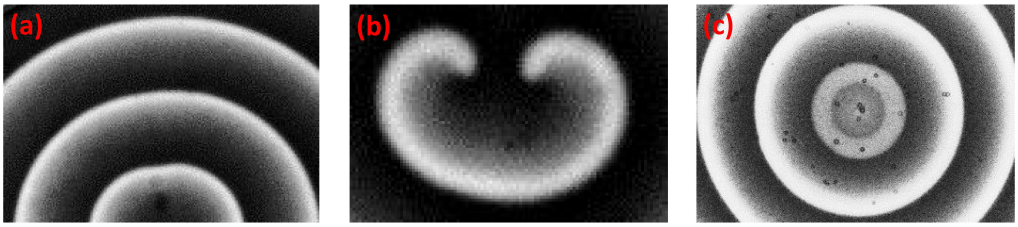

Figure 1.1: Self-organised patterns. (a) Target patterns; (b) A pair of spiral waves; (c) A scroll wave.

Chemical oscillators could also behave as reaction diffusion systems, where the reactants and products could be transported in space by diffusion. Such systems could show a wide range of phenomena, from travelling waves to various self-organised patterns. Zaikin and Zhabotinsky (1970) were the first to observe the periodic propagation of concentric chemical waves, which are called target patterns [29]. When these waves are broken, they could form spirals. The three-dimensional counterpart of those spiral waves is known as scroll waves [29].

1.8 Spiral Wave

1.8.1 How Spiral Wave Forms

When a propagating target wave encounters an obstacle, the obstacle can break the wave and form spiral waves. In the human heart, when normal heart rhythm encounters heterogeneity like scar tissue, a wave break may be possible, which can form spirals. Hitting an obstacle with target waves doesn't necessarily guarantee spiral formation. Two conditions must be met to form spirals: (i) the nature of the obstacle and (ii) the excitability of the system [32]. In our system, i.e., the BZ system, we have used a thin glass slab with sharp edges as an obstacle and manually cut the circular target waves to produce spirals. The excitability of a medium denotes the capacity of the medium to sustain propagating waves, which cannot support the passing of another wave until a certain amount of time has passed, known as the refractory time. For BZ reaction, Winfree has suggested a

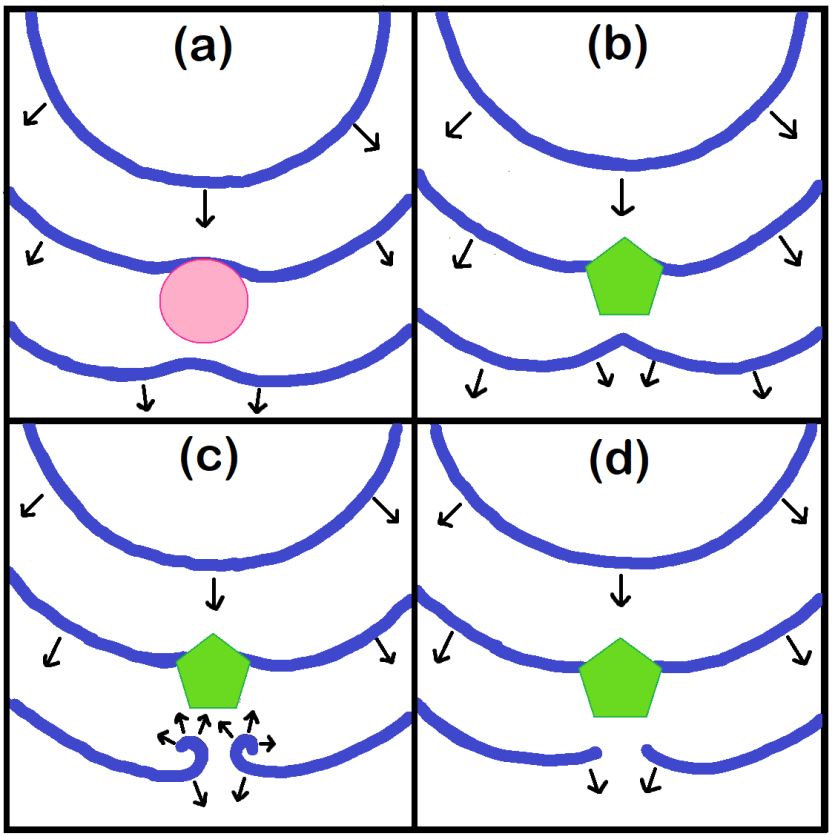

Figure 1.2: Diagram showing how waves interact with objects of varied shapes at different levels of excitability as they propagate. (a) Interaction with round obstacles having smooth surfaces at normal levels of excitability; (b) Interaction with a pentagon-shaped obstacle having sharp edges at normal levels of excitability; (c) Interaction with a pentagon-shaped obstacle having sharp edges at low levels of excitability; (d) Interaction with a pentagon-shaped obstacle having sharp edges at very low levels of excitability.

relationship between excitability (denoted as ϵ) and the concentration of different chemical species in the BZ reaction [39].

$$\epsilon = \frac{k_5}{k_3}\frac{[organics]}{[H^+][BrO_3^-]} \tag{1.1}$$

where [organics]=[BrMA]+[MA] (MA stands for malonic acid), $k_5 = 0.04$ $M^{-1}s^{-1}$, and $k_3 = 40$ $M^{-2}s^{-1}$.

Throughout our simulations, the excitability (ϵ) was maintained at 0.02. For experiments, the excitability (ϵ) was maintained at 0.05.

Fig. 1.2 shows four scenarios to explain the spiral formation concept. Generally, we need a system with low levels of excitability and obstacles with sharp edges to form spirals. In Fig. 1.2(a), the surface is round, and round surfaces are not good for forming spirals. In Fig. 1.2(b), although the surface has sharp edges, the system has a normal level of excitability. By normal level of excitability, we simply mean that the excitability of the system is enough to maintain normal wave activity by fusing the broken wave fronts, which got generated from normal wave fronts after hitting the obstacle. So, waves rapidly rejoin without initiating any wave activity. In Fig. 1.2(c), all conditions are met to form spirals, i.e., low excitability and an

obstacle with a sharp edge. In Fig. 1.2(d), excitability is too low, which makes the broken fronts unable to rotate.

1.8.2 Some Core Concepts of Spiral Wave

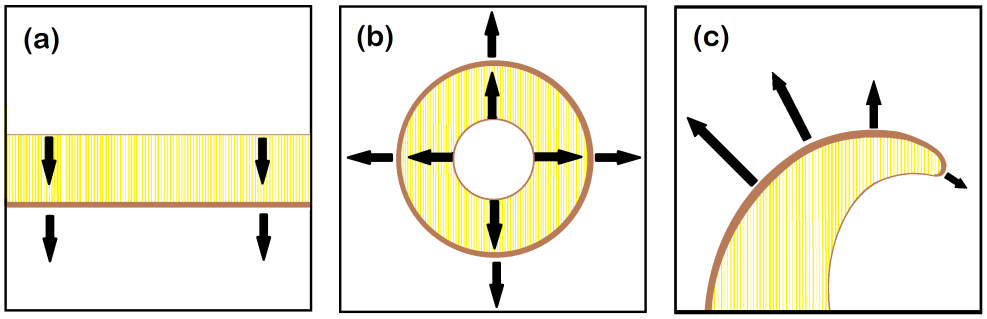

Figure 1.3: Propagating waves of various shapes. (a) Linear wave; (b) Circular wave; (c) Spiral wave.

A recovery band of finite dimension is always followed by the wave front in the case of linear or circular wave propagation [Figs. 1.3(a) and 1.3(b)]. The wave front is shown as a thick brown line. The wave tail (highlighted as a thin brown line) is the final portion of this recovery band [32]. A planner wave and a circular wave both propagate at the same speed, which means that the velocity component visible in the wave fronts of both types of waves often doesn't change over the course of propagation. The wave front and wave tail almost never collide in the case of planar or circular waves. In contrast, spiral waves have a phase singularity, also known as the spiral tip [32], where the wave front and wave tail contact at the same location [Fig. 1.3(c)]. As seen in Fig. 1.3(c), a spiral wave has varying curvature and conduction velocity. A diverging trajectory is followed by points far from the tip, and a converging trajectory is followed by points very close to the tip.

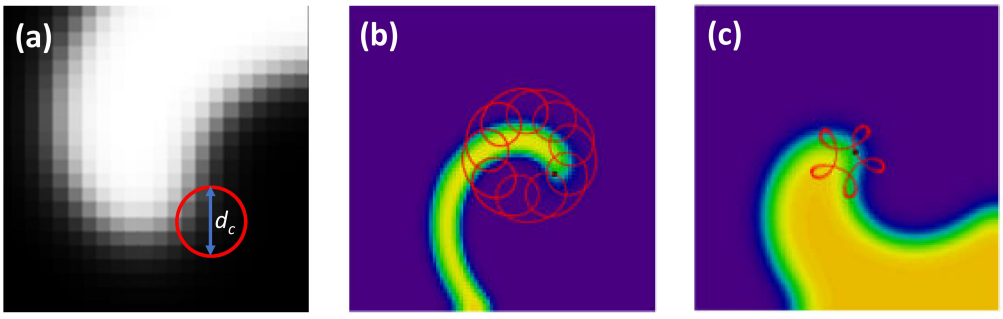

Figure 1.4: Figure showing different kinds of tip trajectories. (a) Circular trajectory; (b) Meandering trajectory having inward petals [33]; (c) Meandering trajectory having outward petals [33].

The movement of a spiral's tip, or more specifically, its tip trajectory, best describes the spiral's dynamics. The tip trajectory of a spiral can be circular [Fig. 1.4(a)] or meandering [Figs. 1.4(b) and 1.4(c)] depending on the system parameters [34, 35, 36]. These meandering tips follow either epicycloid orbits, which resemble

flowers with petals facing inside, or hypocycloid orbits, which resemble flowers with petals facing outward (flowerlike orbits with outward petals) [37, 38, 39]. Additionally, spiral waves have been observed to meander chaotically [40, 41]. our experimental and theoretical model sustains circular trajectories. When the spiral tip makes a full rotation it traverses a circular trajectory, which we define as the core of the spiral. We define the diameter of this core as the spiral core diameter (d_c).

One more important parameter is the wavelength of a spiral. The wavelength of a spiral is the distance between two successive circular waves away from the spiral tip (core), as shown in Fig. 1.5(a). Wavelength can also be measured from a time-space plot, as given below [Fig. 1.5(b)].

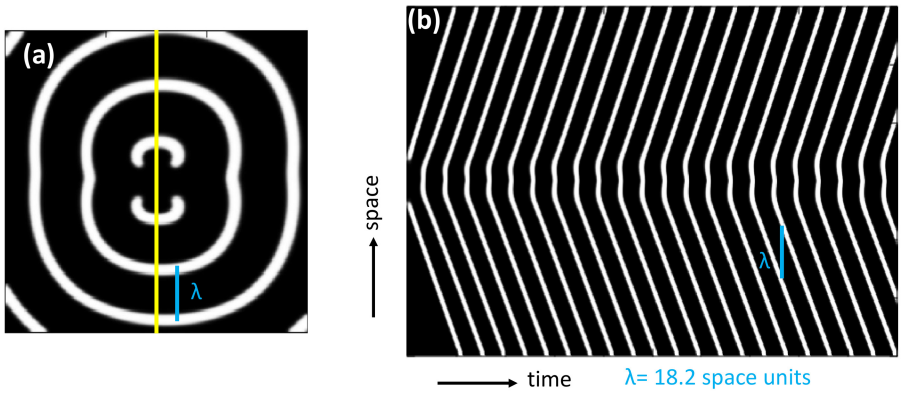

Figure 1.5: Snapshot of a numerical simulation. (b) Time-space plot generated along the yellow line in (a) showing wavelength λ. Time increases from left to right.

1.9 Spiral Wave Interaction Dynamics: Motivation, Recent advances and Objective

Initially, the study of spiral wave activity was limited to chemical and physical systems only. Over time, scientists have discovered the role of spiral waves in some biological systems and processes. Aggregation of slime mould Dictyostelium discoideum is driven by periodic waves of cAMP, which instruct the cells to collect at the aggregation center [42]. Spiral patterns were seen during intracellular Ca2+ release in Xenopus laevis oocytes, which primarily serves as a messenger [43]. According to a study, chicken retinal cells contain spiral waves [44]. In the neocortex, spiral waves have been observed often, both during sleep-like states and pharmacologically induced oscillations. Their findings demonstrate the role of the spiral wave in normal cortical processing and epilepsy [45]. Spiral waves can also occur in the heart [46, 32]. When the normal heartbeat encounters heterogeneities like scar tissue in the heart, there is a chance that a wave will break. A spiral could form as a result of a wave breaking. Arrhythmia might be the result of these spirals. If these spiral waves are not addressed, they have the potential to further fragment and reach a chaotic, turbulent state, making the patient prone to ventricular fibrillation. Ventricular fibrillation is the main cause of the majority of cardiac arrests. Scientists are therefore interested in the control and interaction of

spiral waves. Theoretical investigations revealed that a spiral can interact either repulsively or attractively, depending on the system's properties [47, 48]. Spiral waves, according to one group, can interact in three different ways: (1) Attraction, which leads to annihilation; (2) Repulsion, in which one spiral predominates, pushing or expelling the opposing spiral to the border (3) Repulsion, in which neither spiral exhibits control over the other [49]. In additional studies, the dominance of one spiral wave in a pair of spiral waves [50, 51] has also been demonstrated. Such dominance might result from symmetry breakage [50] and asymmetric perturbation [51]. Scientists have also tried to control the dynamics of the spiral waves by external means like electric field [52], LASER [53], light [54] etc. They carefully manipulated the dynamics with those outside tools to foster interaction. They successfully annihilated the spiral waves, which is important from a medical perspective because annihilation is a non-invasive way to kill or eliminate spiral waves. In Chapter 3, we explored the interaction of the spiral rotors in a reaction diffusion system. We started our study with a two-spiral system having the same phase angle initially. Then we extended our system to 4 spiral rotors and finally to 8 spiral rotors with the same phase angle initially. We used the BZ system for our experimental study, which is one of the best mimic systems to study spiral wave activity. We employed the Barkley model, a generic model for simulating such reaction diffusion systems, for the theoretical work. In chapter 3, the systems we have considered are symmetrical, i.e., they have the same phase angle at the time of initiation. The changing phase angle between the spirals has a prominent impact on the interactive behaviour. So, we have dedicated Chapter 4 to the study of spiral waves, which initially have a phase angle difference.

Pinning spiral waves to impermeable obstacles is a significant problem in cardiac physiology. The irregular polymorphic activity stops when a spiral wave binds to an obstruction in the heart, such as blood vessels or injured tissues, and periodic monomorphic activity then appears [55, 56, 57]. Pinning modifies a spiral wave's fundamental properties, including its rotating frequency, time period, etc. The size of the obstacles must be greater than a predetermined minimum size in order to pin [58]. A recent study on pinning with circular and rectangular obstacles shows that the propagating parameters (i.e., wavelength, wave period, and velocity of pinned spiral waves) increase with the circumference, regardless of the obstacle area [59]. In Chapter 5, we pinned two spiral waves to two different-sized obstacles. Their dynamics are limited by pinning, and their frequency also varies depending on the circumference of the obstacle. Interaction, or coupling, takes place among those pinned spirals after some time. We investigated the potential for phenomena like synchronisation to result from the interplay of pinned spirals with various frequencies.

Bibliography

[1] S. Sinha and S. Sridar, *Patterns in exitable media* (CRC press Tylor & Francis group,6000 Broken Sound Parkway NW, Suite 300 Boca Raton, FL 33487-2742, 2015).

[2] F. Sagues and I. R. Epstein, Dalton Trans. **7**, 1201 (2003).

[3] S. H. Strogatz, *Nonlinear Dynamics and Chaos* (CRC press Taylor & Francis group, 6000 Broken Sound Parkway NW, Suite 300 Boca Raton, FL 33487-2742, 2018).

[4] D. J. Watts and S. H. Strogatz, Nature **393**, 440 (1998).

[5] A. N. Zaikin and A. M. Zhabotinsky, Nature **225**, 535 (1970).

[6] S. Jungblut and C. Dellago, Eur. Phys. J. E **39**, 77 (2016).

[7] D. Nagy, G. Szirmai, and P. Domokos, Eur. Phys. J. D **48**, 127 (2008).

[8] P. Krugman, *The self organizing economy* (Blackwell Publishers,1995).

[9] T. Vicsek and A. Zafeiris, Physics Reports **517**, 71 (2012).

[10] R. V. Drongelen, A. Pal, C. P. Goodrich, and T. Idema, Phys. Rev. E **91**, 032706 (2015).

[11] N. H. P. Nguyen, D. Klotsa, M. Engel, and S. C. Glotzer, Phys. Rev. Lett. **112**, 075701 (2014).

[12] R. Toth, A. F. Taylor, and M. R. Tinsley, J. Phys. Chem. B **110**, 10170 (2006).

[13] A. Pikovsky, M. Rosenblum, and J. Kurths, *Synchronization*: *A Universal Concept* in *Nonlinear Sciences*,(vol. 12. Cambridge university press, 2003).

[14] F. G. Kazanci and B. Ermentrout, SIAM J. Appl. Math., **67**, 512 (2007).

[15] P. Kumar, D. K. Verma, and P. Parmananda, Phys. Lett. A **381**, 2337 (2017).

[16] D. M. Abrams and S. H. Strogatz, Phys. Rev. Lett. **93**, 174102 (2004).

[17] H. Nishimori, N. J. Suematsu, and S. Nakata, J. Phys. Soc. Jpn. **86**, 101012 (2017).

[18] J. M. Cruz, J. Escalona, P. Parmananda, R. Karnatak, A. Prasad, and R. Ramaswamy, Phys. Rev. E **81**, 046213 (2010).

[19] D. K. Verma, H. Singh, A. Contractor, and P. Parmananda, J. Phys. Chem. A **118**, 4647 (2014).

[20] J. M. Cruz, M. Rivera, and P. Parmananda, Phys. Rev. E **75**, 035201(R) (2007).

[21] Y.-N. Li, L. Chen, Z.-S. Cai, and X.-Z. Zhao, Chaos, Solitons and Fractals **17**, 699 (2003).

[22] A. B. Cawthorne, P. Barbara, S. V. Shitov, C. J. Lobb, K. Wiesenfeld, and A. Zangwill, Phys. Rev. B **60**, 7575 (1999).

[23] N. Chakrabarty, A. Jain, N. Lal, K. D. Gupta, and P. Parmananda, Chaos **27**, 013115 (2017).

[24] D. J. DeShazer, R. Breban, E. Ott, and R. Roy, Phys. Rev. Lett. **87**, 044101 (2001).

[25] E. N. Lorenz's, J. Atmos. Sci. **20**, 130 (1963)

[26] D. Ruelle and F. Takens, Commun. Math. Phys. **20**, 167 (1971)

[27] A. T. Winfree, *Timing of Biological Clocks* (Scientific American Library, New Work 1987)

[28] I. R. Epstein and J. A. Pojman, *An Introduction to Nonlinear Chemical Dynamics* : *Oscillations*, *Waves*, *Patterns*, *and Chaos* (Oxford University Press, Inc., 198 Madison Avenue, New York, New Work 10016, 1998)

[29] A. M. Zhabotinsky, Scholarpedia **2(9)**, 1435 (2007)

[30] I. Prigogine, *Time*, *structure and Fluctuation* (The Nobel lecture, 1977)

[31] R. J. Field., E. Koros. and R. M. Noyes, J. Amec. Chem. Soc. **94**, 8649 (1972)

[32] J. Jalife, M. Delmar, J. Anumonwo, O. Berenfeld, and J. Kalifa, *Basic Cardiac Electrophysiology for the Clinician*, 2nd Edn. (Wiley-Blackwell, Oxford, UK, 2009)

[33] S. F. Pravdin, M. A. Patrakeev, and A. V. Panfilov, Phys. Rev. E **107**, 014215 (2023).

[34] G. Li, Q. Ouyang, V. Petrov, and H. L. Swinney, Phys. Rev. Lett. **77**, 2105 (1996).

[35] G. S. Skinner and H. L. Swinney, Physica D (Amsterdam) **48**, 1 (1991).

[36] M. Braune and H. Engel, Chem. Phys. Lett. **211**, 534 (1993).

[37] D. Barkley, Phys. Rev. Lett. **72**, 164 (1994).

[38] D. Barkley and I. G. Kevrekidis, Chaos **4**, 453 (1994).

[39] D. Mahanta, N. P. Das, and S. Dutta, Phys. Rev. E **97**, 022206 (2018).

[40] Z. Q. James, N. Weiss, and A. Garfinkel, Phys. Rev. E **61**, 727 (2000).

[41] D. M. Lombardo and S.-J. Rappel, Phys. Rev. E **99**, 062409 (2019).

[42] F. Siegert and C. J. Weijer, Physica D (Amsterdam) **49**, 224 (1991).

[43] J. Lechleiter, S. Girard, E. Peralta, and D. Clapham, Science **252**, 123 (1991).

[44] N. A. Gorelova and J. Bures, J. Neurobiol. **14**, 353 (1983).

[45] X. Huang, W. Xu, J. Liang, K. Takagaki, X. Gao, and J. Y. Wu, Neuron **68**, 978 (2010).

[46] R. A. Gray, A. M. Pertsov, and J. Jalife, Nature (London) **392**, 75 (1998).

[47] I. S. Aranson, L. Kramer, and A. Weber, Physica D **53**, 376 (1991)

[48] I. S. Aranson, L. Kramer, and A. Weber, Phys. Rev. Lett. **67**, 404 (1991).

[49] M. Ruiz-Villarreal, M. Gómez-Gesteira, C. Souto, A. P. Muñuzuri, and V. Pérez-Villar, Phys. Rev. E **54**, 2999 (1996).

[50] I. Aranson, H. Levine, and L. Tsimring, Phys. Rev. Lett. **76**, 1170 (1996).

[51] I. S. Aranson, L. Kramer, and A. Weber, Phys. Rev. E **48**, R9 (1993).

[52] J. Schütze, O. Steinbock, and S. C. Müller, Nature **356**, 45 (1992).

[53] O. Steinbock, S. C. Müller, Int. J. Bifurcation Chaos Appl. Sci. Eng. **3**, 437 (1993).

[54] K. Agladze, Chaos **6**, 328 (1996).

[55] T. Ikeda, M. Yashima, T. Uchida, D. Hough, M. C. Fishbein, W. J. Mandel, P.-S. Chen, and H. S. Karagueuzian, Circ. Res. **81**, 753 (1997).

[56] Z. Y. Lim, B. Maskara, F. Aguel, R. Emokpae, and L. Tung, Circulation **114**, 2113 (2006).

[57] Y.-H. Kim, F. Xie, M. Yashima, T.-J. Wu, M. Valderrbano, M.-H. Lee, T. Ohara, O. Voroshilovsky, R. N. Doshi, M. C. Fishbein, Z. Qu, A. Garfinkel, J. N. Weiss, H. S. Karagueuzian, and P.-S. Chen, Circulation **100**, 1450 (1999).

[58] T. Ikeda, M. Yashima, T. Uchida, D. Hough, M. C. Fishbein, W. J. Mandel, P.-S. Chen, and H. S. Karagueuzian, Circ. Res. **81**, 753 (1997).

[59] M. Sutthiopad, J. Luengviriya, P. Porjai, M. Phantu, J. Kanchanawarin, S. C. Müller, and C. Luengviriya1, Phys. Rev. E **91** 052912 (2015).

Chapter 2

Methodology

2.1 Theoretical Approach

2.1.1 Reaction-Diffusion System

A non-linear chemist is mostly interested in the theoretical modeling of reaction diffusion systems, where the interplay of reaction and diffusion gives rise to spatiotemporal patterns. Mathematically, they could be modeled using partial differential equations as follows:

$$\frac{\partial u(x,y,z,t)}{\partial t} = f(u) + D\nabla^2 u(x,y,z,t) \tag{2.1}$$

where $u(x,y,z,t)$ is one of the several variables describing the state of a system in time and space (in three dimensions); D is the diffusion coefficient; $f(u)$ is the reaction term; and ∇^2 is the sum of second derivatives with respect to spatial coordinates (the Laplacian) [1].

2.1.2 Theory Behind Diffusion

Flux, J, is used to define the rate of migration of a property. Mathematically speaking, flux is the amount of a given property that passes through a given area in a given time period, divided by the area and length of the interval. In the case of diffusion, we speak of a matter flux of a certain number of molecules per square metre per second; in the case of thermal conduction, we speak of an energy flux and express it in joules per square metre per second; and so on. We multiply the flux by the area A and the time interval Δt, forming $JA\Delta t$, to get the total amount of each property that is transmitted via a given area A in a given time interval Δt.

Fick's first law of diffusion states that the matter flux is proportional to the concentration gradient [2]. According to the law, diffusion will happen more quickly when concentration varies significantly with position as opposed to when it is almost uniform. In the case of uniform concentration, there is no net flux, i.e., $du/dx = 0$, where u is the concentration of particles and x is the direction of flow. Fick's first law in terms of diffusion coefficient and considering a flow along x direction is:

$$J(matter) = -D\frac{du}{dx} \tag{2.2}$$

D is called the diffusion coefficient of u. A positive value of J signifies a flux towards positive x; a negative value of J signifies a flux towards negative x. Because matter flows down a concentration gradient, from high concentration to

low concentration, J is positive if du/dx is negative. Therefore, the coefficient of proportionality must be negative, and we write $-D$.

The diffusion equation, also referred to as Fick's second law of diffusion, establishes a relationship between the spatial variation of a concentration at a point and the rate at which that concentration changes at that point [2]. It is represented by the following formula:

$$\frac{\partial u}{\partial t} = D\frac{\partial^2 u}{\partial x^2} \tag{2.3}$$

We demonstrate how the diffusion equation derives from Fick's first law of diffusion with the following justification:

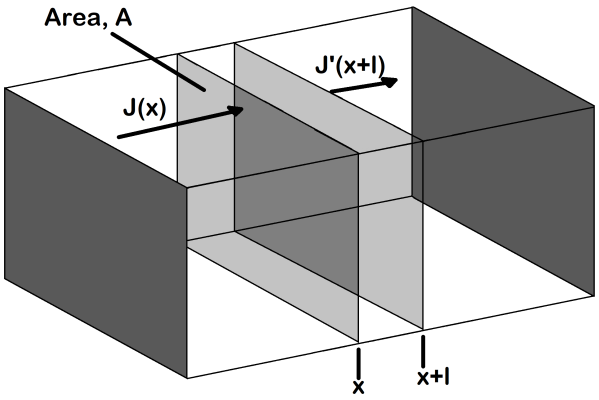

Figure 2.1: Figure showing flux entering at x and flux going out at x+l.

We take into account a small cross-sectional region A, which spans from x to $x + l$ [Fig. 2.1]. Let u at time t be the concentration at x. The amount (number of moles) of particles that enter the slab in the infinitesimal interval dt is $JAdt$; therefore, the rate at which the molar concentration inside the slab (which has volume Al) increases due to the flux from the left is:

$$\frac{\partial u}{\partial t} = \frac{JAdt}{Aldt} = \frac{J}{l} \tag{2.4}$$

Additionally, there is outflow through the right window. This window's flux is J', and the resulting rate of concentration change is:

$$\frac{\partial u}{\partial t} = -\frac{J'Adt}{Aldt} = -\frac{J'}{l} \tag{2.5}$$

Consequently, the net rate of change in concentration is:

$$\frac{\partial u}{\partial t} = \frac{J - J'}{l} \tag{2.6}$$

Each flux is proportional to the concentration gradient at the window. So, by applying Fick's first law of diffusion [Eq. 2.2]:

$$J - J' = -D\frac{\partial u}{\partial x} + D\frac{\partial u'}{\partial x} = -D\frac{\partial u}{\partial x} + D\frac{\partial}{\partial x}\left[u + (\frac{\partial u}{\partial x})l\right] = Dl\frac{\partial^2 u}{\partial x^2} \tag{2.7}$$

Now, the substitution of Eq. 2.7 in Eq. 2.6 gives Eq. 2.3.

In three dimensions,

$$\frac{\partial u(x,y,z,t)}{\partial t} = D \times \left[\frac{\partial^2}{\partial x^2} + \frac{\partial^2}{\partial y^2} + \frac{\partial^2}{\partial z^2}\right] u(x,y,z,t) \tag{2.8}$$

Now, writing in terms of the Laplacian operator, Eq. 2.8 will become:

$$\frac{\partial u(x,y,z,t)}{\partial t} = D \times \nabla^2 u(x,y,z,t) \tag{2.9}$$

Equation 2.9, together with the kinetic rate equations, will give us the reaction-diffusion system expressed as Eq. 2.1

2.1.3 A Numerical Approach to Solve Reaction-Diffusion Systems

Fourth-order Runge-Kutta and Euler are the two most popular methods to solve such reaction diffusion equations with a proper Laplacian stencil and initial conditions. Discretization of the system in a 2D plane as a $n \times m$ lattice or in 3D space as a $n \times m \times l$ lattice, with a proper boundary condition, is necessary to use the Laplace stencil. A systematic mathematical insight into getting such patterns is given below.

Let us consider the 2D version of reaction diffusion system, where u, a reactant, is evolving with time.

$$\frac{\partial u(x,y,t)}{\partial t} = f(u) + D\nabla^2 u(x,y,t) \tag{2.10}$$

The Euler method can be used to get the values of u at different times.
Say, $u(x,y,t_0)$ = known initial concentration
$t - t_0 = dt$, small time interval
$u(x,y,t) - u(x,y,t_0)$ = change in concentration during time dt
$f(u)_{t_0}$ = could be calculated from the initial concentration of reactants.
Now, the value of u at time t and at point (x,y) is given by the following equation:

$$u(x,y,t) = [f(u)_{t_0} + D\nabla^2 u(x,y,t_0)]dt + u(x,y,t_0) \tag{2.11}$$

$u(x,y,t)$ could be used to determine the next successive point, and this way the process will continue to give us a numerical solution for the differential equation. Now, a geometric approach known as the 5-point stencil could be employed to solve the Laplace operator in a discretized geometric space. The geometric arrangement of all the neighbouring points around the point where the function is to be differentiated is shown in Fig. 2.2 along with the mathematical derivation leading to the solution of such an operator.

$$\frac{\partial u(x,y,t)}{\partial x} = \frac{[u(x+\frac{h}{2},y) - u(x-\frac{h}{2},y)]}{h} \tag{2.12}$$

where h is the distance between two successive points and also $dx = h$

$$\frac{\partial^2 u(x,y,t)}{\partial x^2} = \frac{[u(x+h,y) - 2u(x,y) + u(x-h,y)]}{h^2} \tag{2.13}$$

Similarly,

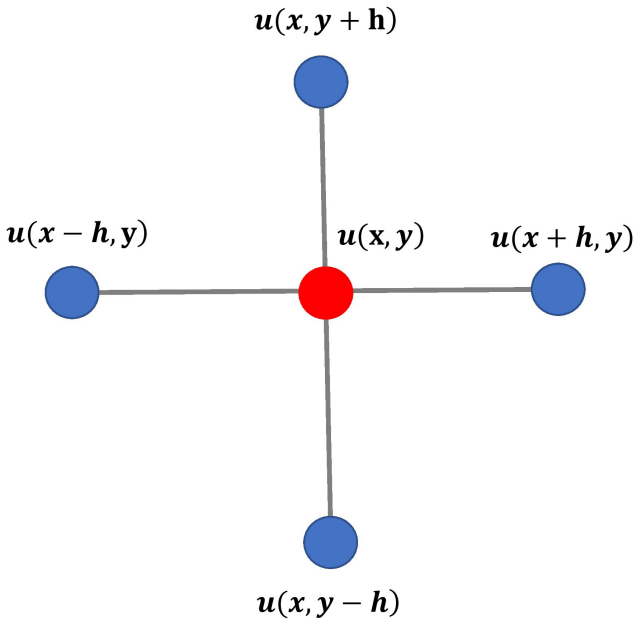

Figure 2.2: 5-point stencil.

$$\frac{\partial^2 u(x,y,t)}{\partial y^2} = \frac{[u(x,y+h) - 2u(x,y) + u(x,y-h)]}{h^2} \tag{2.14}$$

We know,

$$\nabla^2 u(x,y,t) = \left[\frac{\partial^2}{\partial x^2} + \frac{\partial^2}{\partial y^2}\right] u(x,y,t) \tag{2.15}$$

So, from Eqs. 2.13, 2.14, and 2.15, we have:

$$\nabla^2 u(x,y,t) = \frac{[u(x+h,y) + u(x-h,y) + u(x,y+h) + u(x,y-h) - 4u(x,y)]}{h^2} \tag{2.16}$$

Now, using Eq. 2.16 in Eq. 2.11 gives:

$$u(x,y,t) = \left[f(u)_{t_0} + D\frac{[u(x+h,y) + u(x-h,y) + u(x,y+h) + u(x,y-h) - 4u(x,y)]}{h^2}\right] dt + u(x,y,t_0) \tag{2.17}$$

It gives the value of u at a particular point (x, y) in the $n \times m$ lattice at a particular time. Solving for all $n \times m$ points produces the corresponding two-dimensional patterns.

2.1.4 Barkley Model

The Barkley model is one of the most extensively used numerical models to study pattern formation, from target waves to spirals and scrolls. It is given as [3]:

$$\frac{\partial u}{\partial t} = \frac{1}{\epsilon}\left[u(1-u)(u - \frac{v+b}{a})\right] + D_u \nabla^2 u \tag{2.18}$$

$$\frac{\partial v}{\partial t} = u - v + D_v \nabla^2 v \tag{2.19}$$

Figure 2.3: A pair of spiral waves from Barkley model.

This is a more generic model for a reaction-diffusion system. Where u= activator, v= inhibitor, a and b are the parameters, and D_u and D_v are the diffusion coefficients [3].

Throughout our simulations, the diffusion coefficients for the two species are $D_u = D_v = 1.0$, and the parameter values are $a = 0.84$, $b = 0.07$, and ϵ= 0.02. We have used a 5-point Laplacian stencil and have imposed no-flux boundary conditions across the walls.

A spiral wave is found to have its tip in the regions where $u = 0.5$ and $v = a/2$ - $b = 0.35$ [3]. Figure 2.3 shows a pair of spiral waves from a numerical simulation of the Barkley model.

2.1.5 Oregonator Model

The Oregonator model is derived from the FKN mechanism of the BZ reaction. The model consists of the following elementary steps [4, 5]:

$$A + Y \xrightarrow{k_1} X + P \tag{2.20}$$

$$X + Y \xrightarrow{k_2} 2P \tag{2.21}$$

$$A + X \xrightarrow{k_3} 2X + 2Z \tag{2.22}$$

$$2X \xrightarrow{k_4} A + P \tag{2.23}$$

$$B + Z \xrightarrow{k_c} \frac{1}{2} fY \tag{2.24}$$

Where $X = HBrO_2$, $Y = Br^-$, $Z = Ce^{4+}$, $A = BrO_3^-$, $B = CH_2(COOH)_2$, and $P = HOBr$ or $BrCH(COOH)_2$. f is an adjustable stoichiometric factor, and k_c is an adjustable rate parameter. The quantities k_1, k_2, k_3, and k_4 are the real, experimentally derived forward rate constants. The inhibitor species is Z, while the activator species is X. The reactant and product species A, B, and P are often present in significantly larger concentrations and are believed to be constant over the course of a few oscillations, in contrast to the dynamic intermediate species X, Y, and Z [5]. So, considering the law of mass action for X, Y, and Z, we have:

$$\frac{dX}{dt} = k_1[A][Y] - k_2[X][Y] + k_3[A][X] - 2k_4[X]^2 \tag{2.25}$$

$$\frac{dY}{dt} = -k_1[A][Y] - k_2[X][Y] + \frac{1}{2}k_c f[B][Z] \tag{2.26}$$

$$\frac{dZ}{dt} = 2k_3[A][X] - k_c[B][Z] \tag{2.27}$$

Further simplification to dimensionless forms gives the following three rate equations:

$$\epsilon\frac{dx}{d\tau} = qy - xy + x(1-x) \tag{2.28}$$

$$\epsilon'\frac{dy}{d\tau} = -qy - xy + fz \tag{2.29}$$

$$\frac{dz}{d\tau} = x - z \tag{2.30}$$

where,

$$x = \frac{2k_4[X]}{k_3[A]}, y = \frac{k_2[Y]}{k_3[A]}, z = \frac{k_c k_4[B][Z]}{(k_3[A])^2}, \tau = k_c B t, \epsilon = \frac{k_c B}{k_3[A]}, \epsilon' = \frac{2k_c k_4[B]}{k_2 k_3[A]},$$
$$q = \frac{2k_1 k_4}{k_2 k_3}. \tag{2.31}$$

If $\epsilon' < \epsilon$, then a steady state approximation could be made for y in Eq. 2.29, which gives:

$$y = \frac{fz}{q+x} \tag{2.32}$$

The substitution of Eq. 2.32 in Eq. 2.28 gives:

$$\frac{dx}{d\tau} = \frac{1}{\epsilon}\left[x(1-x) - \frac{fz(x-q)}{(q+x)}\right] \tag{2.33}$$

Now, Eqs. 2.30 and 2.33 can be compared with a typical activator-inhibitor model like the Barkley model. Now including diffusion terms into these equations and denoting x, the activator as u, and z, the inhibitor as v, and replacing τ with a general time variable, the equations become:

$$\frac{\partial u}{\partial t} = \frac{1}{\epsilon}\left[u(1-u) - \frac{fv(u-q)}{(q+u)}\right] + D_u\nabla^2 u \tag{2.34}$$

$$\frac{\partial v}{\partial t} = u - v + D_v\nabla^2 v \tag{2.35}$$

The Oregonator Model is defined as Equations 2.34 and 2.35 combined.

2.2 Experimental Approach

2.2.1 The Belousov-Zhabotinsky Reaction

Over the years, chemists were able to create a small number of chemical oscillators in the lab, and some of them accidentally. One of the few well-known chemical oscillators is the Belousov-Zhabotinsky reaction, which, in an undisturbed medium, transforms into a reaction diffusion system and can produce a variety of spatiotemporal patterns, from target waves to spirals and scrolls [6].

The BZ reaction mechanism is quite complicated. Field, Körös, and Noyes formulated a reaction model that takes care of the most important part of the reaction kinetics that gives rise to oscillations in the BZ reaction. This reaction model is often referred to as FKN mechanisms [7]. These mechanical stages of the FKN model are also the foundation of the theoretical Oregonator model. The following ten steps make up this reaction model:

$$HOBr + Br^- + H^+ \rightleftharpoons Br_2 + H_2O \tag{2.36}$$

$$HBrO_2 + Br^- + H^+ \rightarrow 2HOBr \tag{2.37}$$

$$BrO_3 + Br^- + 2H^+ \rightarrow HBrO_2 + HOBr \tag{2.38}$$

$$2HBrO_2 \rightarrow BrO_3^- + HOBr + H^+ \tag{2.39}$$

$$BrO_3^- + HBrO_2 + H^+ \rightleftharpoons 2BrO_2 + H_2O \tag{2.40}$$

$$BrO_2^{\cdot} + Fe^{3+} + H^+ \rightleftharpoons 2HBrO_2 + Fe^{4+} \tag{2.41}$$

$$BrO_2^{\cdot} + Fe^{4+} + H_2O \rightarrow BrO_3^- + Fe^{3+} + 2H^+ \tag{2.42}$$

$$Br_2 + CH_2(COOH)_2 \rightarrow BrCH(COOH)_2 + Br^- + H^+ \tag{2.43}$$

$$6Fe^{4+} + CH_2(COOH)_2 + 2H_2O \rightarrow 6Fe^{3+} + HCOOH + 2CO_2 + 6H^+ \tag{2.44}$$

$$4Fe^{4+} + BrCH(COO)_2 + 2H_2O \rightarrow Br^- + 4Fe^{3+} + HCOOH + 2CO_2 + 5H^+ \tag{2.45}$$

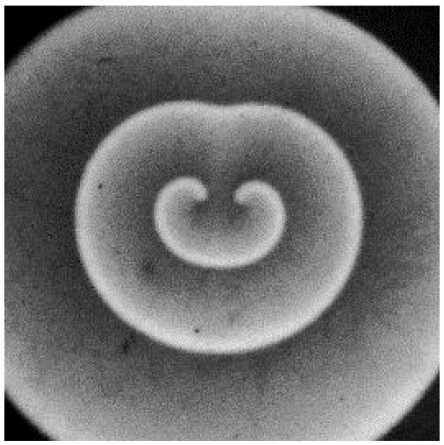

Figure 2.4: A pair of spiral waves from BZ-reaction system.

Dipping silver wire in BZ-reaction is one of the means to initiate the formation of target patterns [8]. Silver wire decreases the Br^- ion concentration by forming

$AgBr$ in its vicinity [8]. Cleaving the target patterns could give rise to spirals. Therefore, the BZ-reaction paved an experimental way to explore various aspects of those wonderful wave patterns. Figure 2.4 shows spiral waves in the BZ system. For detecting the tips of spiral waves and tracing their paths, in-house MATLAB codes were used. The species concentration we used for our reactions is provided in the following table:

Compound	Concentration
Sulphuric acid, H_2SO_4	$0.2M$
Sodium Bromate, $NaBrO_3$	$0.04M$
Malonic acid, $C_3H_4O_4$	$0.04M$
Ferroin	$0.001M$

Table 2.1: BZ-reaction species along with their concentrations.

2.2.2 The Experimental Setup

The reaction is carried out in a Petri dish. A diffused, cold white light source (Dolan Jenner DC950H) is used to illuminate the Petri dish (the system) from below. A charge-coupled device camera was kept right above the system. The camera records the images after a certain time gap (2 seconds in our case). That's how we get the images to analyse the evolving spiral dynamics. The camera has a blue dichroic filter. This filter helps with better imaging by creating a sharp colour difference between the oxidized and reduced forms of the catalyst in the BZ system.

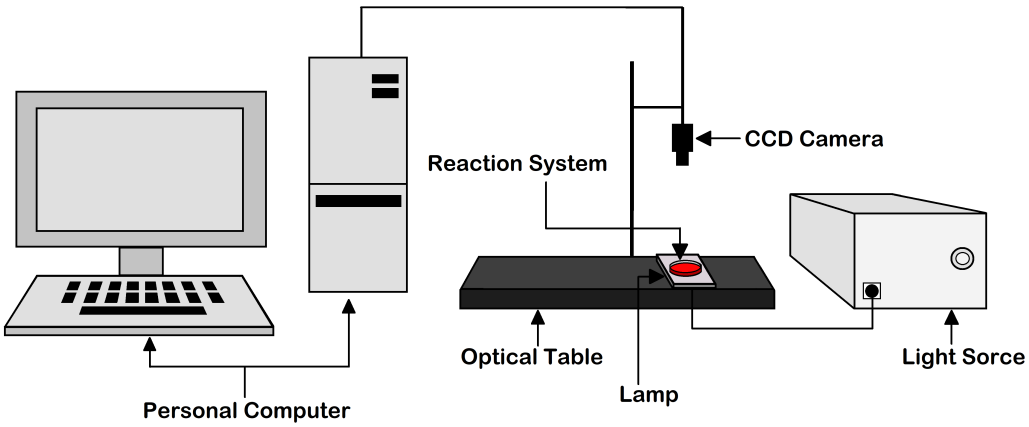

Figure 2.5: Experimental setup.

Bibliography

[1] I. R. Epstein and J. A. Pojman, *An Introduction to Nonlinear Chemical Dynamics : Oscillations, Waves, Patterns, and Chaos* (Oxford University Press, Inc., 198 Madison Avenue, New York, New Work 10016, 1998).

[2] P. Atkins and J. D. Paula, *Atkins' Physical Chemistry*(Oxford University Press, Great Clarendon street, Oxford, OX2 6DP, 2010).

[3] D. Barkley, Physica D **49**, 61 (1991).

[4] I. R. Epstein and K. Showalter, J. Phys. Chem. **100**, 13132 (1996).

[5] R. J. Field, Scholarpedia **2(5)**, 1386 (2007).

[6] J. Jalife, M. Delmar, J. Anumonwo, O. Berenfeld, and J. Kalifa, *Basic Cardiac Electrophysiology for the Clinician*, 2nd ed. (Wiley-Blackwell, Oxford, 2009).

[7] R. J. Field, E. Körös, and R. M. Noyes, J. Am. Chem. Soc. **94**, 8649 (1972).

[8] D. Mahanta, N. P. Das, and S. Dutta, Phys. Rev. E **97**, 022206 (2018).

Chapter 3

Interaction of Multiple Spiral Rotors in a Reaction-Diffusion System

3.1 Introduction

Two-dimensional spiral waves and their three-dimensional counterparts, scroll waves, are responsible for arrhythmia occurring in cardiac systems. The presence of such re-entrant waves is a harbinger of tachycardia and fibrillation in the atria and ventricles of the heart, usually leading to fatal cardiac arrest [1, 2, 3, 4, 5]. These spiral rotors of electrophysiological activities share similar physics with spiral waves that occur in other excitable systems that span across physics, chemistry, biology, and geology [6, 7, 8, 9].

The three-dimensional spatiotemporal dynamics of the heart is accompanied by a measurable scalar electrical value, which can be recorded with an electrocardiogram (ECG). A rapidly drifting electrical rotor in the ventricles of the rabbit heart gives rise to complex excitation patterns manifested in an ECG as ventricular fibrillation (VF). A spiral rotor that gets pinned to an unexcitable heterogeneity will be akin to monomorphic ventricular tachycardia [10]. It has been shown that a single drifting rotor can cause fibrillation in smaller hearts. The human heart is, however, much larger, and VF occurs only in the presence of several such rotors. Hence, the interaction of multiple spiral rotors and the control of their dynamics are of interest to scientists across disciplines.

To date, numerous studies have been performed to achieve the repositioning and annihilation of spiral rotors [11, 12, 13, 14, 15]. The removal of spiral tips from an excitable media by noninvasive methods is a feat worth accomplishing. If one can remove rotating spiral and scroll waves from the cardiac system, it will enable the medical community to better control the diseases related to these waveforms [16]. Existing studies have tried to control the dynamics of spiral waves by modifying the excitability of the system and applying external gradients and target waves [17]. Light [11, 12] and electric field [13] have been used to move the tips of the spirals in a two-dimensional reaction-diffusion system, sometimes leading to annihilation of the waves. High-frequency wave trains have been successfully used to force spirals into defect drifts [18]. Using multiple wave fields, several rotors could even be localized to a particular position. The interaction of rotors in both two and three dimensions with system inhomogeneities has also been a subject of intense study. Theoretical as well as experimental investigations have revealed how the

frequency, position, phase, and nature of spirals can get modified in the presence of inhomogeneities [19, 20, 21, 22].

There are some examples of spiral interaction in the existing literature. Experimentally, instances of suppression and expulsion of one spiral tip by another were observed in the aggregation of Dictyostelium amoebae [23]. Some studies of the interaction of phase singularities (spirals) in the cardiac model are also available [24]. This study demonstrated that a spiral competition instability was responsible for the symmetry breaking of the spiral pair. Numerical studies on the FitzHugh-Nagumo model showed that both like as well as unlike charged spiral vortices (topological charges) can form bound pairs possessing either an axis or a center of symmetry [25]. This charge is attributed to the chirality or the sense of rotation of spiral waves. Corotating spirals are considered to have like charges, and counterrotating spirals are said to be oppositely charged. In yet another study with the complex Ginzburg-Landau equations, it was established that the interaction between well-separated spirals in the particular system is exponentially weak and does not depend on the topological charges [26]. Symmetry-breaking instabilities in a bound state of a spiral pair can also induce the expulsion of one spiral [27], sometimes leading to its elimination at the system boundary [28]. A numerical study of the light-sensitive BZ medium demonstrated how light intensity can modulate the behavior of two counterrotating spirals [29]. In a recent numerical study of the Ferroin-catalyzed BZ system, it was shown that a spiral wave interacting with its axis-symmetric mirror image undergoes attraction when within close distances, leading to annihilation, followed by repulsion, and finally, a region of extremely slow drift as the distance separating them increases [30]. However, such studies on the interaction of spiral rotors are mainly limited to a pair of spirals. Numerical studies on model systems were also expanded to multiarmed vortices [31]. Weijer *et al*. demonstrated from extensive simulations that spirals having same chirality, with tips less than one wavelength apart, can form multiarmed spirals [32].

In three dimensions, experiments with coplanar scroll rings demonstrated that their filaments undergo crossover collisions and reconnect when they are within a core length of each other [33, 34]. On the other hand, the filaments repelled when placed over one another. In yet another study of straight, parallel scroll waves, it was established that the filaments repel only when the interfilament distance was shorter than the wavelength of the scroll waves [35]. When this distance was almost equal to the wavelength, the two scroll waves synchronized.

A detailed study on the interaction of multiple (more than two) spiral vortices with identical frequencies, showing spontaneous annihilation and repulsion, and also establishing the exact distances at which the nature of the interaction changes, is yet to be carried out. It remains to be seen if the limiting distances for the interaction of several spiral rotors are exactly the same as those for a pair of spiral tips, or if they differ [30]. If they do differ, we aim to understand the causes of such variation.

In the current paper, we revisit the problem of spiral wave interaction and extend it further. By employing numerical as well as experimental methods, we explore the dynamics of multiple spiral rotors around each other. We show with experimental evidence the spontaneous annihilation of vortices (without employing any external force). We carry out detailed simulations with the Barkley model for one, two, and four spiral pairs by varying the mutual distances between them. It is observed that, with increasing distance between the rotors, attractive potentials become repulsive. Our simulations reveal different interaction zones with

a transition from an attractive to a repulsive zone and a further transition from this repulsive zone to a zone of no interaction. The important role of the wave connecting two rotors has also been established. We additionally carried out experiments in thin layers of a chemical reaction-diffusion system. We have chosen the Ferroin-catalyzed Belousov-Zhabotinsky (BZ) [7] reaction for the study of the spiral dynamics. Several experiments have been carried out, varying the distances between pairs of spiral tips. Our experimental results corroborate well with the numerical predictions. The phenomena of spiral repulsion and spiral attraction leading to annihilation have been successfully demonstrated for a system of up to eight rotors. Additionally, several intriguing observations have been made for a system of multiple spiral tips, like spontaneous symmetry breaking.

3.2 Numerical Model

The generic two-variable Barkley model is often employed for the study of reaction-diffusion systems [36]. We have chosen this model for our study as it is quite versatile and can be applied to different experimental systems. It has been widely used to explore the dynamics of spiral and scroll waves in the BZ system [13, 37, 38]. The Barkley model is also closer to the FitzHugh-Nagumo model, which is often used to model cardiac waves.

In the presence of diffusion, the Barkley model can be written as follows:

$$\frac{\partial u}{\partial t} = \frac{1}{\epsilon}\left[u(1-u)(u-\frac{v+b}{a})\right] + D_u\nabla^2 u \tag{3.1}$$

$$\frac{\partial v}{\partial t} = u - v + D_v\nabla^2 v \tag{3.2}$$

Here, u is the activator, and v is the inhibitor. In the BZ system, u and v are qualitatively related to the concentrations of bromous acid and the oxidized form of ferroin, the catalyst, respectively. $D_u = D_v = 1.0$ are the diffusion coefficients of the two species. For our simulations, we have chosen the parameter values of $a = 0.84$, $b = 0.07$, and $\epsilon = 0.02$. In chemical reactions, most species diffuse with approximately the same diffusion coefficient [36], supporting our choice of equal diffusion coefficients. This, along with our parameter set, describes a system in which spiral and scroll waves undergo rigid rotation [20, 39], as is the case with our experimental system for the chosen chemical recipe. A time interval of $\Delta t = 0.012$ time units and a step size of $\Delta x = 0.35$ space units were chosen. We employed no-flux (Neumann) boundary conditions on all sides.

The two-dimensional space (of area 105×105 space units) was divided into 300×300 cells of dimension 0.35×0.35 space units each. A five-point Laplacian stencil was used to discretize the space. For initiating a pair of spiral waves, the concentrations of u and v are taken to be 0.0 across the entire space, except for a thin strip in the middle. Here three long strips of isoconcentration lines (with a width of two cells or 0.7 space units each) representing the front ($u = 0.9$, $v = 0$), middle ($u = v = 0.7$), and back or refractory area ($u = 0$, $v = 0.9$) of the wave are taken as the initial conditions for starting a plane wave. The length of the strip varied from experiment to experiment and ranged from 10 cells, or 3.5 space units to 110 cells, or 38.5 space units. Our rotors are initiated far from the system boundary.

Using an explicit finite difference method for space, we converted the system of partial differential equations into ordinary differential equations and proceeded to integrate them by employing the fourth-order Runge-Kutta method. Simulations were repeated using a nine-point stencil, yielding the same results. This choice of parameter values and identical diffusion coefficients can initiate and sustain stable, nonmeandering spirals with a circular core of diameter $d_s = 1.8$ space units. The average wavelength of the spirals (λ) far from the core is around 18.2 space units, while the average time period is 5.3 time units. The wavelength (as well as the time period) is measured from the time-space plot by averaging over several wavelengths (periods) [17]. The spiral tip is defined as the intersection of the isoconcentration lines, $u = 0.5$ and $v = a/2 - b = 0.35$ [18, 36].

3.3 Numerical Results and Discussion

3.3.1 A Single Spiral Pair(A Two Rotor System)

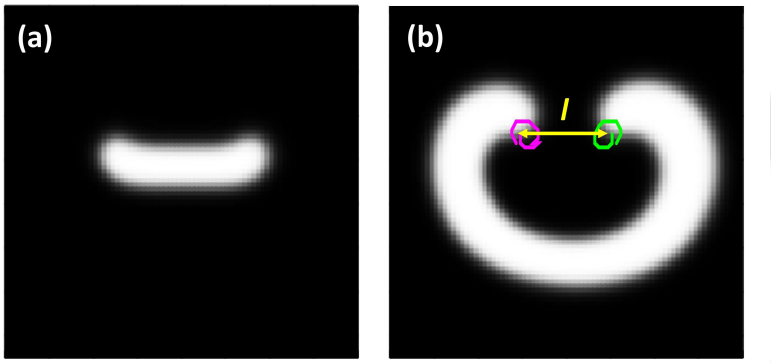

Figure 3.1: Two counterrotating spirals. (a) Snapshot of an initial waveform at 0.72 time units after initiation; (b) Snapshot of the waveform after first rotation at 7.92 time units with system parameter l. The area of each snapshot is 28×28 space units.

We begin our simulations with the simplest case: a single spiral pair. These are two counterrotating spirals with the same initial phase angles, and they arise out of a single plane wave. We refer to these two spiral rotors as initially joined by a wave. Fig. 3.1(a) shows an initial waveform, and Fig. 3.1(b) shows two counterrotating spirals generated from this initial plane wave, along with tip trajectory and system parameter l. The distance between the centers of the two circular cores (shown as the tip trajectory in Fig. 3.1(b)) of the spirals, measured after the first rotation, is considered to be the initial length l.

No Interaction

When (l) is quite large, e.g., $l = 19.75$ space units in Fig. 3.2, the two spirals keep on rotating around their circular cores. The tip trajectories up to the specified time are shown in Figs. 3.2(a)−3.2(c), with a superimposed spiral snapshot taken at the specified time. There is no visible or measurable movement of the spiral cores. The x-coordinate vs. time plots of the tip trajectories corresponding to Figs. 3.2(b) and 3.2(c), respectively, are shown in Figs. 3.2(d) and 3.2(e). It further confirms that the oscillations stay within the same range. The number of

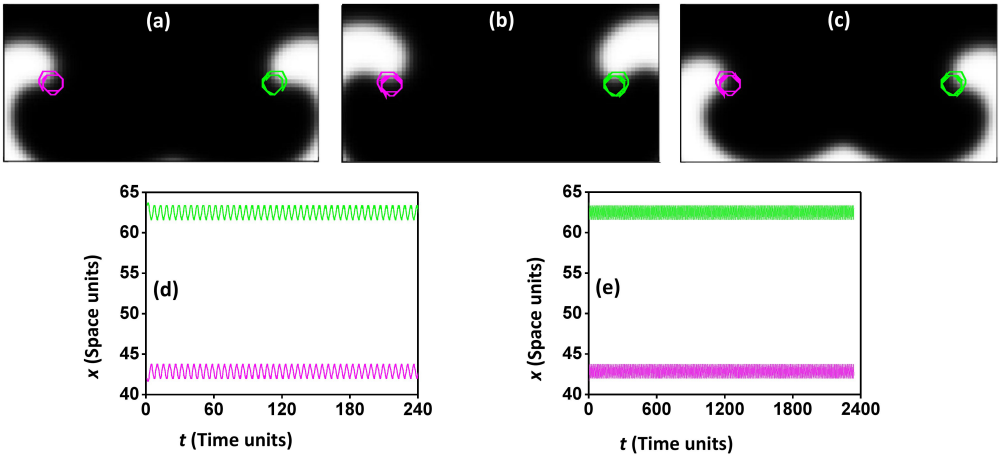

Figure 3.2: A pair of two counterrotating spirals showing no interaction for $l = 19.75$. Snapshots of spirals along with superimposed tip trajectories at $t =$ (a) 24, (b) 240, (c) 2400 in normalized time units. The area of each snapshot is 28×14 space units. (d) and (e) are x-coordinate vs. time plots for the initial and later parts of the simulations, respectively.

oscillations in Fig. 3.2(e) is so high that the peak positions are hardly discernible, yet the x-range remains constant.

Repulsion

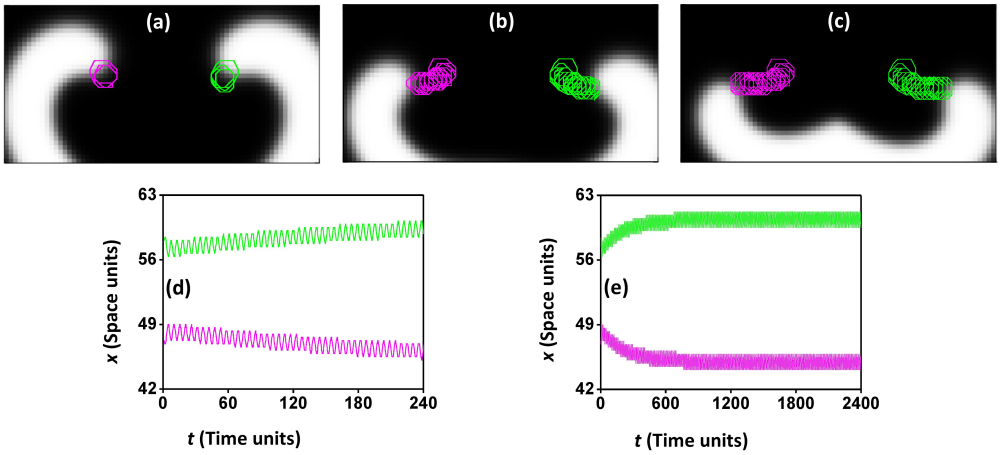

Figure 3.3: A pair of two counterrotating spirals showing repulsion for $l = 9.25$. Snapshots of spirals along with superimposed tip trajectories at $t =$ (a) 24, (b) 240, (c) 2400 in normalized time units. The area of each snapshot is 24.5×12.25 space units. (d) and (e) are x-coordinate vs. time plots for the initial and later parts of the simulations, respectively.

As the cores are brought closer, we can observe an immediate repulsion between them, which pushes them apart until the distance between them is a little less than one wavelength. Here, they continue rotating around a fixed circular orbit. Fig. 3.3 shows one such experiment where the initial value of l is 9.25. However, in this case, the right tip travels slightly lower than the left one, breaking the symmetry

barely. As we keep decreasing the initial distance between the cores, this repulsion phenomenon is observed until $l = 8.2$.

Attraction

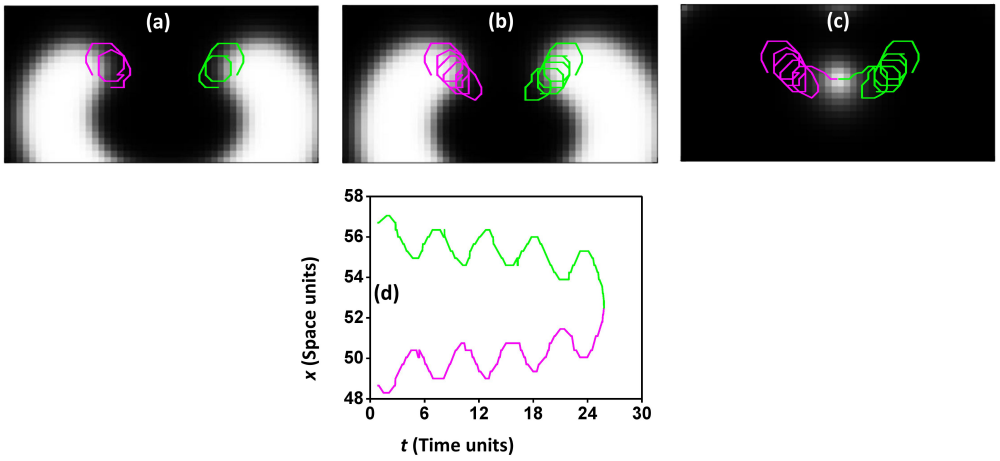

Figure 3.4: A pair of two counterrotating spirals showing attraction and annihilation for $l = 6.65$. Snapshots of spirals along with superimposed tip trajectories at $t =$ (a) 12.5, (b) 23.5, (c) 25.9 in normalized time units. The area of each snapshot is 17.5×8.75 space units. (d) is the x-coordinate vs. time plot.

Below $l = 8.2$, there is a sudden change from repulsive behavior to an attractive one. In Fig. 3.4, an example of attractive interaction between the cores of a spiral pair, which are initially 6.65 space units apart, is seen. The two vortices are observed to trace a curved path that brings them close together and finally annihilates them. It is to be noted that 1.8 space units is the diameter of a noninteracting spiral core for the chosen parameter range. Hence, we observe for this numerical experiment [Fig. 3.4] that though the value of l is many times the core diameter $l > 3.6 \times d_s$, still, the spiral rotors do attract each other and eventually annihilate. The annihilation of two counterrotating spirals that lie within one core length of each other had been previously observed in the literature [25]. However, in our study, we found that the spirals attract even when they are farther apart, as long as they are less than 8.2 space units apart. When the distance between the spiral tips is less than 4.9 space units, the spiral rotors do not complete one full rotation. Instead, their strong mutual attraction forces them to annihilate each other before that. In all our simulations, we measure the value of l by considering the position of the centers of the individual rotors if an invisible boundary existed between the two tips, stopping their interaction.

Phase Diagram

A phase diagram constructed from the behavior of two interacting spiral cores is shown in Fig. 3.5. There are three clearly marked regions in the phase diagram: Attraction leading to annihilation ($8.2 > l$), repulsion ($16.4 \geq l \geq 8.2$), and no interaction ($l > 16.4$). Interestingly, we may observe that when $l > \lambda - d_s = 16.4$, the spirals do not interact. Let us call this value the critical distance, d_c. On the other hand, the interaction changes from repulsive to attractive at exactly half of this critical value, i.e., $l = 1/2\ (\lambda - d_s) = 8.2$. Two counterrotating spirals

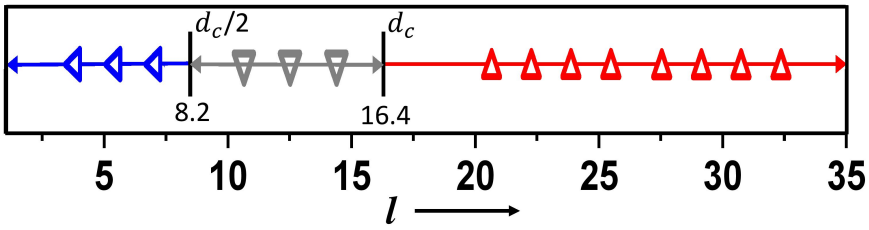

Figure 3.5: Phase diagram of two counterrotating spirals.

initiated from the same wave begin to rotate at a maximum distance ($l_{max} = l + d_s = 20$) and then come closer to each other as the two tips rotate in. This means that the maximum distance l_{max} between the two spiral tips must be more than one wavelength ($\lambda = 18.2$ space units) for there to be no interaction between them. In our numerical system, whenever there was any motion of the spiral core, that happened from the beginning (right after initiation) until that time when the spiral rotors attracted each other and eventually got annihilated or reached a distance where the movement ceased. This is similar to the observations made in [30] where the authors report that a spiral attracts its mirror image on a no-flux boundary when the distance between them is less than 0.28λ, repels beyond that until a distance of 0.82λ, and then there is a very slow drift.

3.3.2 Two Spiral Pair(A Four Rotor System)

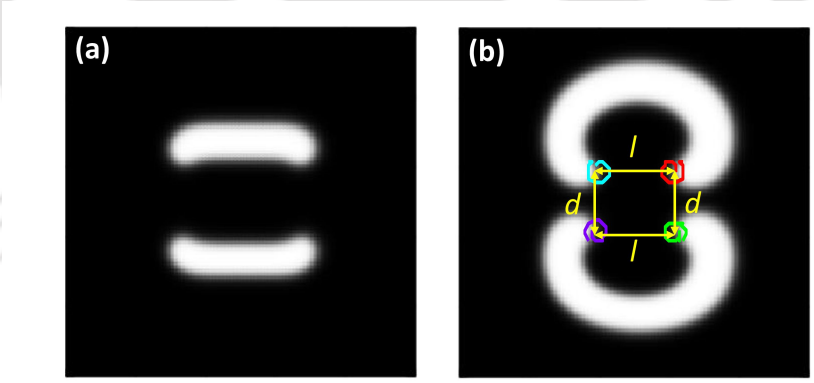

Figure 3.6: A four-rotor system. (a) Snapshot of two initial waveforms at 0.72 time units after initiation; (b) Snapshot of waveforms after first rotation at 7.2 time units with system parameters l and d. The area of each snapshot is 35×35 space units.

Next, we carry out simulations with two spiral pairs (a four-rotor system). We initiate this system of four rotors by placing two parallel plane waves with their refractory zones, or wave tails, facing each other [Fig. 3.6(a)]. As the wave expands, two pairs of counterrotating spirals are formed. The two spirals that are created at either end of a plane wave are referred to as spiral twins, and the initial distance between the centers of their cores is defined as "l" [Fig. 3.6(b)]. The initial distance separating a spiral core from its nearest neighbor (other than the twin) is defined as "d" [Fig. 3.6(b)]. For the case of two spiral pairs or four

rotors, we place the two plane waves along the horizontal (hence l is the horizontal distance between two neighboring rotors, and d is the vertical distance).

For studying a system of four spiral rotors, we initiate a completely symmetrical arrangement so that the lines joining the centers of every rotor to its nearest neighbors will form a rectangle (square for equal l and d values). We carried out several simulations by varying the initial horizontal distance between the cores (l) and the vertical nearest-neighbor distance (d). By doing so, we observed different kinds of synergistic phenomena between the spiral tips.

Horizontal Annihilation

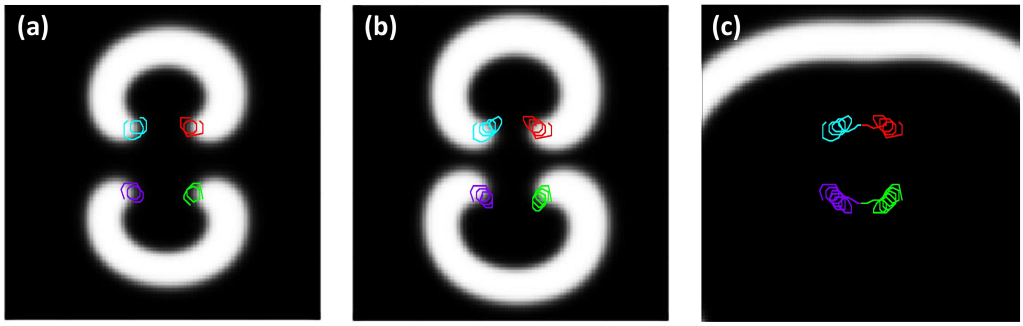

Figure 3.7: Horizontal annihilation of spiral rotors, for $l = 7.4$ and $d = 7.0$. Snapshots of spirals along with tip trajectories at $t =$ (a) 12, (b) 19.2, and (c) 33.6 in normalized time units. The area of each snapshot is 35×35 space units.

Figure 3.7 depicts an example where mutual collapse occurs between the cores of a spiral pair due to annihilation along l. We later refer to this kind of annihilation as horizontal annihilation for a system of two spiral pairs. The trajectories superimposed on the snapshots are the paths traced out by the tip of the spiral waves. It helps us get an idea of the movement of the spiral rotor. As time progresses, the tips get closer, indicating an attractive interaction between the two cores of the initially formed spiral pairs.

An individual spiral tip is influenced by all the rotors close to it. For a system with two spiral pairs initially facing each other, there are two rotors nearest to an individual spiral tip: one placed along l, that is, at the far end of the initial mother wave, and the other placed along d, that belongs to a neighboring spiral wave pair. In this example, $l = 7.4$ space units and $d = 7.0$ space units, both smaller than the limiting distance, $d_c/2 = 8.2$. Here, even though l is larger than d, the spirals choose to attract horizontally, along the distance l. This unexpected dynamics of the spiral tips requires more exploration.

Vertical Annihilation

Figure 3.8 is another instance of the annihilation of vortices between two spiral pairs facing each other. Two spiral tips that initially belong to different spiral pairs start attracting each other along the vertical distance d until they finally annihilate each other. This event is later referred to as vertical annihilation. The spiral rotors may have chosen vertical annihilation over horizontal in this example because of the very low value of d (=6.3) as compared to l (=15.75), the latter 2.5 times the value of d.

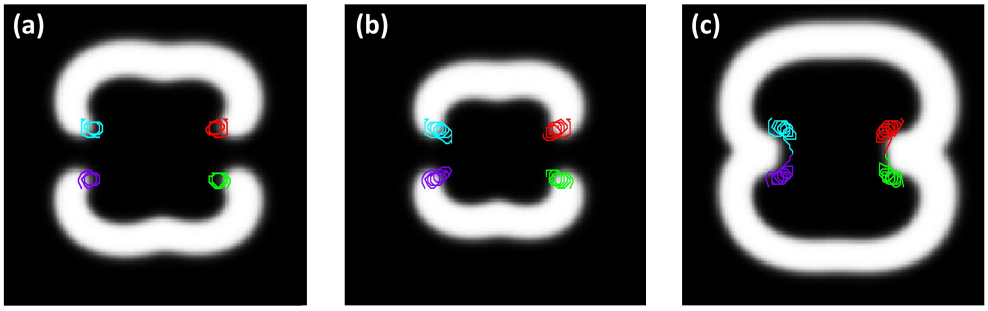

Figure 3.8: Vertical annihilation of spiral rotors, for $l = 15.75$ and $d = 6.3$. Snapshots of spirals along with tip trajectories at $t =$ (a) 14.4, (b) 26.4, and (c) 29.04 in normalized time units. The area of each snapshot is 35×35 space units.

Annihilation and Repulsion (Spontaneous Symmetry Breaking)

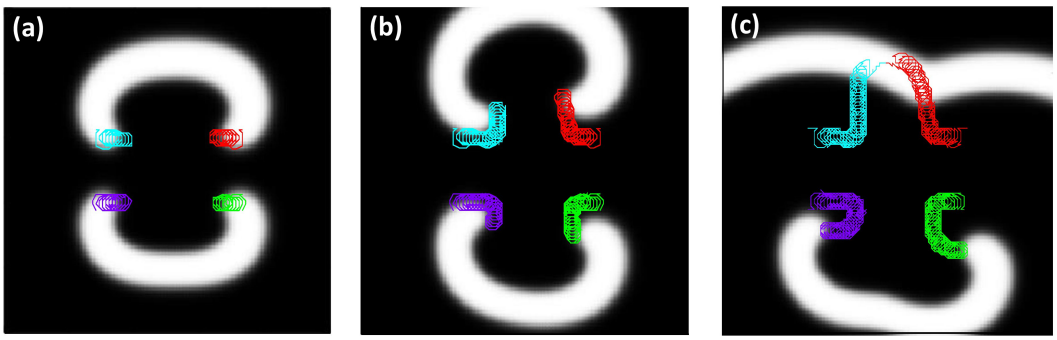

Figure 3.9: Simultaneous repulsion between one pair and annihilation between the other, for $l = 14.35$ and $d = 7$. Snapshots of spirals along with tip trajectories at $t =$ (a) 60, (b) 180, (c) 480 in normalized time units. The area of each snapshot is 35×35 space units.

Figure 3.9 illustrates some remarkable phenomena. Here $l = 14.35$ and $d = 7.0$. Even though l is still quite larger than d ($l = 2.05 \times d$), we can observe an initial attraction along l for both spiral pairs. After covering a certain distance, however, the spiral rotors become strongly repulsive and start moving in the vertical direction, away from the middle. For the bottom pair, this results in a complete U-turn, as the two spiral tips initially approach each other, turn in the negative y direction, and after a while, again start moving horizontally apart. On the other hand, in the top pair, after initially attracting horizontally for a while, they start moving away in parallel (like a bound state) towards the positive y direction before attracting each other once again, finally leading to the annihilation of the spiral pair. This is a very good example of symmetry-breaking instability. It indicates a cooperative effect among the spirals. It is noteworthy that the value of d here is smaller than $1/2d_c$, which would point towards an attractive interaction in the vertical direction in a simpler situation (a single spiral pair). Nonetheless, for a system of four rotors, the tip of a spiral wave is influenced by multiple rotors. This modifies its trajectory, and we often end up with such complicated dynamics and spontaneous symmetry breaking.

Repulsion

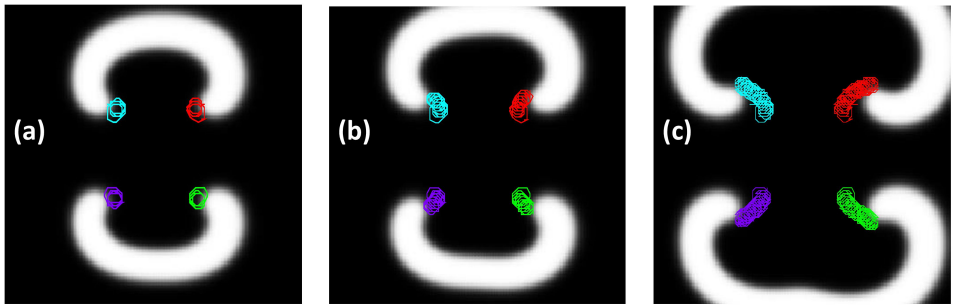

Figure 3.10: Repulsion between the spiral rotors, for $l = 10.15$ and $d = 9.8$. Snapshots of spirals along with tip trajectories at $t =$ (a) 30, (b) 96, and (c) 2160 in normalized time units. The area of each snapshot is 35×35 space units.

In Fig. 3.10, $l = 10.15$ and $d = 9.8$, both values greater than $d_c/2$. Here, initially, the repulsion is vertical, but after some time, the tips start tracing almost diagonal trajectories away from their initial positions.

No Interaction

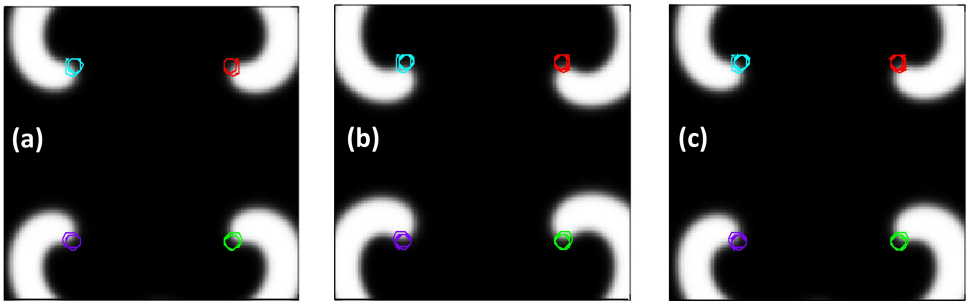

Figure 3.11: No interaction for $l = 19.3$ and $d = 21.2$. The area of each snapshot is 35×35 space units.

With very high d and l values, the dynamics of the waves become independent of each other (no interaction), as seen in Fig. 3.11, where $l = 19.3$ and $d = 21.2$, both greater than the critical distance d_c.

Phase Diagram

Figure 3.12 summarizes the results of all our numerical experiments with two spiral pairs. As was observed in the results of Fig. 3.7 to Fig. 3.11, spiral tips are influenced by all rotors lying in their vicinity, leading to a plethora of tip dynamics. Since we start with two identical spiral wave pairs facing each other, we try to compare the attraction or repulsion faced by a rotor due to its spiral twin and the other rotor closest to it, which belongs to a different pair of spirals. This phase diagram gives us a better understanding of the interactive effects between the spiral rotors. When the distance between two rotors is very low, they show strong attraction towards each other, leading to mutual annihilation. Depending on the values of l and d, they attract either horizontally or vertically. It is observed that

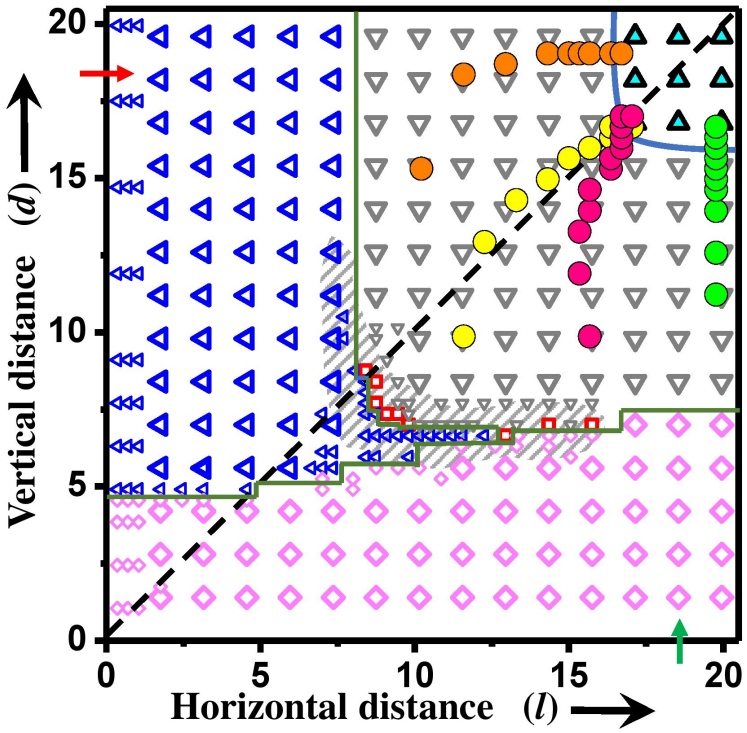

Figure 3.12: Phase diagram of the interaction between two pairs of spirals. The triangles, diamonds, and squares depict the type of interaction for a given simulation with fixed l and d values. Open magenta diamonds depict vertical annihilation; open blue left-pointing triangles depict horizontal annihilation; gray downward-pointing triangles depict repulsion; and the cyan-filled black-bordered upward-pointing triangles depict no interaction between any rotor. The red squares are the cases where one of the pairs attracts and annihilates while the other pair repels and moves away from each other. The various regions have been separated by solid lines, which are only qualitative in nature. The shaded region denotes the occurrence of the complicated dynamics of spiral tips, as in Figs. 9 and 15. Four numerical experiments have been traced here, with the changing l and d values of their spiral cores depicted by closed-colored circles of a unique color. It shows how the rotors move from different zones of repulsive interaction into the noninteracting zone. The red and olive arrows mark the $d = 18.2$ and $l = 18.55$ lines, respectively.

for all d values less than 4.9 space units, the spirals undergo vertical annihilation. As mentioned earlier, this is the minimum distance of separation of a spiral rotor from its neighbors to complete one full rotation. As the plane waves start curling in, one spiral rotor encounters its neighbor from the other spiral pair before it comes into the vicinity of its own twin. So, when the d distances are low ($<$4.9), they annihilate vertically even before they can complete the first rotation (see Fig. 3.13 for a representative example of the tip trajectory in this case).

With increasing l and d values, there is a transition from the attractive zone to the repulsive zone. However, the phase diagram is asymmetric, along a diagonal line (broken line in Fig. 3.12) drawn across $l = d$. This can be attributed to the difference in the strength of interaction, specifically attraction (as the noninteractive zone is symmetric along the diagonal), between the two kinds of neighbors. As the system transitions, the highest value of d for which vertical annihilation is found

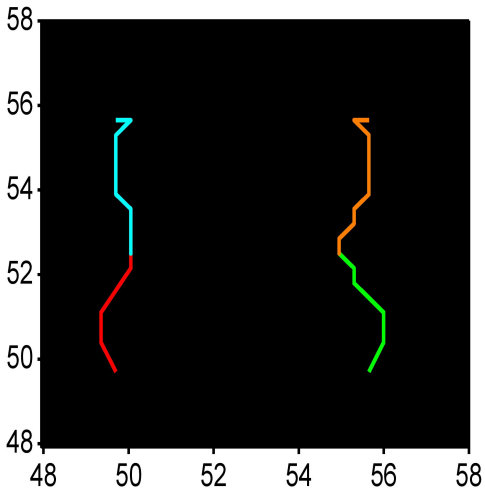

Figure 3.13: Tip trajectories for four spiral rotors showing vertical annihilation for l=4.55 and d=4.2.

is seven space units, whereas horizontal annihilation was observed for l values as large as 12.25. The higher limiting values of l as compared to d for attraction leading to annihilation (horizontal and vertical, respectively) indicate some kind of stronger attractive power between spirals that are initially joined by the same wave and warrant further investigation.

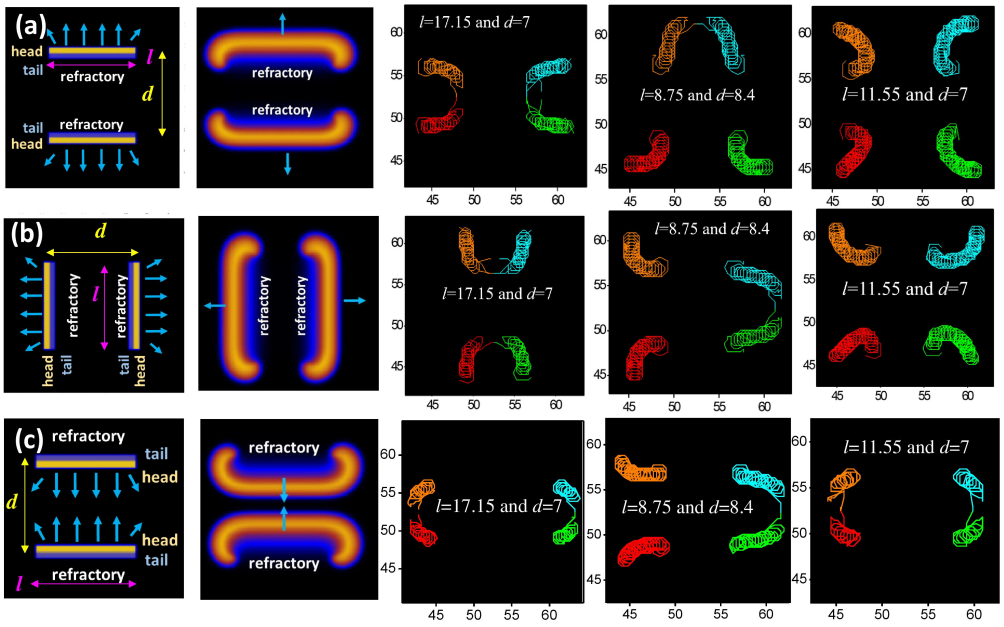

Figure 3.14: Simulation results show a comparison of the change in initial wave placement for a couple of spiral pairs. Top panel (a) shows snapshots and trajectories for various sets of l and d values for l placed horizontally, and initial conditions are the same as taken throughout the paper. Here, the leading edges of the waves initially move away from each other. Panel (b) shows the trajectories for the same sets of initial l and d values as in panel (a); however, l here is placed vertically. Bottom panel (c) shows the case where the leading edges of the waves initially move towards each other along d. Here, the final trajectories change as the interactions between the excitation waves change.

We have already mentioned that changing coordinates does not change the relationship between the spiral tips. Additional simulations by initiating two pairs of spirals in the vertical direction, where l lies parallel to the y-axis, show that the phase diagram remains unchanged for any orientation of the spirals as long as their relative l and d distances are maintained. Comparative results for these two kinds of simulation are shown in Figs. 3.14(a) and 3.14(b). This confirms that our observations do not arise from any numerical error or bias along a particular direction. Rather, in both of these kinds of simulations (as well as all our experiments reported later), we have initiated a pair of waves, which have their trailing edges facing each other. This results in an inhibition of the attractive interaction between the initial waveforms. If the initial waves are horizontally placed, there would be an inhibition along d. Eventually, when the waves expand and merge, the new vertical waves move toward each other, with their leading edges facing one another. This results in a comparatively stronger attraction of the spiral rotors along l. This is the reason for our observation that one spiral is more attracted to its twin (born from the same initial wave). Changing the direction of the wave head and its repolarizing tail would reverse our observations. If the leading edges of the initial horizontal waves faced each other, they would attract more along the vertical, resulting in a stronger attractive interaction along d. Some examples are given in Fig. 3.14(c). For such a system, the spirals will not be more strongly attracted by their twins but by their other nearest neighbor, resulting in a higher limiting value (for attraction followed by annihilation) for the vertical d distance than the horizontal l distance. We would also expect the phase diagram (Fig. 3.12) to change for such a system.

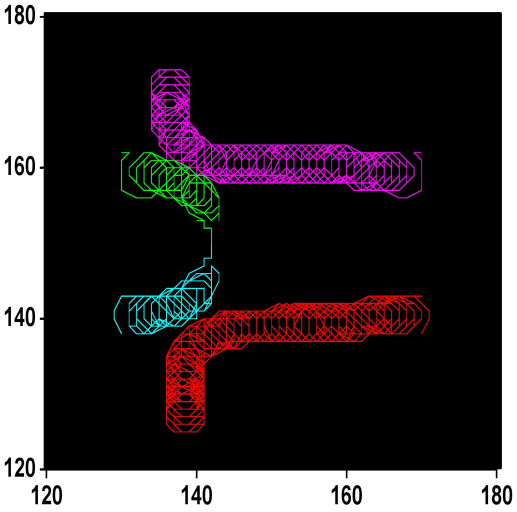

Figure 3.15: Tip trajectories for four spiral rotors showing spontaneous symmetry breaking for $l = 12.95$ and $d = 6.65$. The right pair of counterrotating spirals travel left as a bound state before separating as they approach the left pair of spirals.

In Fig. 3.12, the transition from attraction to repulsion cannot be defined by a sharp (l, d) line; instead, it is a thin region (shaded area in Fig. 3.12) within a range of l and d values. The systems in the transition region could have three kinds of interactions: the spirals may attract and annihilate, they might all repel, or there could be a case of simultaneous attraction and repulsion in the system (depicted by the red squares in Fig. 3.12). Figure 3.9 is an example of such mixed dynamics. This unusual dynamics arises due to the symmetry-breaking cooperative effect of

the spiral waves. The relative motion induced by this effect is quite complicated and may often give rise to completely unexpected dynamics. Tip trajectories for one such numerical experiment ($l = 12.95$, $d = 6.65$) are given in Fig. 3.15. There are also some points where l is greater than half the critical distance, like for $l = 10.2$ and $d = 6.3$, where horizontal annihilation is observed in Fig. 3.16. Although, for this particular point, $l = 1.6 \times d$ and $l > d_c/2$, whereas $d < d_c/2$, the spirals still approach along l and annihilate. Again, this shows that the spiral vortices feel a stronger attraction for their horizontal neighbor (when initiated in this way) than for other neighbors that may be closer to them. However, the presence of the other spiral pair enables this horizontal annihilation between the tips of the spiral wave, which would not have been achieved for a single spiral pair having $l > d_c/2$. Barring these few exceptions, for $l > d_c/2$ and $d > d_c/2$, there exists a large zone of spiral repulsion. With further increase in the vertical and horizontal distances (beyond d_c), all interaction vanishes. Here, from the repulsive to the no-interaction zone, the transition is very sharp, with clear (l, d) demarcating lines along the critical distance (16.8 space units). We have additionally traced the trajectories

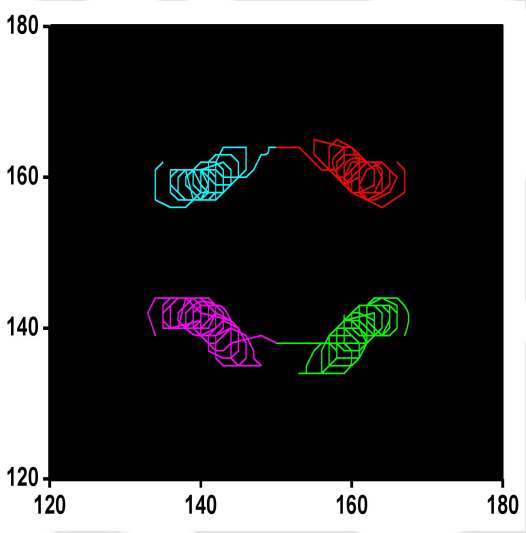

Figure 3.16: Interaction of two spiral pairs showing attraction and annihilation for l=10.2 and d=6.3.

of four numerical experiments in Fig. 3.12 (marked by full circles). All the points lie in the repulsive zone at their initiation and are traced until that point, where the relative motion of the tips ceases. One may observe that the l and d values change spontaneously towards the zone of no interaction. When both distances are much smaller than the critical value of 16.4 space units, for, e.g., the yellow circles that start from (11.55, 9.8), the vertical as well as the horizontal distance increases as the pairs move towards the zone of no interaction (16.4, 16.4). They, however, do not trace an exact straight line. The vertical distance (d) increases faster than the horizontal distance (l), as seen from the curved path of the yellow circles. This points towards the stronger repulsion of the trailing edges of the horizontal waveforms along the vertical when the rotors are linked to the spiral arm of their initial twin, thus separating them vertically. On the other hand, when one of the initial distances is beyond the critical distance, e.g., in the experiment depicted by the green circles, where the initial distances are (19.4, 11.2), only the other distance (vertical in this case) increases all along the path until it reaches the noninteracting zone.

A comparison of the phase diagrams of single and double spiral pairs [Figs. 3.5 and 3.12] shows some similarities and dissimilarities. A careful observation of Fig. 3.12 reveals that for a fairly large value of d (>16.4), the system is in the no-interaction zone in the vertical direction. Again, for $l > 16.4$, it reaches the no-interaction zone in the horizontal direction. For both of these conditions, the individual pair of spirals that lie close by behave as they would in the absence of any other rotors (as in Fig. 3.5). In the case of the former ($d > d_c$), as l increases (for, e.g., along $d = 18.2$, marked by a red arrow in Fig. 3.12), we can observe horizontal annihilation followed by repulsion and then no interaction. Similarly, in the latter case ($l > d_c$), vertical annihilation is followed by repulsion and no interaction as the d value is raised from small to large (for, e.g., along $l = 18.55$, marked by an olive arrow in Fig. 3.12). The presence of the neighboring rotors for lower d and l values brings about the complicated dynamics observed in the system [Figs. 3.9, 3.10, 3.15, and 3.16]. From this observation, we may wonder if an increase in the number of interacting spiral cores might lead to more intricate dynamics.

3.3.3 An Eight Rotor System

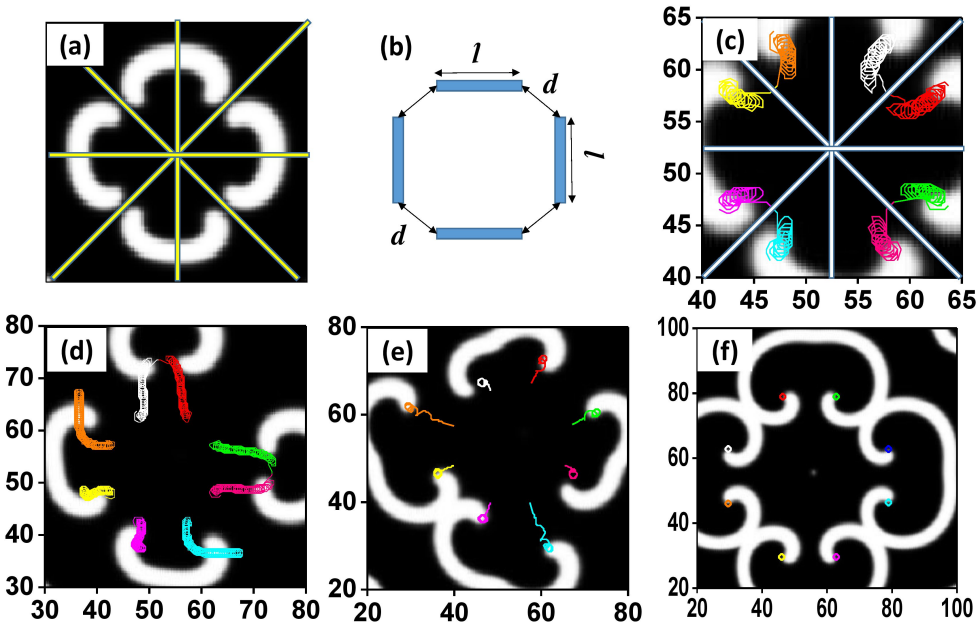

Figure 3.17: Interactions between four pairs of spirals. (a) Snapshot of one numerical experiment at $t = 40.8$ normalized time units for $l = 10.1$ and $d = 6.9$ normalized space units. (b) System design showing the initial placement of waves and corresponding definitions of d and l in these cases. (c) Tip trajectory for $l = 10.1$ and $d = 6.9$. (d) Tip trajectory for $l = 9.0$ and $d = 7.7$. (e) Tip trajectory for $l = 9.5$ and $d = 12.5$ (for the purpose of simplicity, only tip positions at intervals equal to the time period of the spirals, 5.34 time units, are shown here). (f) Tip trajectory for $l = 16.8$ and $d = 23.2$.

Finally, we extended our system to eight spiral cores. We designed a very symmetrical system of spirals in order to be able to clearly observe any symmetry-breaking dynamics. Figure 3.17(a) depicts such a system. In Fig. 3.17(b), we again define our distance parameters l and d as the initial distance between the cores in

a spiral pair and the shortest distance between the two nearest cores belonging to different spiral pairs, respectively. We initiate four spiral pairs having the exact same dimensions and spaced equally apart, forming a kind of closed system with a fourfold degeneracy in the initial waveforms [Fig. 3.17(a)].

In such a symmetric system, we observe mainly four kinds of interactions. A sample of each type is illustrated in Fig. 3.17. Figure 3.17(c) shows mutual annihilation between diagonal pairs of spirals due to a small d (= 6.9) value, as compared to l (= 10.1). Here, each of the spiral pairs behaves almost symmetrically. In Fig. 3.17(d), l = 9.0 and d = 7.7. Here, both annihilation and repulsion are observed simultaneously. The loss of symmetry in this case, is probably due to a symmetry-breaking cooperative effect. The spiral pairs travel like bound states for a distance before the asymmetry sets in, making some pairs repel and others attract and annihilate. This case is similar to that seen in the case of two spiral pairs [Fig. 3.9]. Figure 3.17(e) shows the repulsion of all the spirals. Here l = 9.5 and d = 12.5, both larger than $1/2d_c$. Although their direction of transition is quite symmetric, the velocity is different for different rotors. Some spirals have traveled larger distances compared to others in an equal amount of time. Hence, the repulsion experienced by all the spirals is not uniform throughout. When the spirals are farther away from each other, they do not show any visible interaction, as depicted in Fig. 3.17(f), where l = 16.8 and d = 23.2.

3.4 Experimental Methods

The BZ reaction system provides a convenient way to study the behavior of spiral waves experimentally. A suitable concentration range that sustains spirals was chosen for our experiments. The final concentrations of the reactants are [H_2SO_4] = 0.2 M, [$NaBrO_3$] = 0.04 M, [malonic acid] = 0.04 M, and [ferroin] = 0.001 M. We prepare a homogenous mixture of 0.8 % (w/v, final concentration) agarose gel in millipore water (having a resistivity of 18.2 MΩ cm) with constant stirring and moderate heating. Then it was allowed to cool slightly with continued stirring so as to keep the mixture homogeneous throughout. Now the other reactants (in water) are added to the stirred solution sequentially. When the mixture is just above the gelling temperature, it is poured into a Petri dish of 8 cm diameter and allowed to cool. The BZ gel layer has a thickness of 2 mm. All experiments are carried out at room temperature (22 ± 1 °C). The reaction system was illuminated from below by using a diffused, cold white light source (Dolan Jenner DC950H). We observe the reaction mixture from above with a charge-coupled device camera (mvBlueFOX 22a), which is connected to a personal computer. A blue dichroic filter was attached to the camera for better imaging. We recorded the images at 2 second intervals. The spiral tips were detected by analyzing the snapshots using an in-house interactive program written on the MATLAB platform. The tips were recognized as the points near the spiral head with the highest curvature. In the presence of aerial oxygen, the excitability of the BZ system reduces with time, the waves become slower, and the time period increases [40]. However, we have covered our reaction to minimize this effect. Moreover, we use only experimental data recorded during the first 3 hours after initiating the reaction. During this period, the wavelength and time period of the waves do not change.

The recipe of the BZ reaction that was chosen for these experiments generated a rigidly rotating spiral wave with core diameter d_s = 0.09 cm, an average wavelength, λ = 0.48 cm, and a rotation period of 367 seconds. The wavelength and

timeperiods were measured just like in the case of the numerical simulations, as depicted in [17]. A single spiral pair was generated in the usual way by cleaving a circular wave with a thin glass plate. In order to generate two pairs of spirals, first two circular waves are initiated in close proximity to each other, by dipping two silver wires (Aldrich 99.9% purity) into the reaction gel for a few seconds. The silver helps in catalyzing the reaction, and hence initiates a circular target wave. The waves are allowed to expand and to come closer together. Finally, they are cleaved in such a way that we generate two pairs of spirals, facing one another. The system of spiral waves generated in this manner is similar to what we obtained for our numerical simulations [Fig. 3.1(b)]. Though the initial waveforms in our experiments were curved [Fig. 3.19(a)], instead of straight [Fig. 3.1(a)], the direction of their rotation is the same as that of our numerical simulations. The leading edge of the two initial waves moves away from each other. The distance between the circular waves at the time of cleaving has a special importance as the value of d, or the vertical distance between the center of the spiral cores, depends on it. One more important parameter is the horizontal distance between the centers of the two spiral cores in a pair generated from a single circular wave, l. Special care was taken to maintain these distances by ensuring that the initial target waves are of the same size, and they are cut almost at the same time to obtain similar d and l values between both pairs.

3.5 Experimental Results

3.5.1 One Pair System: The Phase Diagram

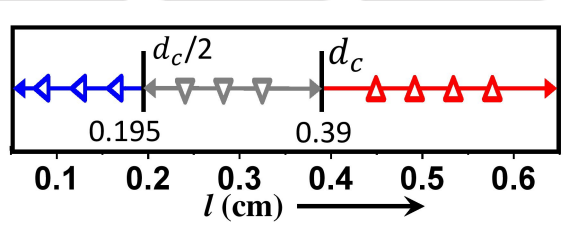

Figure 3.18: Phase diagram of the interaction between the two cores of a counterrotating spiral pair in experiments. Blue left-pointing triangles depict annihilation, gray downward-pointing triangles portray repulsion, and the open red upward-pointing triangles represent no interaction between the two rotors.

Our simulation results for two spirals (Figs. 3.1−3.5) were verified by our experiments with a single excitation wave having two counterrotating spirals at either end. We have designed a phase diagram for a pair of spirals in an experimental system [Fig. 3.18], in keeping with the results of the numerical simulations, in order to graphically demonstrate the various kinds of interactions observed in our experiments. The critical distance, $d_c = 0.39$ cm, is one beyond which all interactions cease, and the distance $d_c/2$ marks the switch between repulsion and attraction. Analyzing with respect to the wavelength and core size, as we did in our simulations, here the critical distance of interaction is equal to $d_c = \lambda - d_s = 0.48 - 0.09 = 0.39$ cm. So, the inter-core distance below which we should observe annihilation is expected to be $1/2d_c = 0.195$ cm.

3.5.2 Two Pair System (Four Spirals)

We carried out a series of experiments with two pairs of spirals by varying the distances d and l, which allowed us to observe the different kinds of interactive phenomena predicted by the simulations. We discuss representative examples of each kind here. However, the initial conditions were not always as symmetric as in simulations. For example, the distance l (= 0.185 cm) in the experiment shown in Fig. 3.19 is an average of 0.17 cm (top pair) and 0.20 cm (bottom pair). There are several factors for this. The exact moment of multiple target wave initiation by several silver wires may not be perfectly coordinated due to local microscopic inhomogeneities in hydrogel density or temperature. Once the waves are formed and start to expand, they are cleaved using a thin object. This also involves errors and noise, and however much care is taken, the two l and d values may not be exactly equal as in a simulation.

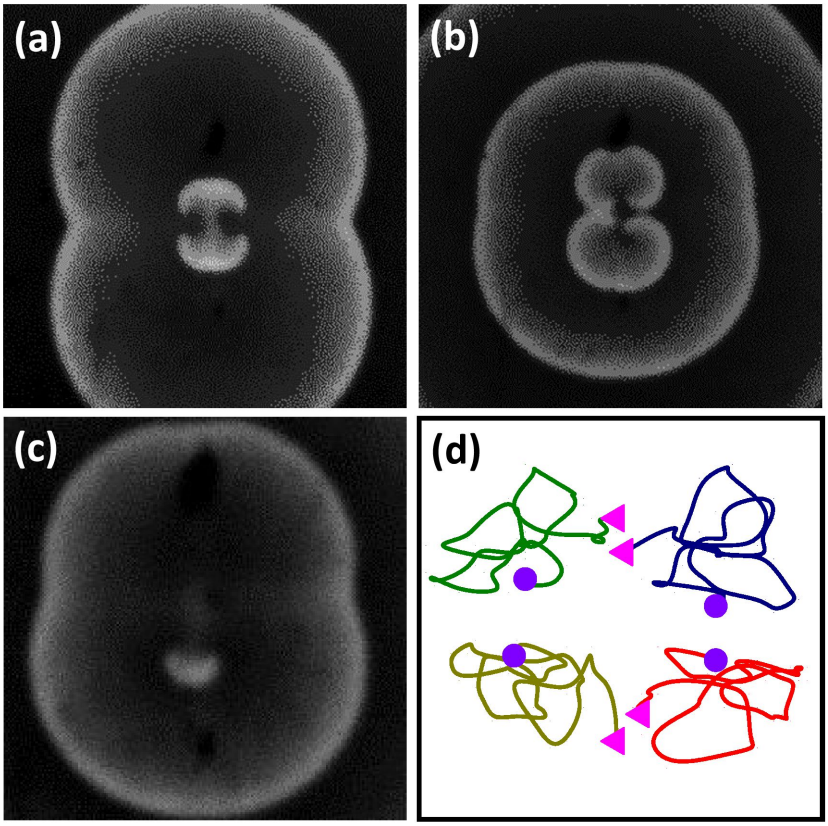

Figure 3.19: Annihilation of two pairs of spiral waves. Snapshots at (a) 8.47 min, (b) 27.28 min, and (c) 32.14 min after initiation of the reaction. Area of each snapshot is 2.95 cm × 2.95 cm. (e) Tip trajectories (colored curves) showing attraction and annihilation. The trajectory of each tip has been given a unique color for clarity. Closed circles designate the initial position of every individual rotor, and the triangles are the final positions prior to the moment of annihilation (at 27.33 min). The area shown in the box is 0.55 cm × 0.55 cm. Initially, d = 0.14 cm, l = 0.185 cm.

Figures 3.19(a)−3.19(c) depict the time evolution of two spiral pairs leading to annihilation. This is similar to the example shown in Fig. 3.7. The tip trajectories in Fig. 3.19(d) portray how a pair of rotors annihilate along the distance l. Here

the initial distances are $d = 0.14$ cm and $l = 0.185$ cm. It is to be noted here that attraction leading to annihilation occurs even when the initial distance between the rotors is more than two times the core diameter ($l = 2.05 \times$ core diameter). The same has been observed in the case of numerical studies too. Even though the initial distance in the vertical direction d is smaller than the initial horizontal distance l, the spiral tips attract along the horizontal, once again establishing the fact that the force of attraction is much stronger along the direction of wave motion. In this experiment, however, both l and d are less than $1/2d_c$.

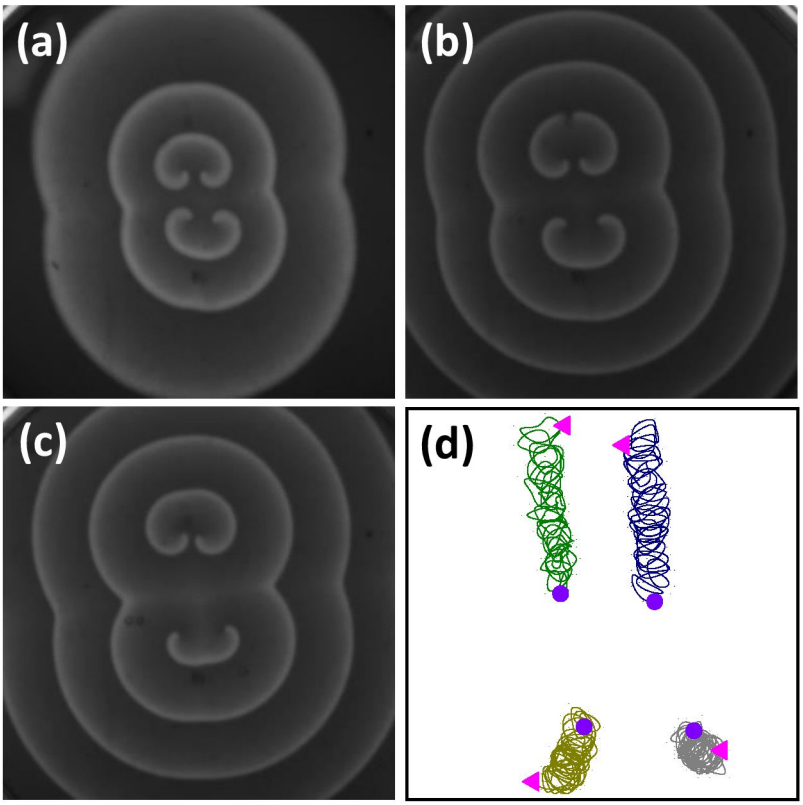

Figure 3.20: Repulsion between two pairs of spiral waves. Snapshots at (a) 19 min, (b) 88 min, and (c) 174 min after initiation of the reaction. The area of each snapshot is 3.8 cm $\times$ 3.8 cm. (d) Tip trajectories showing repulsion. The circles and triangles designate the initial and later (at 72.0 min) positions of the individual rotors, respectively. The area shown in the box is 0.75 cm $\times$ 0.75 cm. Initially $d = 0.295$ cm, $l = 0.31$ cm.

On the other hand, the experiment illustrated in Fig. 3.20 shows an increasing distance between spiral tips with time. This experiment is an example of spiral repulsion, as seen earlier in our simulations [Fig. 3.10]. The values of d and l are 0.34 cm and 0.25 cm, respectively. Although the d values are greater than the l values, the tips repel each other vertically. Due to a slight asymmetry in the initial conditions ($l = 0.23$ cm between the top pair and 0.27 cm between the bottom pair, and $d = 0.32$ cm in the left pair and 0.36 cm in the right pair), the symmetry is further broken in the system as the reaction progresses. The tip trajectories [Fig. 3.20(d)] exhibit the divergent, yet unsymmetrical, dynamics of the rotors over time. All initial distances here (d and l) lie between $1/2d_c$ and d_c. Hence, the repulsion of the tips is in keeping with our theoretical predictions. Interestingly,

one may observe the simultaneous movement of the top spiral pair away from the initial positions, just like in a bound state [29].

3.5.3 Four Pair System (Eight Spirals)

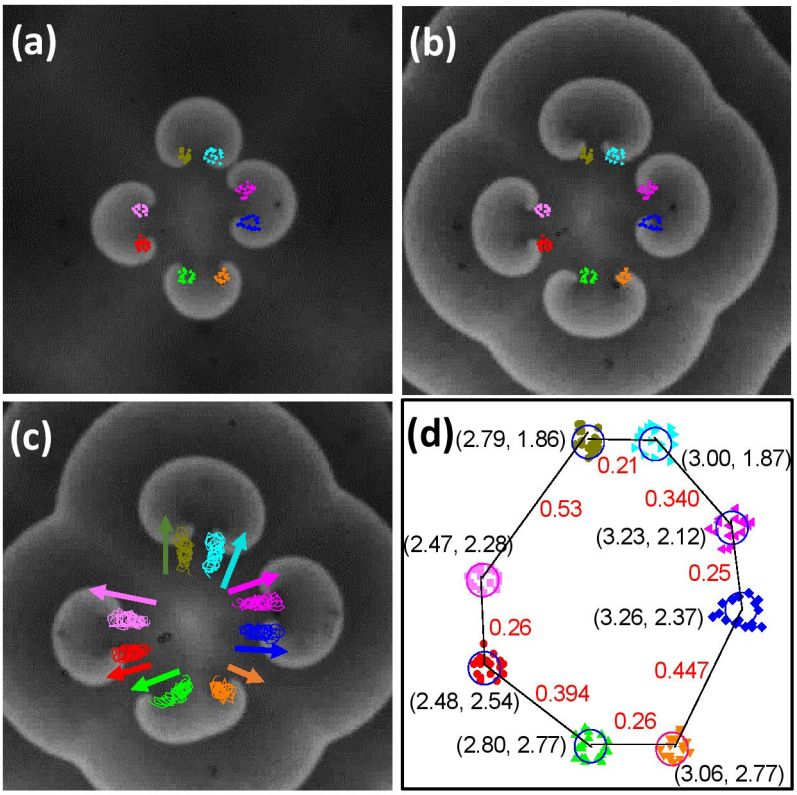

Figure 3.21: Repulsion between four pairs of spiral waves. Snapshots covering an area of 2.95 cm × 2.95 cm at (a) 6.07 min, (b) 56.57 min, and (c) 138.93 min after the initiation of the reaction. (d) Initial positions of the spiral cores (round curves tracing the dots, which are the positions of the spiral tip during the first rotation of the vortex). The coordinates of the center of the circular cores have been noted in cm (in black), while the distance (in cm) between the center of the cores is given in red. The tip trajectories have also been juxtaposed over the snapshots.

We also carried out experiments with four spiral pairs. We initiated the waves by cleaving four circular waves generated adjacent to each other in a square arrangement. The first example is Fig. 3.21, where only repulsive interaction was observed between the spirals. The d values here ranged between 0.34 cm and 0.53 cm, while the l values ranged in the order of 0.21 cm to 0.26 cm. All d values, except one (0.34 cm on the top right), are greater than the critical distance (d_c = 0.39 cm), while the l values are all less than d_c but greater than $1/2d_c$. One would predict the spiral rotors to repel their twins and not interact strongly with the other neighbors. However, we observe that all the spiral rotors move away from the center while (almost) maintaining the initial symmetry. As l values increase very slightly between the tips, the d values are seen to increase more. The only spiral pair that somewhat breaks this symmetry is the one initiated at $y = 2.77$ [shown in Fig. 3.21(d)], the right tip [initially at (3.06, 2.77)], which is probably

pinned to a small bubble that has been formed in its vicinity, seen just below the orange core of the tip in Fig. 3.21(b). This stops its expected movement in the outward direction like the other rotors, while the left tip travels downward, and the l value for this pair increases appreciably.

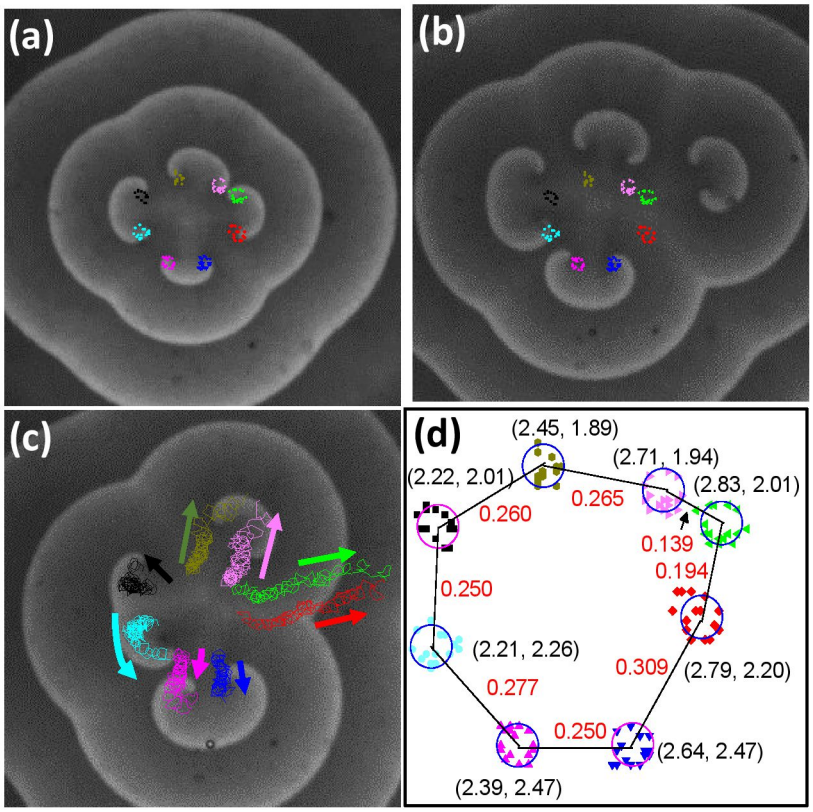

Figure 3.22: Annihilation of one pair of rotors following a strong repulsive interaction between four pairs of spiral waves. Snapshots at (a) 19 min, (b) 116.1 min, and (c) 188.47 min after the initiation of the reaction. Each snapshot covers an area of 2.95 cm × 2.95 cm. (d) Initial positions of the spiral cores with the coordinates of the centers mentioned in cm. The distance (in cm) between the center of each core with its two nearest neighbors is given in red. The tip trajectories of the eight rotors have also been superimposed over the snapshots.

Figure 3.22 shows an experiment where a strong repulsive interaction was observed, followed by the annihilation of a wave pair. The range of d values in this example is 0.139−0.309 cm, while l ranges between 0.194 cm and 0.265 cm. This system has an inherent asymmetry right from the initiation [Figs. 3.22(a) and 3.22(d)]. Hence, one might expect some very unique dynamics to arise out of the wave interactions. A quick glance at the initial inter-rotor distances points to only two values ($d = 0.139$ cm in the top-right corner and $l = 0.194$ cm for the right spiral pair) being in the attractive range. All other distances are in the repulsive zone. The core initiated at (2.83, 2.01) and depicted with green, left-pointing triangles is in the attractive zone of both the cores in its vicinity. So there will be competition to attract this one rotor from its two neighbors. As time progresses, the spiral wave pair on the right is expelled farther to the right by the rest of the rotors [Fig. 3.22(b)]. This is an unexpected movement of the green rotor. Even though it was very close to its pink neighbor (core depicted by right-pointing triangles) [Figs.

3.22(a) and 3.22(d)], it moved away from it and traveled with its twin (the core of red diamonds). At this stage, the three spiral wave pairs that remain at the center of the reaction chamber display a threefold symmetry among themselves [Fig. 3.22(b)]. Subsequently, the spiral wave at the top eventually rotates (as a pair) in the clockwise direction, as it also moves away from the center. Meanwhile, the spiral pair that had been expunged to the right moves farther away, and its two rotors start experiencing mutual attraction, and the vortices eventually undergo annihilation at around 138.5 min (after the initiation of the reaction). This annihilation of the wave may be attributed to its l value of 0.194 cm, which is marginally lower than $1/2d_c$.

3.6 Discussion

We have carried out a detailed analysis of the interaction of counterrotating spiral pairs. Through our experiments and numerical simulations, we have confirmed what is known about the dynamics of two spiral rotors and further probed whether it is possible to explain the behavior of more than two spiral vortices based on spiral wave-pair interactions. We have been able to uncover some previously unexplored behavior which establishes that a simple reduction to spiral pairs fails. Spiral waves, in proximity, would attract each other and finally annihilate. A slight change in the initial distance could make two attracting rotors highly repulsive. We have successfully established a critical distance of interaction between the rotor pairs, whether they have single or multiple neighbors. While the transition from attractive to repulsive interaction occurs across a range of d and l values for more than two rotors, for the simplest case of two rotors, this occurs at 8.2 space units in numerical simulations and 0.195 cm in experiments. As we increase the initial distance further, beyond a particular distance, all interactions between the spirals cease to exist. In numerical simulations, the value is 16.4 space units, and for our experiments, it was found to be 0.39 cm. This critical distance is equal to the difference between the wavelength of the spiral wave and its core diameter.

A preliminary investigation into the dynamics of interacting spiral rotors for different parameter values and also different model systems, like the two-variable Oregonator model, has been carried out. The main results reported in our study hold well in all these situations. Across the systems, we have observed a priority for attractive interaction between the spiral rotors along the direction of wave motion. For a similar initial condition as ours, it has been seen in numerical as well as experimental experiments that a vortex is heavily attracted by its twin, sometimes even when the distance separating it from a neighboring rotor (belonging to another spiral wave pair) is much lower.

We also observed some very interesting symmetry-breaking dynamics in the spiral waves. Existing literature supports the phenomenon of symmetry breaking in two- and three-component reaction-diffusion processes. The dominance of one spiral over the other in a spiral pair, leading to symmetry breaking, was earlier demonstrated in numerical simulations [25, 26], as well as in experiments [27]. With our experiments and simulations, we show that a system with multiple spirals, all having the same frequency initially, can also undergo symmetry-breaking dynamics, even if the initial distances separating them are equal, leading to an uneven geometry as time progresses. We show that in our system, the spiral tips keep on rotating with the same frequency (or time period) while they trace unsymmetrical trajectories, leading to an overall asymmetry in the system without

any necessary dominance of one tip over the other. Unlike the results shown in [27], the cores of our spirals remain fixed at the no-interaction zone, and there is no visible oscillation of the inter-core distance. While some groups [23, 29] claim that a three-component model is required to show the symmetry-breaking instability of spiral pairs, Ruiz-Villarreal *et al.* [27] have shown that such instability is indeed possible in a two-component FitzHugh-Nagumo model. The former groups believe that symmetry breaking requires the presence of a third field whose feedback results in strong interaction between the spiral rotors [23]. However, the results presented in our current study seem to support those by Ruiz-Villarreal *et al.* [27], as we successfully demonstrate the symmetry-breaking instability in a two-variable Barkley model system. The parameter range through which the two-variable Barkley model displays symmetry breaking is also substantial. Spontaneous symmetry breaking can still be observed for a set of parameters entirely different from our current set ($a = 1.1$, $b = 0.18$, $\epsilon = 0.01$, $dt = 0.012$, $dx = 0.35$, $D_u = 1.0$, $D_v = 0.0$). This set of parameters with a non-diffusing recovery variable ($D_v = 0.0$) is often chosen to model systems where the catalyst is immobilized [29, 36]. All the observations made with our parameter values can also be observed in this system. However, it may be expected that the exact value of the critical distance may change with changing parameters. A simple change in the value of the excitability parameter ϵ changes the nature of the spirals (time period, frequency, wavelength, and tip trajectory or core size) [17]. Hence, it can be expected that the critical distance might also change under these circumstances, though it will always be less than one wavelength. For both sets of parameter values that we have thoroughly investigated, we observed the formation of bound states by some pairs of counterrotating spirals (Figs. 3.9, 3.15, and 3.17(d)). This is in keeping with the results shown in [29]. Similar observations have also been made in many of our experiments (Figs. 3.20−3.22). However, a sudden asymmetry in the system brought about by some local inhomogeneities may result in the bound states losing their stability. The spiral pairs, in these cases, may attract and annihilate (Figs. 3.9, 3.17(d), and 3.22) or even repel (Fig. 3.15), after having traveled as a bound state for a long distance. Reducing the grid size does hasten the onset of the symmetry-breaking instability (as mentioned in [27]), and increasing grid sizes leads to a more symmetric system. However, for multiple spirals (more than two), we found that symmetry breaking is observed even for high grid sizes (0.5 space units). Our experiments show that symmetry breaking is an inherent quality of excitable systems with multiple excitable centers. The results of our numerical simulations are in keeping with that idea. The presence of numerical noise in simulations or microscopic variation of system parameters in experiments can make a system starting from symmetrical initial conditions evolve into one of striking asymmetry as time progresses. An initial dissymmetry, however small, blows up with time, and the system diverges into complete asymmetry.

The results obtained for the interactive behavior of these two-dimensional spiral waves are somewhat different from those known about their three-dimensional counterparts, the scroll waves. These three-dimensional scroll waves can be thought of as a stack of spirals or an extension of a two-dimensional spiral along the third dimension. When neighboring scrolls approach each other, their constituent spirals can annihilate if they have opposite senses of rotation. Depending on the distance between the filaments, such a phenomenon can lead to the "reconnection" of the scroll waves. In experiments with scroll rings, we had shown in an earlier study [33] that the circular filaments attract each other and reconnect when they are less

than one core diameter apart. Repulsion between the waveforms was also found for a particular orientation of the filaments, which was believed to be due to the proximity of corotating spirals. Scroll rings with positive filament tension undergo spontaneous shrinkage and eventually disappear. Hence, it is difficult to establish quantitatively the repulsive influence of the constituent spirals on the dynamics of two neighboring scroll rings. In another experimental study of parallel and straight scroll waves [35], it was shown that they repel each other when they are separated by distances greater than $\frac{2}{3}\lambda$ but smaller than one wavelength. Here, the authors could not initiate pairs of scroll waves that were closer than $\frac{2}{3}\lambda$ in their experiments. Hence, for three-dimensional scroll waves, a critical distance for the sudden flipping of attractive interaction to give way to repulsion is not yet known in the literature. However, in our current study, we observe that the attraction between rotors is felt over a distance that is many times greater than the core diameter. Numerically, for our chosen parameters, the distance was found to be 4.5 times the core diameter, while experimentally, we have observed attractive interaction at least up to 2.2 times the core diameter (both of which are close to half a wavelength). It would be interesting to probe the system of 3D scroll waves to ascertain if its constituent spirals also attract until such distances that are close to half of a wavelength.

3.7 Conclusion

In conclusion, we have successfully quantified the nature of spiral wave interaction as a function of wave properties. A critical distance for the interaction of two spiral waves has been established. This measure could be used to understand the dynamics of multiple rotors. For systems of two, four, and eight spiral cores, we have demonstrated the possibilities of spiral attraction leading to annihilation, repulsion, and no interaction. As the number of rotors increases, more complicated dynamics come to light. In the presence of additional rotors, a pair of spirals in the repulsive zone can undergo attraction followed by annihilation. Spontaneous symmetry breaking is also observed, inducing the spiral tips to trace intriguing tip trajectories. We have validated by several examples and comparisons that the dynamics of the spiral rotors also depend on the motion of the spiral wave arm. If the initial waves are moving away from each other, the rotors that will originate from the two ends of a single wave will attract each other more strongly than other rotors from neighboring spiral waves.

Spiral rotors of this kind play a vital role in the fibrillatory conduction of the cardiac muscles by activating the atria at exceedingly high frequencies [10]. The present study illuminates the nuances of spiral wave interaction and may facilitate a better understanding of the interaction of rotors in the atria and ventricles. Since we have shown how the interaction of neighboring spiral tips can bring about their drift within the excitable medium or their annihilation, our results have strong implications for understanding the dynamics of such rotors in the cardiac system. The drift of otherwise non-meandering spiral rotors due to interaction with nearby spirals can transform monomorphic tachycardia into polymorphic tachycardia, and even the life-threatening Torsades de pointes, in the presence of several rotors. Contrarily, the mutual attraction of rotors leads to the annihilation of spiral pairs will point towards the quenching of tachycardia or fibrillation in the heart muscles.

Further analysis of the velocity of attraction and repulsion should shed more light on the interaction dynamics. It remains to be seen whether the velocity

of these interactions would take the form of Yukawa potentials, as was found in the case of three-dimensional scroll rings [33, 41]. Future studies could try to uncover the cause of the symmetry-breaking dynamics that are observed in systems with multiple spiral rotors. Another interesting question is how the spiral velocity fields change as a function of model parameters. Also, detailed simulations of the interaction of spirals with varying phase differences, for both counter- and corotating spirals, will be worth exploring.

Bibliography

[1] J. Jalife, M. Delmar, J. Anumonwo, O. Berenfeld, and J. Kalifa, *Basic Cardiac Electrophysiology for the Clinician*, 2nd ed. (Wiley-Blackwell, Oxford, 2009).

[2] F. H. Fenton, E. M. Cherry, and H. M. Hastings, Chaos **12**, 852 (2002).

[3] F. X. Witkowski, L. J. Leon, P. A. Penkoske, W. R. Giles, M. L. Spano, W. L. Ditto, and A. T. Winfree, Nature (London) **392**, 78 (1998).

[4] J. Christoph, M. Chebbok, C. Richter, J. Schröder-Schetelig, P. Bittihn, S. Stein, I. Uzelac, F. H. Fenton, G. Hasenfuß, R. F. Gilmour Jr., and S. Luther, Nature (London) **555**, 667 (2018).

[5] S. Luther, F. H. Fenton, B. G. Kornreich, A. Squires, P. Bittihn, D. Hornung, M. Zabel, J. Flanders, A. Gladuli, L. Campoy, E. M. Cherry, G. Luther, G. Hasenfuss, V. I. Krinsky, A. Pumir, R. F. Gilmour, Jr., and E. Bodenschatz, Nature (London) **475**, 235 (2011).

[6] O. Steinbock, F. Siegert, S. C. Müller, and C. J. Weijer, Proc. Natl. Acad. Sci. USA **90**, 7332 (1993).

[7] I. R. Epstein and J. A. Pojman, *An Introduction to Nonlinear Chemical Dynamics*: *Oscillations*, *Waves*, *Patterns*, *and Chaos* (Oxford University Press, 198 Madison Avenue, New York, New Work 10016, 1998).

[8] S. Jakubith, H. H. Rotermund, W. Engel, A. von Oertzen, and G. Ertl, Phys. Rev. Lett. **65**, 3013 (1990).

[9] J. Lechleiter, S. Girard, E. Peralta, and D. Clapham, Science **252**, 123 (1991).

[10] J. Jalife, R. A. Gray, G. E. Morley, and J. M. Davidenko, Chaos **8**, 79 (1998).

[11] O. Steinbock and S. C. Müller, Int. J. Bifurcation Chaos Appl. Sci. Eng. **3**, 437 (1993).

[12] K. I. Agladze, Chaos **6**, 328 (1996).

[13] J. Schütze, O. Steinbock, and S. C. Müller, Nature (London) **356**, 45 (1992).

[14] J. Schlesner, V. S. Zykov, H. Brandtstädter, I. Gerdes, and H. Engel, New J. Phys. **10**, 015003 (2008).

[15] M. Braune and H. Engel, Phys. Rev. E **62**, 5986 (2000).

[16] J. Jalife, J. Cardiovasc. Electrophysiol. **14**, 776 (2003).

[17] D. Mahanta, N. P. Das, and S. Dutta, Phys. Rev. E **97**, 022206 (2018).

[18] S. Dutta and O. Steinbock, Phys. Rev. E **83**, 056213 (2011).

[19] B. T. Ginn and O. Steinbock, Phys. Rev. Lett. **93**, 158301 (2004)

[20] S. Dutta and O. Steinbock, J. Phys. Chem. Lett. **2**, 945 (2011).

[21] F. M. Zanotto and O. Steinbock, Phys. Rev. E **103**, 022213 (2021).

[22] E. Nakouzi, J. F. Totz, Z. Zhang, O. Steinbock, and H. Engel, Phys. Rev. E **93**, 022203 (2016).

[23] I. Aranson, H. Levine, and L. Tsimring, Phys. Rev. Lett. **76**, 1170 (1996).

[24] N. Tomii, M. Yamazaki, T. Arafune, K. Kamiya, K. Nakazawa, H. Honjo, N. Shibata, and I. Sakuma, Am. J. Physiol.: Heart Circ. Physiol. **315**, H318 (2018).

[25] E. A. Ermakova, A. M. Pertsov, and E. E. Shnol, Physica D **40**, 185 (1989).

[26] I. Aranson, L. Kramer, and A.Weber, Physica D **53**, 376 (1991).

[27] M. Ruiz-Villarreal, M. Gómez-Gesteira, C. Souto, A. P. Muñuzuri, and V. Pérez-Villar, Phys. Rev. E **54**, 2999 (1996).

[28] R. R. Aliev, V. A. Davydov, T. Kusumi, and T. Yamaguchi, Netsu Sokutei **24**, 194 (1997).

[29] I. Schebesch and H. Engel, Phys. Rev. E **60**, 6429 (1999).

[30] J. F. Totz, H. Engel, and O. Steinbock, New J. Phys. **17**, 093043 (2015).

[31] R. M. Zaritski and A. M. Pertsov, Phys. Rev. E **66**, 066120 (2002).

[32] B. Vasiev, F. Siegert, and C. Weijer, Phys. Rev. Lett. **78**, 2489 (1997).

[33] N. P. Das and S. Dutta, Phys. Rev. E **91**, 030901(R) (2015).

[34] D. Mahanta and S. Dutta, Phys. Rev. E **100**, 022222 (2019).

[35] J. Kupitz and M. J. B. Hauser, J. Phys. Chem. A **117**, 12711 (2013).

[36] D. Barkley, Physica D **49**, 61 (1991).

[37] H. Dierckx, I. V. Biktasheva, H. Verschelde, A. V. Panfilov, and V. N. Biktashev, Phys. Rev. Lett. **119**, 258101 (2017).

[38] N. P. Das and S. Dutta, Phys. Rev. E **96**, 022206 (2017).

[39] S. Alonso, Ralf Kahler, A. S. Mikhailov, and F. Sagués, Phys. Rev. E **70**, 056201 (2004).

[40] O. Steinbock, C. T. Hamik, and B. Steinbock, J. Phys. Chem. A **104**, 6411 (2000).

[41] M.-A. Bray and J. P. Wikswo, Phys. Rev. Lett. **90**, 238303 (2003).

Chapter 4

Effect of Sense and Phase of Rotation on the Interaction of Spirals

4.1 Introduction

Spiral waves, when in close proximity, can interact with each other. Theoretical studies on spiral vortex interaction showed that after a certain distance between spiral cores, the interaction decreases exponentially [1]. Attraction or repulsion was seen among the vortices at short distances, which subsequently created relative motion among them [1, 2, 3]. This attraction could induce annihilation also [4]. Annihilation was also established experimentally by controlling the relative motion among the vortices with the help of external means like LASER [5], light [6], electric field [7] etc. Experimental evidence on the annihilation of spiral waves without the help of external agents is very rare, except in some instances showing the suppression and expelling of one spiral by another [8, 4]. Symmetry-breaking instabilities in a bound state of a spiral pair [9, 10, 2] can also lead to the formation of states with one dominant spiral, i.e., the suppression and expelling of one spiral by another [10]. Studies were also expanded to systems with multiple vortices. Symmetry breaking in multi-armed vortices (unstable) [9, 11, 12, 13, 5] is very common, but there are instances where stable structures result that maintaining symmetry throughout [9].

In our recent study, we showed that two counterrotating spiral waves placed symmetrically (spiral waves having zero phase angle difference) with a very short separation between them attract each other [14]. As the distance increases, this attractive interaction becomes repulsive. After a certain distance, which we call the critical distance (d_c), all interaction ceases [14]. The interaction can be easily understood by monitoring the tip trajectory. In this study, we explored the effect of phase difference and the nature of rotation (chirality) on the interaction of two spiral cores. Here, our approach is numerical. The generic Barkley model was employed for carrying out our numerical experiments. We started our simulation with two counterrotating phase mismatched spiral waves, where we observed the critical distance (d_c) of interaction increase with an increase in phase angle difference. For two counterrotating spirals, at higher phase angle differences, we don't observe any kind of attractive interaction. Then we studied the interaction between two corotating spiral waves. For corotating spirals, the critical distance (d_c) of interaction decreases with an increase in phase angle difference. The critical distance (d_c) of

interaction is highest for a spiral pair having a zero phase angle difference. For two such corotating spirals, we don't get any kind of attractive interaction at any phase angle difference, including the zero phase angle difference.

4.2 Numerical Model

We utilized the generic two-variable Barkley model for numerical simulation. It is one of the best systems to study spiral and scroll waves in reaction-diffusion systems [15, 16]. The model is given as:

$$\frac{\partial u}{\partial t} = \frac{1}{\epsilon}\left[u(1-u)(u-\frac{v+b}{a})\right] + D_u\nabla^2 u \tag{4.1}$$

$$\frac{\partial v}{\partial t} = u - v + D_v\nabla^2 v \tag{4.2}$$

where u represents the activator and v represents the inhibitor. D_u and D_v are diffusion coefficients of u and v respectively. $D_u = D_v = 1.0$ in our system. The values of system parameters are $a = 0.84$, $b = 0.07$, and $\epsilon = 0.02$. The fourth-order Runge-Kutta method, a 5-point Laplace stencil, and a zero-flux boundary condition were used to solve the differential equations numerically. The area was discretized into 300×300 grid points with a step size of $\Delta x = 0.35$ (arbitrary space units) and a time interval of $\Delta t = 0.012$ (arbitrary time units). This system can sustain spiral waves of the same frequency. A spiral with a circular core of 1.8 space units can be initiated and maintained using these parameter values and identical diffusion coefficients. The average spiral far from the core has a wavelength of about 18.2 space units and a period of 5.3 time units.

4.3 Numerical Results and Discussion

Our system consists of a pair of spiral waves with an initial mismatch in their phase angles. Both corotating and counterrotating scenarios were considered, and simulations were divided into two sets accordingly. One set of simulations was done for a corotating spiral pair and the other for a counterrotating spiral pair. Both sets of simulations consist of a pair of spiral waves with phase angle differences of 45°, 90°, 120°, and 180° at the time of initiation.

For maintaining the phase angle difference in a spiral pair, we initially generated two single spirals with a phase angle mismatch of 90°. We just changed the sense of rotation of one spiral wave for the counterrotating set. To keep the cores of the spirals in a fixed position, we pinned the individual spirals with the same size heterogeneity. The heterogeneities were kept within the same y-range. After some time, the heterogeneities were removed, and that's how we get spiral pairs with 90° phase differences whose cores lie within the same y-range. For the other phase angle differences, one spiral was created a little later than the other. Depending on the time difference of initiation, we created spiral pairs with 45°, 135°, and 180° angle differences.

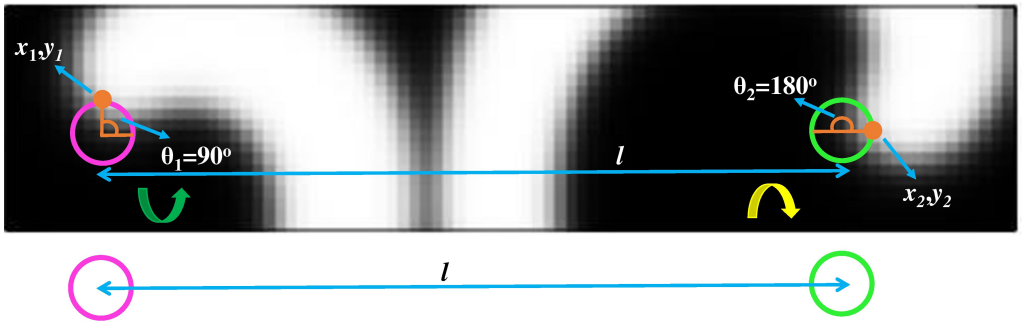

Figure 4.1: Snapshot of two counterrotating spiral waves having a phase angle difference of 90°with superimposed tip trajectory (first rotation) along with the parameters of the numerical experiment (position, angle, and distance). The white regions represent areas of heightened wave activity.

4.3.1 A Pair of Counterrotating Spirals with 90° Phase Angle Difference

Figure 4.1 shows a snapshot of a typical numerical experiment with two counterrotating spirals having a phase angle difference of 90° along with the parameters of the numerical experiment (position, angle, and distance). The phase of the spiral shown here was taken at t=18 time units, and the tip trajectory was also taken until the same time, when they had just completed the first rotation. The distance between the centres of the tip trajectory of the very first rotation is defined as l, which is also shown below the snapshot for a clear understanding. The position of the tip at any given time is defined by (x_i,y_i). (x_1,y_1) is for the left tip, and (x_2,y_2) is for the right tip. The phase angle of each spiral tip with respect to the line along l is defined by θ_1 and θ_2 respectively. Here, $\theta_1 = 90°$ and $\theta_2 = 180°$. The arrows point in the direction of rotation. The green arrow shows the anticlockwise sense, whereas the yellow arrow shows the clockwise sense. The way they interact depends on the value of l. The detailed explanations are given in the following sections:

No Interaction

When the l distance between the cores is very high ($l > 18.2$), no visible interaction is seen between the tips. The tips keep rotating around the same core, as seen in Fig. 4.2. When $l > 18.2$ space units, both the spiral arms become exposed enough to screen their cores from the other (neighboring) spiral arm. Figure 4.2(a) shows the tip trajectory for the first rotation and the spiral snapshot at 17.4 time units. Similarly, Figs. 4.2(b) and 4.2(c) too show the tip trajectory and spiral snapshots at later periods. The spiral core remains in the same position in all the figures indicating no visible interaction among the tips. Figures 4.2(d) and 4.2(e) are the time vs. x-coordinate plots up to the time corresponding to Figs. 4.2(b) and 4.2(c), respectively, i.e., t = 240 time units and t = 1801 time units, respectively. It further confirms the fact that the oscillations remain within the same range. In Fig. 4.2(e), the number of oscillations is so high that we can hardly see the peak positions, but the x-range is constant throughout.

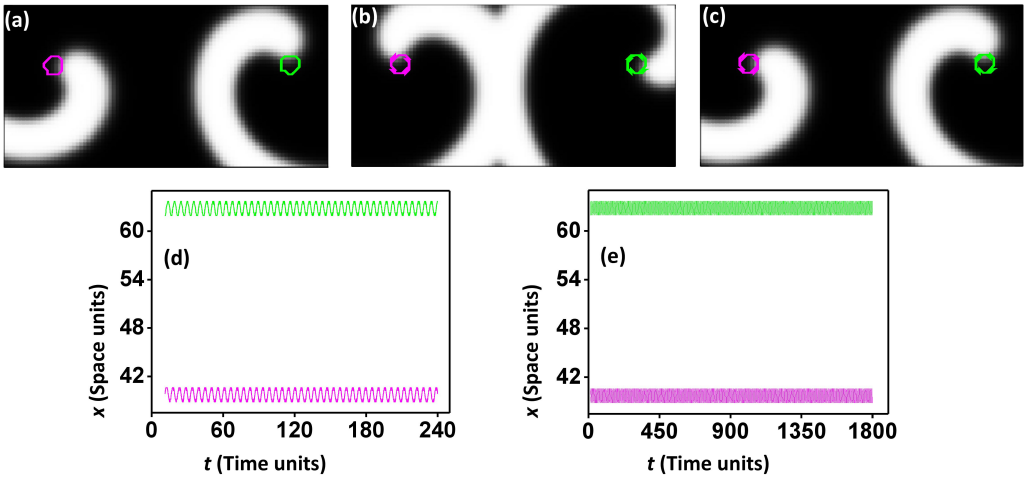

Figure 4.2: Spiral rotors at a separation ($l = 23.1$), fall in the no-interaction zone. Snapshots of spirals along with superimposed tip trajectories at $t =$ (a) 17.4, (b) 240, and (c) 1801 in normalized time units. The area of each snapshot is 31.5 × 15.75 space units. (d) and (e) are x-coordinate vs. time plots for the initial and later parts of the simulations, respectively.

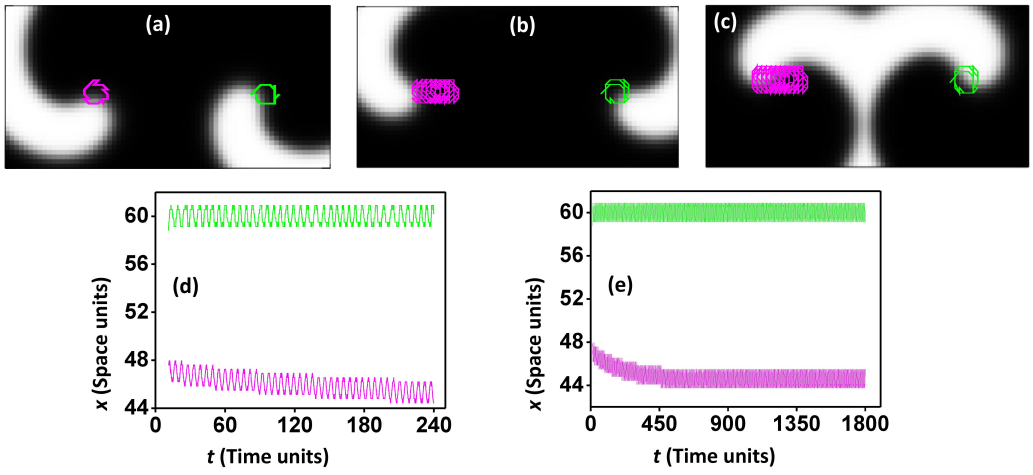

Figure 4.3: Spiral rotors at a separation ($l = 12.95$), fall in the repulsive zone. Snapshots of spirals along with superimposed tip trajectories at $t =$ (a) 15.36, (b) 240, and (c) 1800 in normalized time units. The area of each snapshot is 24.5 × 12.25 space units. (d) and (e) are x-coordinate vs. time plots till $t =$ (d) 240 and (e) 1800 time units, respectively.

Repulsion at the Range $11.9 \leq l \leq 18.2$

When $l \leq 18.2$, they interact with each other. For $7.7 \leq l \leq 18.2$, the interaction is repulsive. Figure 4.3 shows the same. Figures 4.3(a)−4.3(c) are the tip trajectories of the spiral tips till the respective time mentioned, along with the superimposed spiral snapshot at the respective time mentioned. There is a clear drift of the magenta spiral core, and the drift increases with time, whereas the green spiral core remains in the same position. The drift or repulsion can be explained by Figs. 4.3(d) and 4.3(e) as well. Figs. 4.3(d) and 4.3(e) are the x-coordinate vs. time plots of tip trajectories corresponding to Figs. 4.3(b) and 4.3(c), respectively. As the number of rotations is low in Fig. 4.3(b), oscillations can easily be seen in

Fig. 4.3(d). Fig. 4.3(c) has too many rotations, so they become very close and take the form of a band in Fig. 4.3(e). The x-range is the same for the green oscillations. The x-range for magenta oscillations shifts with time until 500 time units (as can be seen from Fig. 4.3(e)), and finally, they have come to a constant position. It means that the repulsion stops after 500 time units and at this stage, the separation becomes 15.5 space units.

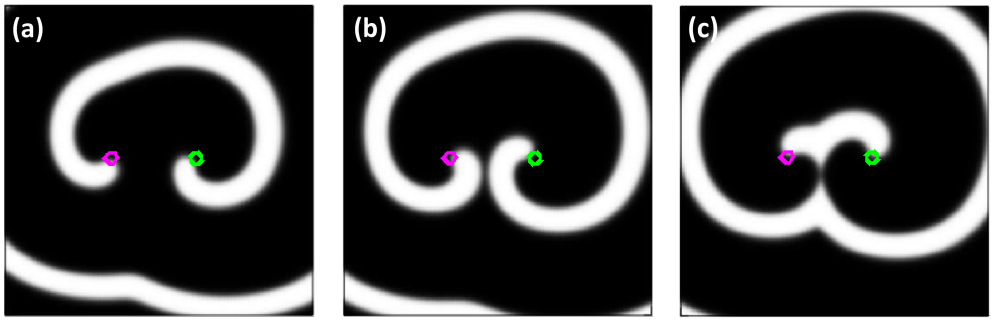

Figure 4.4: One spiral drifts for $l = 12.95$. Snapshots of spirals along with tip trajectories at $t =$ (a) 47.52, (b) 48.72, and (c) 49.92 in normalized time units. The area of each snapshot is 49×49 space units.

Here, one interesting thing to note is that only one spiral is getting repelled, and the other one remains in the same position. This is due to the fact that the spiral arm of the green spiral (spiral having a green tip trajectory), which is ahead, screens its own spiral from the magenta spiral arm. Hence, the green (right) spiral is less exposed to the magenta (left) spiral arm. The magenta spiral arm, on the other hand, cannot screen its own spiral from the green spiral arm. As can be seen from Fig. 4.4, the spiral arm generated by the green tip is approaching the magenta tip and finally hitting the tip. At each hit by the green spiral arm, the cyan spiral core gets shifted a little bit. This bit-by-bit shifting continues until the magenta spiral arm becomes exposed enough to screen its own spiral tip from the green spiral arm. At this particular distance, all interaction ceases.

Repulsion at the Range $7.7 \leq l \leq 11.9$

Figure 4.5 is another instance of repulsion where both tips are getting repelled. Figures 4.5(a)−4.5(c) show tip trajectories along with the superimposed spiral snapshot. It shows how both spiral cores are getting away from each other. Figures 4.5(d) and 4.5(e) are the x-coordinates vs. time plots corresponding to Figs. 4.5(b) and 4.5(c), respectively. Figure 4.5(d) depicts the initial oscillations, and Fig. 4.5(e) depicts oscillations for a long time till all interactions stop.

Phase angle resetting happens for phase angle mismatched spiral waves when their cores are within the interacting limit. When spiral cores are beyond the interacting distance ($l > d_c$), then the phase angle difference remains the same as in the very beginning, even after thousands of rotations. With decreasing l values, the rate of phase angle resetting increases. The phase angle reset happens in the direction of decreasing phase difference. In this case [Fig. 4.5], the phase angle difference decreases within a few rotations. So, here in Fig. 4.5, one of the spiral arms is not exposed enough to screen its own core, like in Fig. 4.3. That's why both spirals are drifting or being repelled. This repulsion continues till 500 time units and the separation becomes 15.12 space units at this stage.

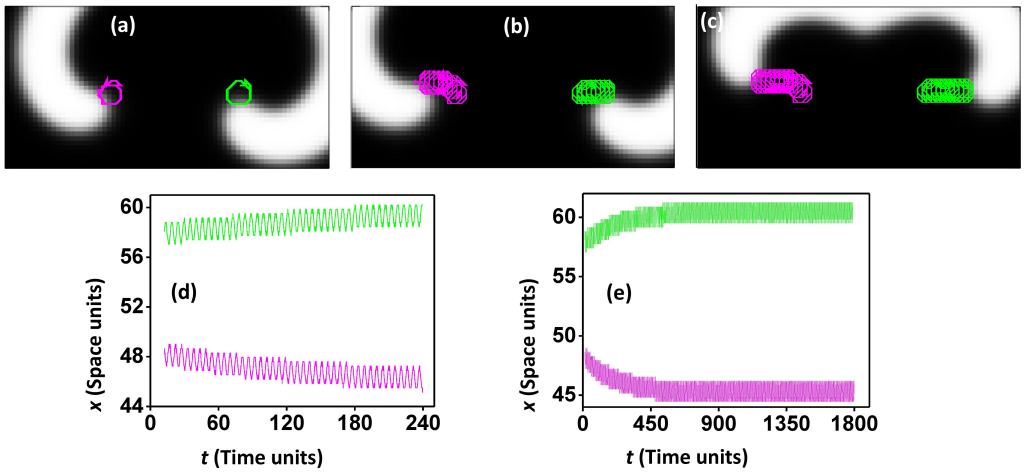

Figure 4.5: Spiral rotors at a separation (l = 9.8), fall in the repulsive zone. Snapshots of spirals along with tip trajectories at t = (a) 14.4, (b) 240, and (c) 1800 in normalized time units. The area of each snapshot is 24.5 × 12.25 space units. (d) and (e) are x-coordinate vs. time plots till t = (d) 240 and (e) 1800 time units, respectively.

Attraction

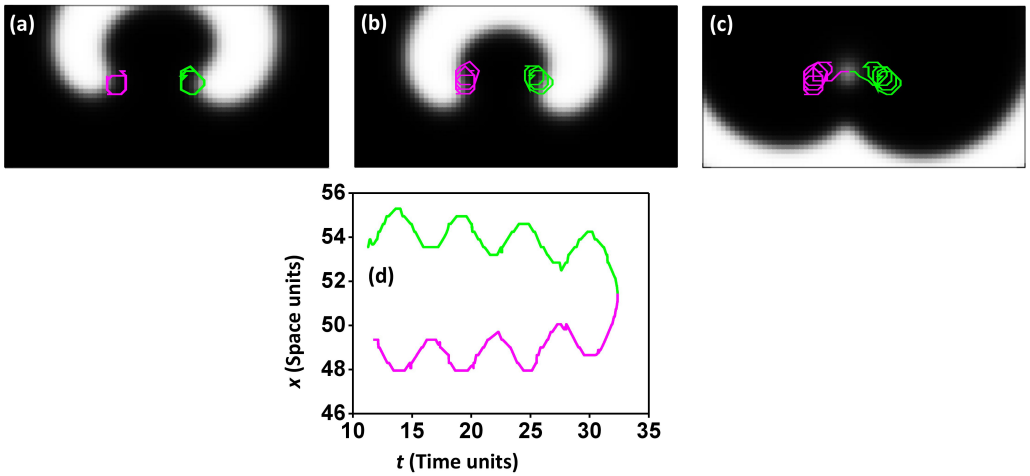

Figure 4.6: Spiral rotors at a separation (l = 5.6), which falls in the attractive zone. Snapshots of spirals along with the superimposed tip trajectories at t = (a) 13.44, (b) 24, and (c) 32.4 in normalized time units. The area of each snapshot is 24.5 × 12.25 space units. (d) is the x-coordinate vs. time plot till t = 32.4 time units.

When $l < 7.7$, they showed attraction. Like the previous figures, Figs. 4.6(a)−4.6(c) also shows the tip trajectories until the respective time mentioned, along with the superimposed spiral snapshot. As time progresses, the tips are getting closer to being annihilated. The x-coordinate vs. time plot in Fig. 4.6(d) depicts the spiral cores getting attracted to each other and finally joining.

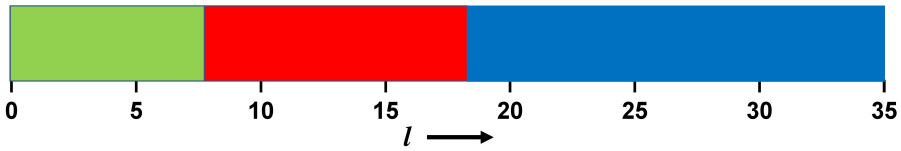

Figure 4.7: Phase Diagram for a pair of counterrotating spirals with a 90° phase angle difference.

Phase Diagram

Finally, we summarised our results into a one-dimensional phase diagram [Fig. 4.7]. The green area represents the attractive zone, the red area represents the repulsive zone, and the blue area represents the no-interaction zone. The critical distance (d_c), the distance at which all interaction ceases, for a 90°mismatched spiral pair is 18.2. It's higher than for two counterrotating pairs with a zero phase angle difference, where d_c = 16.4, and they also follow the law $d_c = \lambda$ - d_s. In this particular case, this law doesn't hold, i.e., $d_c \neq \lambda$ - d_s. The point where attractive potential becomes repulsive is 7.7. It's also not following the half-critical distance rule. The half-critical distance rule says that for a pair of spiral waves placed along l, i.e., the y-coordinates of the spiral tips are the same for a few initial rotations with the same phase angle, and the value at which the attractive potential becomes repulsive is exactly half the critical distance (d_c).

4.3.2 A Pair of Counterrotating Spirals with 45° Phase Angle Difference

Figure 4.8(a) shows a pair of counterrotating spiral waves with a phase angle mismatch of 45°. When $l < 7.35$, they show attractive interaction. Figure 4.8 (b) shows an instance of annihilation. At the beginning of the simulation, they were l = 7 space units apart. With time, as can be seen from Fig. 4.8(b), the spiral waves (cores) are gradually approaching each other in every rotation, and finally, they annihilate at t = 97.44 time units. This can also be understood from the x-coordinate vs. time plot [Fig. 4.8(f)], which corresponds to Fig. 4.8(b). With time, the tips approach each other, and finally, they join. When $7.35 \leq l \leq 17.85$, they show repulsion. Figs. 4.8(c) and 4.8(g) show such an instance where both tips are drifting. Initially, they were placed at l = 9.45 space units separation. As this separation comes under the repulsive zone, they start pushing each other away. The pushing continues until the separation is good enough for each spiral arm to screen its individual spiral cores. When $12.6 \leq l \leq 17.85$, we see only one spiral drift [Figs. 4.8(d) and 4.8(h)]. Here, l = 12.95 space units. The reason behind only one spiral drift is already explained in Fig. 4.4. When $l > 17.85$, the spiral arms get enough space to screen their individual cores. Hence, all interaction ceases after l = 17.85 space units. Figures 4.8(e) and 4.8(i) show the same for l = 22.75 space units. Figure 4.8(j) is the phase diagram for this particular case. The green area represents attraction, and the red area represents repulsion, which starts at 7.35 and continues until 17.85. After 17.85, all interaction vanishes (the blue area).

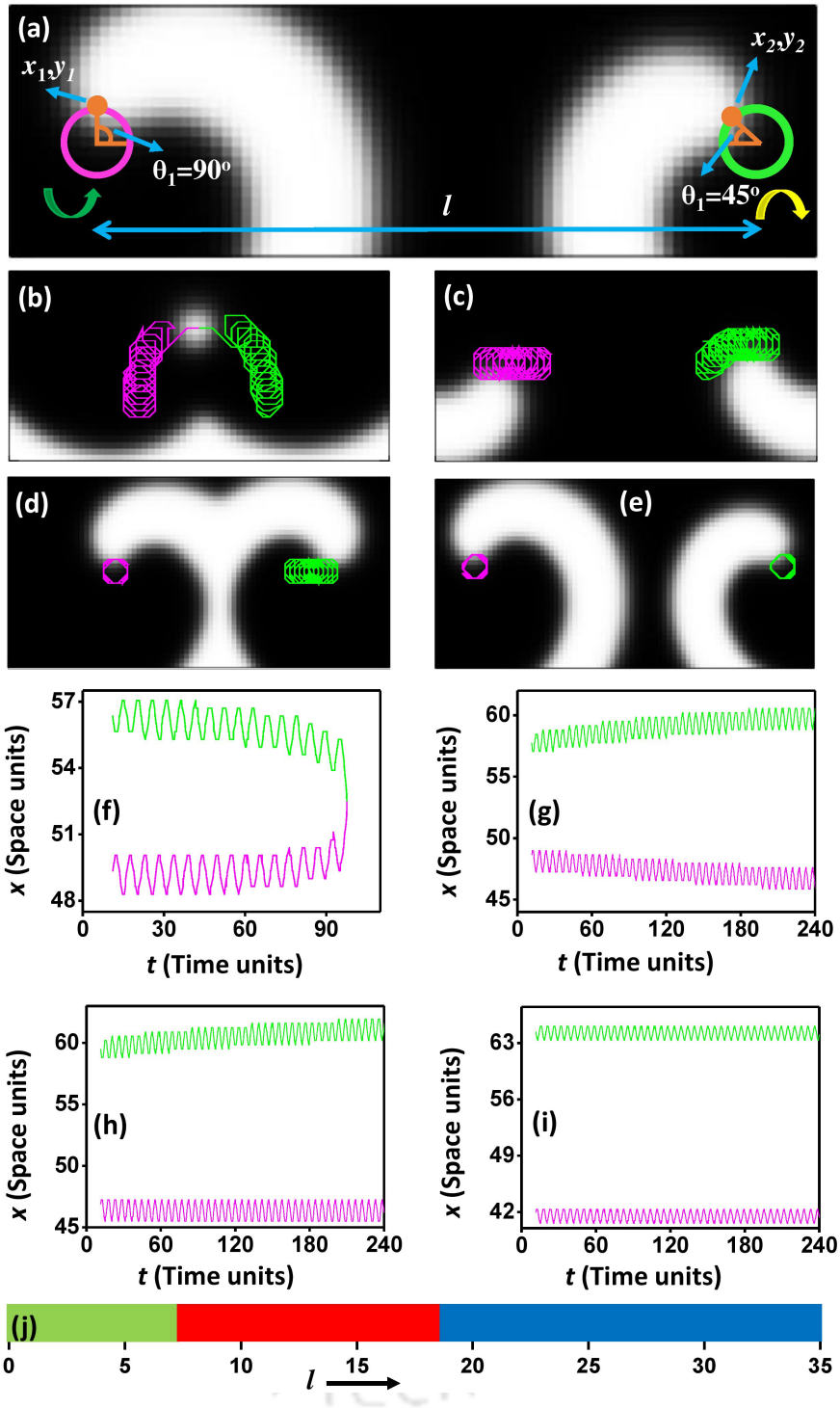

Figure 4.8: (a) Snapshot of two counter-rotating spiral waves having a phase angle difference of 45° with the superimposed tip trajectory of the very first rotation (Magenta and green circles) along with the parameters of the numerical experiment (position, angle, and distance). (b) Annihilation for $l = 7$; (c) Repulsion for $l = 9.45$; (d) One spiral drift/repulsion for $l = 12.95$; (e) No-interaction for $l = 22.75$. (f), (g), (h), and (i) are x-coordinate vs. time plots corresponding to (b), (c), (d), and (e), respectively. (j) Phase diagram.

4.3.3 A Pair of Counterrotating Spirals with 135° Phase Angle Difference

Figure 4.9 shows a pair of counterrotating spirals having a phase angle mismatch of 135°. With a higher phase angle difference, we don't get any kind of attractive

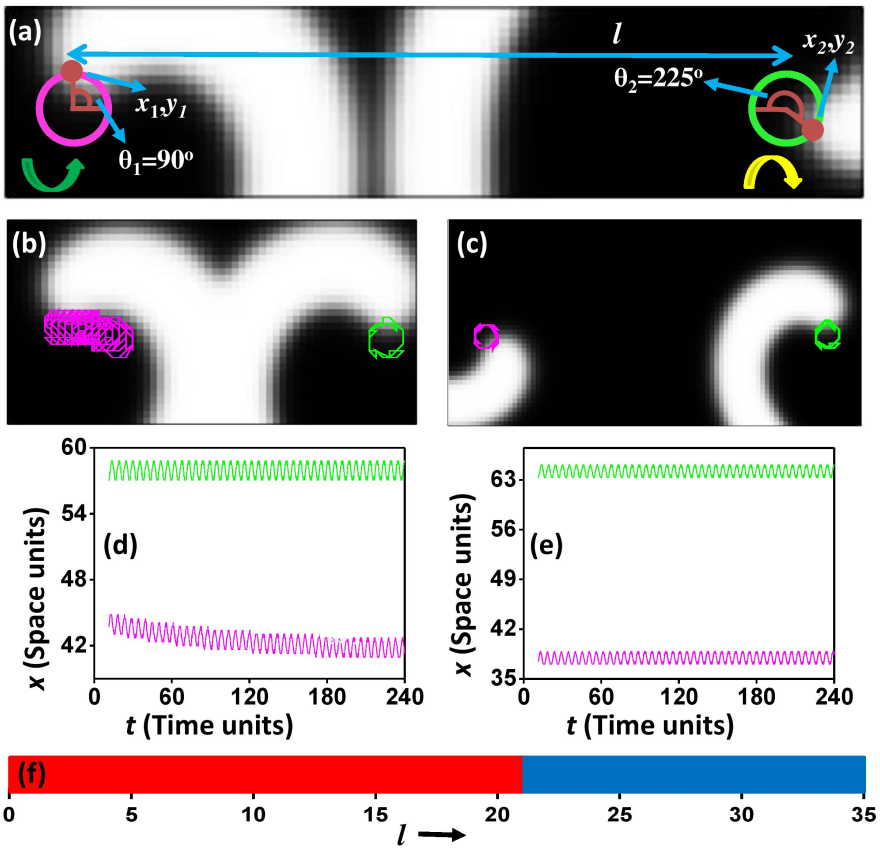

Figure 4.9: (a) Snapshot of two spiral waves having a phase angle difference of 135° with the superimposed tip trajectory of the very first rotation (Magenta and green circles) along with the parameters of the numerical experiment (position, angle, and distance). (b) One spiral drift or repulsion for $l = 14$, (c) No-interaction for $l = 26.25$. (d) and (e) are x-coordinate vs. time plots for (b) and (c), respectively. (f) Phase diagram.

interaction. This is due to the fact that one spiral arm remains much ahead of the other spiral arm. In other words, one spiral arm, the one that is ahead, reaches relatively closer to the other spiral core. This advanced spiral arm can easily screen its own spiral core. So, there is no possibility of attraction. But this advanced arm, if within the interacting distance (critical distance, d_c), can repel the other spiral core. Within critical distance (d_c), the lagging spiral arm, the one that is relatively far from the other spiral core, won't get time to shield its own spiral core. Figures 4.9(b) and 4.9(d) demonstrate such an instance of repulsion where one spiral core is getting drifted by the other spiral arm. When the two cores are separated by the critical distance (d_c), they show no interaction [Figs. 4.9(c) and 4.9(e)]. They keep rotating within the same circular core. Figure 4.9(f) is the phase diagram for this particular case where, within critical distance (d_c), we see one spiral drift (repulsion). The critical distance (d_c) here is 21 space units.

4.3.4 A Pair of Counterrotating Spirals with 180° Phase Angle Difference

Figure 4.10(a) shows a snapshot of a counterrotating spiral pair having a phase angle mismatch of 180°. As in Fig. 4.9 (135° case), we see only repulsive interac-

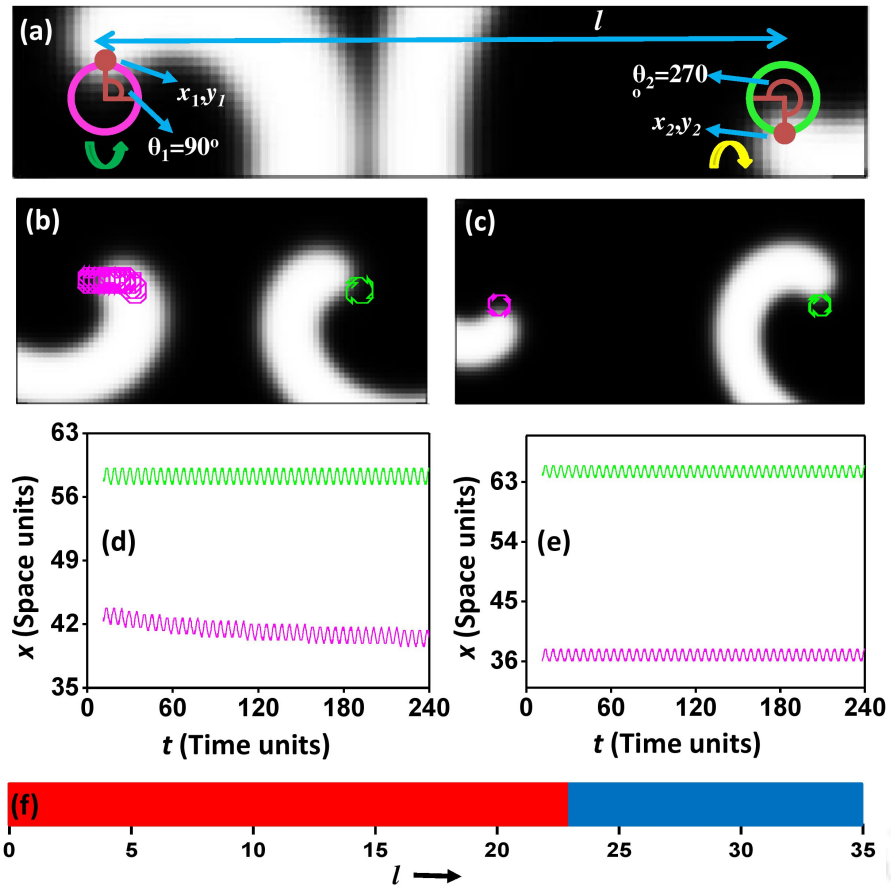

Figure 4.10: (a) Snapshot of two spiral waves having a phase angle difference of 180° with the superimposed tip trajectory of the very first rotation (Magenta and green circles) along with the parameters of the numerical experiment (position, angle, and distance). (b) One spiral drift or repulsion for $l = 15.4$; (c) No-interaction for $l = 27.65$. (d) and (e) are x-coordinate vs. time plots corresponding to (b) and (c), respectively. (f) Phase diagram.

tion here, where one spiral gets drifted and the other spiral remains in its initial position [Figs. 4.10(b) and 4.10(d)]. At critical distances and beyond, all interaction ceases [Figs. 4.10(c) and 4.10(e)]. Figure 4.10(f) shows the phase diagram for this particular case, where we see one spiral drift till $l = 22.75$ space units, and after that, they enter the no-interaction zone.

4.3.5 A Pair of Corotating Spirals with 90° Phase Angle Difference

For a pair of corotating spiral waves, we don't get any kind of attractive interaction. Within critical distance (d_c), we get only repulsive interaction. The sense of rotation of the right spiral has been changed to make both of them anticlockwise. Figure 4.11 is a typical example of a numerical experiment with two corotating spiral pairs with an initial phase difference of 90°. As can be seen from Fig. 4.11(a), one spiral arm remains much ahead (the left spiral arm). This spiral arm can easily screen its own spiral core. On the other hand, the other spiral arm (the right arm) is not advanced enough to save its own core, which gets drifted by the advanced arm. The parameters assigned here are the same as before. If $l \leq$

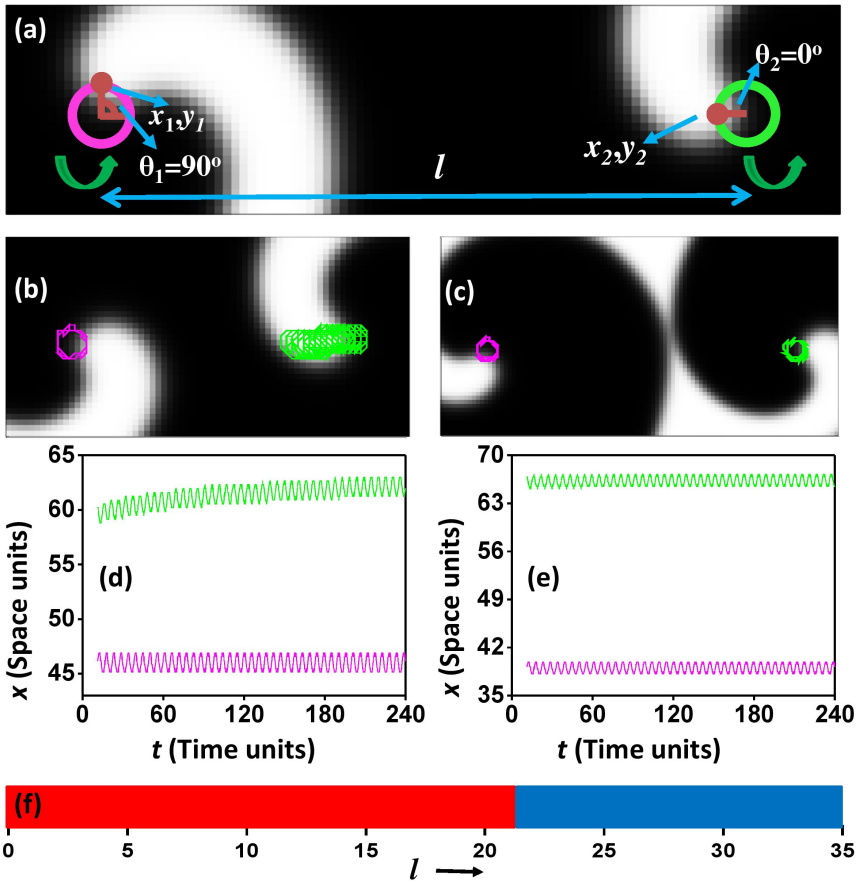

Figure 4.11: (a) Snapshot of two corotating spiral waves having a phase angle difference of 90°with the superimposed tip trajectory of the very first rotation (Magenta and green circles) along with the parameters of the numerical experiment (position, angle, and distance). (b) One spiral drift or repulsion for l = 13.65; (c) No-interaction for l = 27.3. (d) and (e) are x-coordinate vs. time plots corresponding to (b) and (c), respectively. (f) Phase diagram.

21.0, the zone becomes repulsive [Fig. 4.11(b) and 4.11(d)], and if $l > 21.0$, the zone becomes non-interacting [Fig. 4.11(c) and 4.11(e)]. The phase diagram [Fig. 4.11(f)] explains the same.

4.3.6 Corotating Spiral Pairs with 45°, 135° and 180° Phase Angle Difference

As explained previously, we don't get any kind of attractive interaction between the two co-rotating spiral pair cases for any phase angle difference. The critical distances (d_c) for 45°, 135°, and 180° are 22.75 space units, 19.25 space units, and 17.5 space units, respectively.

4.4 Phase Angle Difference vs. Critical Distance (d_c)

For two counter-rotating spirals, with an increase in phase angle difference, the distance at which they can interact (d_c) increases [Fig. 4.12(a)]. This is due to

the fact that with an increase in phase angle difference, one spiral arm becomes more advanced and closer to the other spiral core. On the other hand, for two corotating spirals, the critical distance (d_c) decreases with an increase in phase angle difference [Fig. 4.12(b)]. For two corotating spirals, one spiral arm will always remain ahead compared to the other spiral arm (the left spiral in Fig. 4.11(a)). That advanced spiral can easily screen its own core from the other spiral arm. That's why this spiral always remains unaffected. The advancement of the other spiral arm increases with an increase in phase angle difference, which in turn increases its screening capacity. Hence, the critical distance (d_c) decreases with an increase in phase angle difference for two corotating spirals.

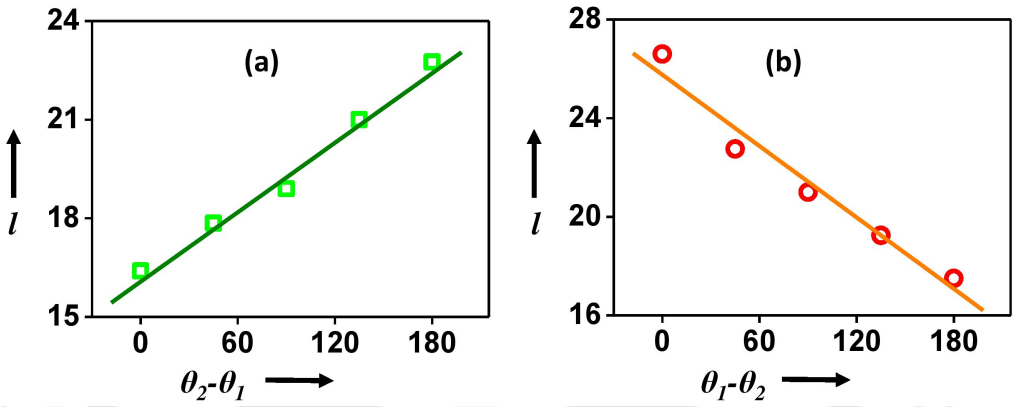

Figure 4.12: Variation of critical distance (d_c) with increasing phase angle difference. (a) For counterrotating pairs; (b) For corotating pairs.

4.5 Discussion

We have carried out a detailed analysis of the interaction of two spiral waves, both corotating, and counterrotating, by varying the initial conditions. In our recent study, we showed that for two symmetrically placed (θ_2 - θ_1 = 0) counterrotating spirals, the distance within which the spirals interact, i.e., the critical distance, is $d_c = \lambda$ - d_s, where λ = wavelength and d_s = core diameter [14]. The distance where the nature of interaction changes (from attractive to repulsive) is exactly half the critical distance (d_c) [14]. When there is an initial phase angle mismatch between the spirals, they no longer follow this rule, i.e., $d_c \neq \lambda$ - d_s, and the distance at which attractive potential becomes repulsive is not equal to half the critical distance ($\neq d_c/2$).

In the existing literature, the interactive behavior was mainly shown as a function of the distance separating the spirals and system parameters [1, 2, 3, 14]. Here, our study mainly focuses on the dependence of interacting behavior as a function of (i) the sense of rotation and (ii) the initial phase angle difference. We established both attractive and repulsive interactions for counterrotating spirals having a low phase angle difference at the time of initiation when they are within the critical distance (d_c). Only repulsive interaction was found for corotating spirals and counterrotating spirals having a high phase angle difference at the time of initiation when present within the critical distance (d_c).

Existing studies show the symmetry-breaking dynamics in a spiral pair can lead to the formation of states with one dominant spiral [4, 10]. One spiral acts as a

forcing wave, causing the drift of the other spiral toward the boundary [4, 8, 10]. We, too, have found one spiral drift where one spiral, the dominant one, expels the other wave, but this drift continues until the characteristic critical distance (d_c) of that particular pair. Symmetry breaking in spirals is a common phenomenon, but there are instances where symmetry is maintained throughout. In our system, we have started from an asymmetric state (mismatched phase angle). There are instances, especially in the repulsive regime of corotating spiral waves and counterrotating spirals with high phase angle differences, where this asymmetry blows up, and we get extreme cases like one spiral drift. We have also found symmetric states in the attractive regime of counterrotating spirals, where phase resetting from an initial asymmetric state leads to such symmetry.

4.6 Conclusion

In conclusion, we can say that we have established the dependence of critical distance (d_c) on the sense of rotation of spiral waves and the initial phase angle difference between two spirals in a pair. For two counterrotating spirals, the distance to which they can interact increases with an increase in phase angle difference. At higher phase angle differences, two such counterrotating spirals don't show any kind of attractive interaction, i.e., within critical distance (d_c), they show only repulsion. For two corotating spirals, the distance to which they can interact decreases with an increase in phase angle difference. Corotating spirals show only repulsive interaction within the interacting zone ($l < d_c$). A complete asymmetric state, like one spiral drift, was seen in the repulsive regime of corotating spiral waves and counterrotating spiral waves with higher phase angle differences. Counterrotating spirals with a low phase angle difference also show one spiral drift at the extreme right of the repulsive regime, i.e., at a higher l value of the repulsive regime. Symmetric annihilating states were also found in the attractive regime of the counterrotating spiral waves.

In the future, it will be interesting to see how interactive behavior and symmetry are affected by increasing the number of rotors. A number of combinations of clockwise and anticlockwise rotors having different initial phase angles can be studied. One more interesting thing to explore is how system parameters like excitability affect the dynamics of our current system. Throughout our simulations, we have observed phase resetting. It will be worth exploring if such phase-resetting dynamics lead to synchronization and chimera in the case of three or more rotor systems with different initial phases.

Bibliography

[1] I. S. Aranson, L. Kramer, and A. Weber, Physica D **53**, 376 (1991)

[2] E. A. Ermakova, A. M. Pertsov, and E. E. Shnol, Physica D **40**, 185 (1989).

[3] I. S. Aranson, L. Kramer, and A. Weber, Phys. Rev. Lett. **67**, 404 (1991).

[4] M. Ruiz-Villarreal, M. Gómez-Gesteira, C. Souto, A. P. Muñuzuri, and V. Pérez-Villar, Phys. Rev. E **54**, 2999 (1996).

[5] O. Steinbock and S.C. Müller, Int. J. Bifurcation Chaos Appl. Sci. Eng. **3**, 437 (1993).

[6] K. Agladze, Chaos **6**, 328 (1996).

[7] J. Schütze, O. Steinbock, and S. C. Müller, Nature **356**, 45 (1992).

[8] I. Aranson, H. Levine, and L. Tsimring, Phys. Rev. Lett. **76**, 1170 (1996).

[9] I. S. Aranson, L. Kramer, and A. Weber, Phys. Rev. E **47**, 3231 (1993).

[10] I. S. Aranson, L. Kramer, and A. Weber, Phys. Rev. E **48**, R9 (1993).

[11] R. M. Zaritski and A. M. Pertsov, Phys. Rev. E **66**, 066120 (2002)

[12] B. Vasiev, F. Siegert, and C. Weijer, Phys. Rev. Lett. **78**, 2489 (1997).

[13] K. I. Agladze and V. I. Krinsky, Nature **296**, 424 (1982).

[14] H. Kalita and S. Dutta, Phys. Rev. E **105**, 054213 (2022).

[15] D. Barkley, M. Kness, and L. S. Tuckerman, Phys. Rev. A **42**, 2489 (1990).

[16] D. Barkley, Physica D **49**, 61 (1991).

Chapter 5

Rotational Synchronization of Pinned Spiral Waves

5.1 Introduction

The footprints of synchronization are often found in nature, like in the flashing of fireflies and the chirping of crickets. They are also encountered across other diverse systems, such as pendulums, clocks, lasers, and applauding audiences [1]. From population dynamics [2] to the firing of neuronal cells [3], the rhythmic nature of oscillators dictates the dynamical behavior of the system. Spontaneous synchronization is also encountered in spatially distributed oscillators in biological systems, such as the rhythmic electrochemical waves in the heart [4] or the glycolytic oscillations in suspensions of yeast cells [5]. Examples of chemical systems exhibiting synchrony are the mercury beating heart [6] and rhythmic oscillations of catalytic particles in the Belousov-Zhabotinsky (BZ) reaction [7]. The behavior of these coupled chemical and biological oscillators found a mathematical description in the seminal work of Kuramoto [8]. His model was later extended to the study of various nonidentical coupled oscillators, irrespective of the origin of the system, like Josephson junctions [9], which are superconducting rotator arrays. Ensembles of rotors coupled electrically, mechanically, optomechanically, chemically, or biologically have been widely investigated [1, 10, 11, 12, 13]. These theoretical as well as experimental studies have revealed a wide range of rotational behavior, such as in-phase and antiphase locking [9, 14], amplitude death [15], lag synchronization [13], cluster formation [12], and chimera states [16].

In order to study the rotational synchronization of spirals, it is helpful to arrest the translational motion of the spiral cores. Spiral waves are known to anchor to inexcitable heterogeneities in a process called pinning [17]. In cardiac tissues, a rotor can attach itself to a discontinuity like scar tissue, resulting in stationary rotating activity [18]. Several studies on the pinning of spiral rotors to different geometries of obstacles have been carried out [19, 20, 21]. Pinning modifies the frequency of the rotor by elongating its rotation period [22]. However, the innate nature of the spiral as a rotor remains unperturbed during the process. We propose to look at the interaction of two rigidly rotating spirals anchored to circular disks. By varying the size of the disk, we are able to control the frequency of our rotors, enabling us to study both the frequency and phase synchronization of the spiral waves. A recent numerical study explored the asymmetric interaction of arrays of pinned spiral oscillators rotating with the same frequency [23].

Here we explore the synchronization of two counterrotating pinned spiral waves,

both experimentally and numerically. We carry out experiments in the BZ reaction using unexcitable circular heterogeneities of varying sizes as pinning anchors. We begin by exploring the interaction of two identical oscillators, where we find complete synchronization in frequency and phase. By changing the size of one heterogeneity, we are able to initiate two rotors with different characteristic frequencies. We then vary the distance between the two spirals and explore the changing nature of synchronization between the rotors. Numerical simulations based on a generic reaction-diffusion model are also carried out. These studies corroborate our experimental results while providing additional insights into the subtle dynamics of the rotational motion of these reentrant excitation waves.

5.2 Experimental Methods

Our BZ system consists of a solution of $0.16M$ sulfuric acid, $0.04M$ sodium bromate, $0.04M$ malonic acid, and $0.001M$ ferroin embedded in a 0.8 wt./vol % agar gel matrix. The solutions are prepared with Millipore water. All experiments are carried out in Petri dishes of 6 cm diameter at room temperature (23 $\pm$ 1 °C). The thickness of the reaction gel is maintained at around 2 mm. A plane wave is initiated in the center of the circular dish, far from the system boundaries, by inserting the tip of a silver wire into the reaction mixture for a few seconds. When the circular wave reaches the desired dimension, we cleave it with the help of a thin glass slide. The free ends of the wave now curl in to form a pair of counterrotating spiral waves. Subsequently, a chemically inert rubber cylinder, with a height equal to the thickness of the reaction layer, is placed near each tip of the spiral. The system is illuminated from below with a diffused, cold white light source and is observed by a charge-coupled device camera (mvBlueFOX 220a) mounted over it. A blue dichroic filter is used on the camera for better imaging. The images are recorded on a personal computer every 2 seconds and are later analyzed by using interactive, in-house MATLAB codes. The spiral tip position is recognized as the point of highest curvature touching the unexcitable disk (shown in Fig. 1).

5.3 Experimental Results

Figure 5.1(a) shows a snapshot of a typical experiment. The two tips of the spiral are anchored to two different-sized rubber disks of diameters d_1 and d_2. A magnified version of the area around the heterogeneities is shown in Fig. 5.1(b). The tips of the two spirals are located at (x_1, y_1) and (x_2, y_2), respectively, both measured in relation to the individual centers of the i^{th} disk, with (x_{ci}, y_{ci}) considered the origin. The distance between the centers of the circular beads is called l. The phase angles of each spiral tip with respect to the line joining the centers are denoted by θ_1 and θ_2, respectively. The motion of the pinned spiral rotor can be monitored by noting the position of the spiral tip (x_i, y_i) at any given time. The phase angle can be calculated as:

$$\theta = \tan^{-1}\left(\frac{y_i}{x_i}\right) \tag{5.1}$$

Various experiments are carried out by changing the size of the cylinders and the distance separating them. We chose typical disk sizes of 1.8, 2.7, and 3.6 mm. It is known that a spiral anchored to an unexcitable heterogeneity moves

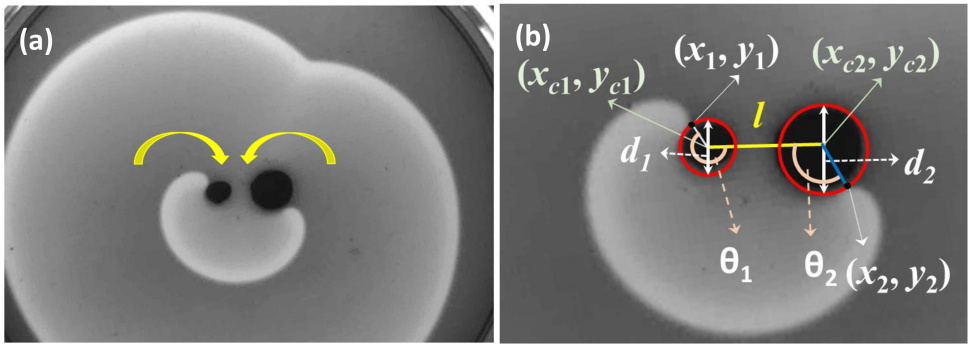

Figure 5.1: Experiments to study the synchronization of two pinned spiral waves. (a) Snapshot of a typical experiment with two differently sized disks. The area of the snapshot is 30.7×30.7 mm^2. (b) Magnified central area of (a), showing the pinned rotors and defining the parameters of the experiment (position, angle, and distance) described in the text.

slower than a free spiral [22]. When pinned to a cylindrical disk, the spiral core is determined by the circular perimeter of the disk, around which it rotates. Hence, the larger the disk, the slower the frequency of rotation. The time period of a free spiral (obtained with the current chemical recipe) is 10.1 min, its core diameter is 1.09 mm, and its wavelength is 9.94 mm [24]. The time periods for the pinned spiral rotors have been calculated for systems where the two spiral tips are pinned to identical obstacles (circular disks with the same diameter). For $d_1 = d_2 = 1.8$, 2.7, and 3.6 mm, the time periods are approximately $T = 12.0$, 18.0, and 24.0 min, respectively.

5.3.1 Complete Synchronization

An experiment using two identical disks is shown in Figs. 5.2(a)−5.2(d). Here, both disks have diameters of 1.8 mm. The plots of x_i and y_i versus time are shown in Figs. 5.2(a) and 5.2(b), respectively. The two counterrotating spirals are placed side by side. Hence, if the initial phases of the two spirals are the same (i.e., $\theta_1 = \theta_2$ at $t = 0$), then the y-coordinates of the tips will increase and decrease simultaneously, while the two x-coordinates will have an opposing trend. The same is also observed in the phase plots shown in Figs. 5.2(c) and 5.2(d). This is an example of complete synchronization (in frequency and phase) between two counterrotating spirals. The y positions will be in-phase synchronized and the x positions out-of-phase synchronized. This is also called mirror synchronization [25] or mixed synchronization [15]. Since we maintain similar initial conditions in all our experiments and simulations, we compare only the y positions in all subsequent figures.

5.3.2 Lag Synchronization

Figure 5.3 shows an example of synchronization between two spiral rotors initially having different frequencies. The two spiral tips are pinned to disks of diameters $d_1 = 1.8$ mm and $d_2 = 2.7$ mm, with $l = 12.15$ mm. For the sake of convenience, henceforth, we refer to the smaller obstacle as d_1 and the larger obstacle as d_2. Initially, the spiral pinned to the smaller disk [black curve in Fig. 5.3(b)] rotates

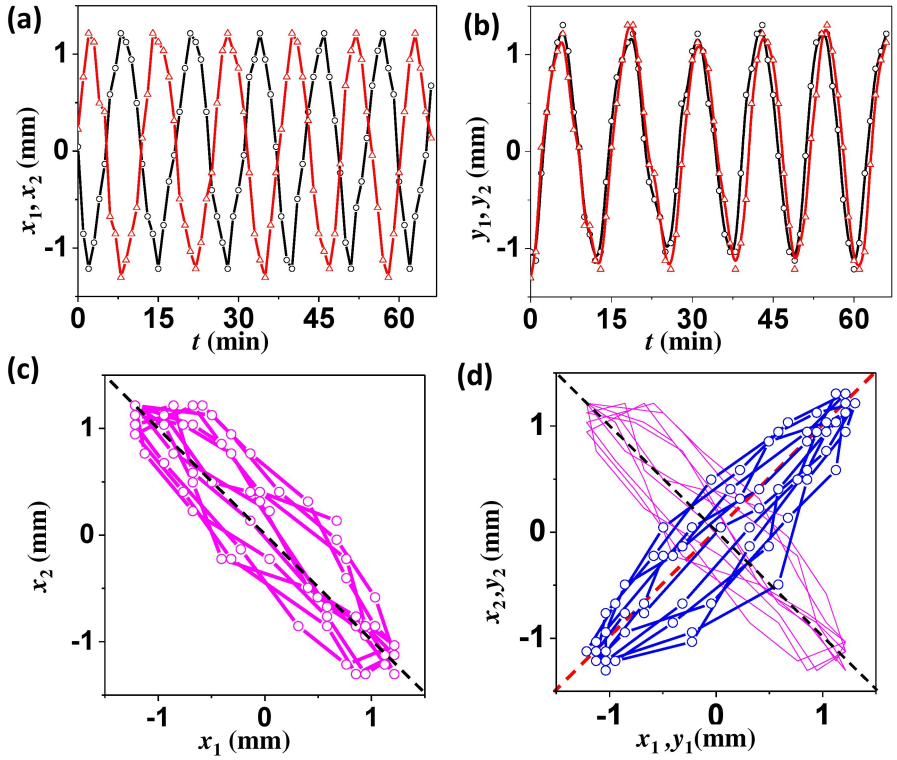

Figure 5.2: Synchronization of two spiral rotors pinned to identical circular disks of diameters $d_1 = d_2 = 1.8$ mm and separated by a distance of $l = 4.68$ mm. The time evolutions of the (a) x and (b) y positional coordinates of rotors 1 (black circles) and 2 (red triangles) are shown. (c) Phase portrait of the x positions of the two rotors, with a black dashed line of slope -1. (d) Plot of y_1 versus y_2 (thick blue line with circles) showing in-phase synchronization. The corresponding x plot has been added in the background (in magenta) to show the emergence of mirror synchrony. The black and red dashed lines in (d) have slopes of -1 and +1, respectively.

faster than the other rotor ($T_1 = 12$ min and $T_2 = 18$ min). A plot of the phase angle with time is depicted in Fig. 5.3(c). It shows the incoherence in the rotational phase during the initial stages of oscillations. After several periods, it is observed that the two spirals rotate with the same frequency ($T = 12$ min). This is evident from the time plot of the y-coordinate [Fig. 5.3(f)]. However, here the two rotors do not synchronize completely in phase, but they have a slight lag. This is unlike the case of identical oscillators. The excitation wave emitted by a spiral rotor annihilates on touching another wave from a different spiral or target source. When both oscillators have an equal frequency, the wave arms emitted by them meet midway between the two rotors (at $l/2$) when they are initiated with almost the same phase. In the case of an initial mismatch of spiral frequencies, the waves emanating from the faster rotor (obstacle 1) gain over the slower one (obstacle 2). As it slowly invades the space of the second rotor, it accelerates it. Finally, when the waves from the smaller obstacle touch the larger obstacle, it generates a faster second rotor. So, the frequency of rotor 2 is modified to match that of rotor 1. In this experiment, the time required for synchronization is around 58 min.

The phase diagram (y_1 versus y_2) of the two oscillators in the early part of the experiment fills the whole region [Fig. 5.3(d)]. This is expected due to the lack of frequency synchronization between the two rotors. In the later part of the

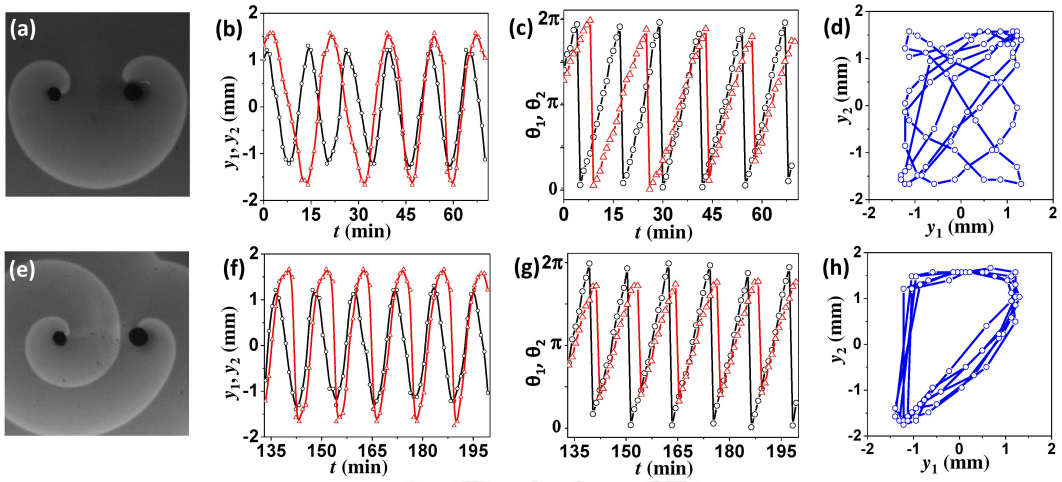

Figure 5.3: Synchronization of two rotors having different initial frequencies. Here d_1 = 1.8 mm, d_2 = 2.7 mm, and l = 12.15 mm. Snapshot of the experiment at (a) t= 8 mins and (b) t= 154 mins. The area of each snapshot is 3.3×3.3 cm^2. Data from (a)−(d) the initial stage of the experiment and (e)−(h) the post-synchronization stage are depicted. (b) and (f): Time evolution of the y positions of the two rotors; (c) and (g): Plots of phase angles θ_1 and θ_2 versus time, (d) and (h): Phase portraits of the y-coordinates. Black curves with circles are for the smaller rotor (rotor 1), and red curves with triangles are for the larger rotor (rotor 2) in (b), (c), (f), and (g). This coloring scheme is maintained throughout the paper for the time evolution of position (y_i) and angle (θ_i) coordinates.

experiment, we get a closed curve known as a Lissajous figure, which is a signature of frequency synchronization. However, the curve has a flat area around y_1 = -1.3 mm [Fig. 5.3(h)]. A close look at the position plot [Fig. 5.3(f)] will reveal a jump of oscillator 2 from $y_2 > 1.3$ to values of $y_2 <$ -1.3 within two data points, recorded 1 min apart. This happens due to a phase resetting that occurs when the paths of the two oscillators cross. This interesting phenomenon is explained in more detail in Fig. 5.4. A close inspection of Fig. 5.3(c) shows a decreasing trend in the maximum value of θ_2 (red triangles). Upon synchronization, it can be observed that the phase angle of the larger rotor oscillates between 0.6π and 1.7π. This is also a manifestation of the phase resetting of the slower rotor by the faster one.

5.3.3 Phase Jump

Figure 5.4 shows the wave-resetting dynamics around two rotors that differ more drastically in size (d_1 = 1.8 mm and d_2 = 3.6 mm). Four snapshots have been chosen at intervals of 3.2 min each after synchronization has been reached. Once their frequencies have synchronized, the time required for the wave to complete one rotation around the larger obstacle has to match the time required to circulate around the smaller disk. As soon as the wave arm of the faster rotor touches the other heterogeneity, the phase angle of the latter is reset.

Here it is important to note the chirality of the two rotors. The larger rotor around d_2 rotates in an anticlockwise fashion and has negative chirality, while the smaller rotor around d_1 rotates in a clockwise manner and can be said to have positive chirality [Fig. 5.4(a)]. As the spiral tips, now having the same speed, rotate around their individual pinning sites, the spiral around d_2 does not

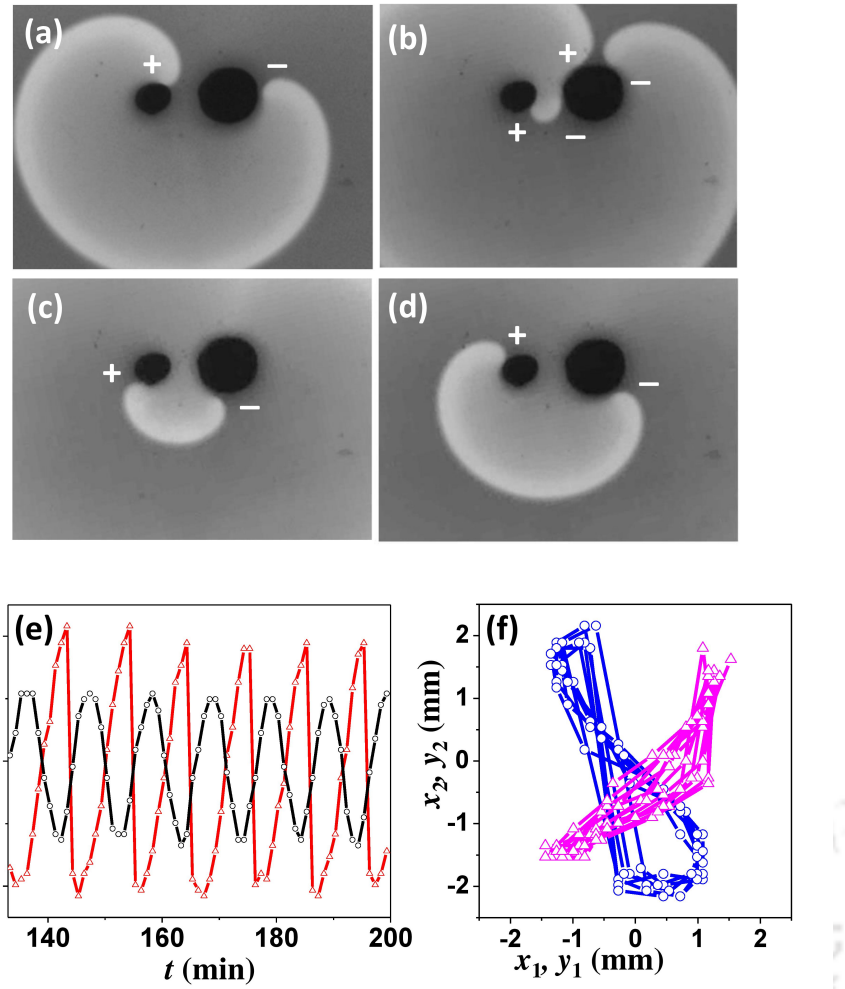

Figure 5.4: Experiment depicting phase resetting during synchronization. The two rotors are pinned to unexcitable disks of diameters $d_1 = 1.8$ mm and $d_2 = 3.6$ mm and placed at a distance of $l = 4.86$ mm from each other. (a)−(d): Wave dynamics during phase resetting of the slower rotor (right) by the faster one. Snapshots were taken at (a) 114.8, (b) 118, (c) 121.2, and (d) 124.4 min after the introduction of the pinning obstacles. The area of each snapshot is 23×17 mm^2. (e) Plots of the y position as a function of time at a later stage of the experiment. (f) Phase plots of x_i (magenta triangles) and y_i (blue circles) show mixed synchronization.

make a full round before the expanding wave from the first rotor touches the larger heterogeneity. The heterogeneity splits the wave, initiating a pair of spirals having opposite chirality on the second (larger) obstacle, both moving in opposite directions [Fig. 5.4(b)]. The newly formed positive spiral moves towards the original negative spiral on the obstacle, finally colliding with it and annihilating each other [Fig. 5.4(c)]. Its negative counterpart remains on the obstacle and continues its rotation until it comes across a newly formed positive spiral from the next colliding wave. So, for a very short time, there are actually three spiral tips on the larger obstacle [Fig. 5.4(b)].

The y-coordinate plot for the two spiral rotors during the later stages of the experiment, after synchronization has been reached, is shown in Fig. 5.4(e). The value of y_2 plunges from its maximum to its minimum. These two positions correspond to the spiral tip at the top and bottom of disk 2, at times close to those in

Figs. 5.4(b) and 5.4(c), respectively. Due to this sudden resetting of the phase of rotor 2 and its larger size, the two oscillators seemingly synchronize in an out-of-phase manner [Fig. 5.4(e)]. The phase portraits of x and y also support this idea [Fig. 5.4(f)]. The x and y plots still have opposing slopes, pointing towards mixed synchronization. However, they can no longer be said to be mirror synchronized, as the two rotors are no longer identical, and this is reflected in the difference between the x- and y- phase portraits, unlike what was seen in Fig. 5.2. Here the x plot is in-phase locked, while the y plot is out-of-phase locked [Fig. 5.4(f)]. This can be considered an example of the interchange of rotational synchronization.

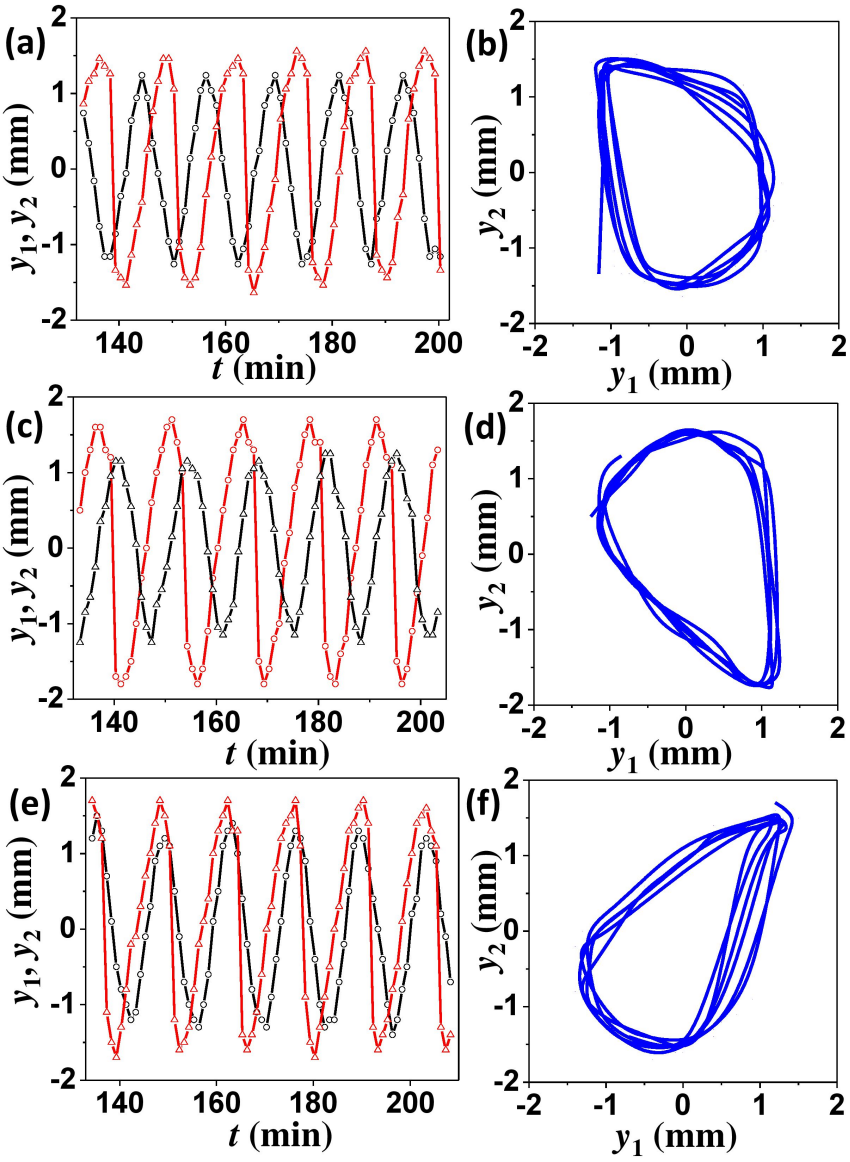

Figure 5.5: Varying nature of synchronization with increasing inter-pin distance. Experiments with $d_1 = 1.8$ mm and $d_2 = 2.7$ mm are shown for (a) and (b) $l = 4.4$ mm, (c) and (d) $l = 8.15$ mm, and (e) and (f) $l = 10.7$ mm. (a), (c), and (e): Plots of the position coordinates with time after synchronization has been reached. (b), (d), and (f): Relative positions of y_1 versus y_2, corresponding to the same time frame depicted in (a), (c), and (e), respectively.

5.3.4 Effect of Distance (l) on Synchronization Behavior

In order to explore the effect that the distance between the two rotors has on the synchronization behavior, we vary the l value between a set of two oscillators. Figure 5.5 shows a series of experiments with $d_1 = 1.8$ mm, and $d_2 = 2.7$ mm, and l values of 4.4, 8.15, and 10.7 mm. In every case, we observe frequency synchronization after several rotations. The nature of phase synchronization is, however, slightly different in the three cases. They can phase lock in almost-complete synchrony [Figs. 5.5(e) and 5.5(f)] or have a constant phase lag [Figs. 5.5(a)−5.5(d)]. While in the case of $l = 4.4$ mm [Figs. 5.5(a) and 5.5(b)], we find that the phase resetting occurs at the beginning of the positive y_1 slope, near its minimum value, for $l = 8.15$ mm [Figs. 5.5(c) and 5.5(d)], it occurs at the end of the y_1 slope, near its maximum. Contrarily, for $l = 10.7$ mm [Figs. 5.5(e) and 5.5(f)] and for $l = 12.15$ mm [Figs. 5.3(e)-5.3(h)], phase jumps take place at the beginning and end of the decay of y_1, respectively. The increasing values of the inter-disk distance l should be noted here.

5.3.5 Synchronization Time (t_S) vs. Distance (l)

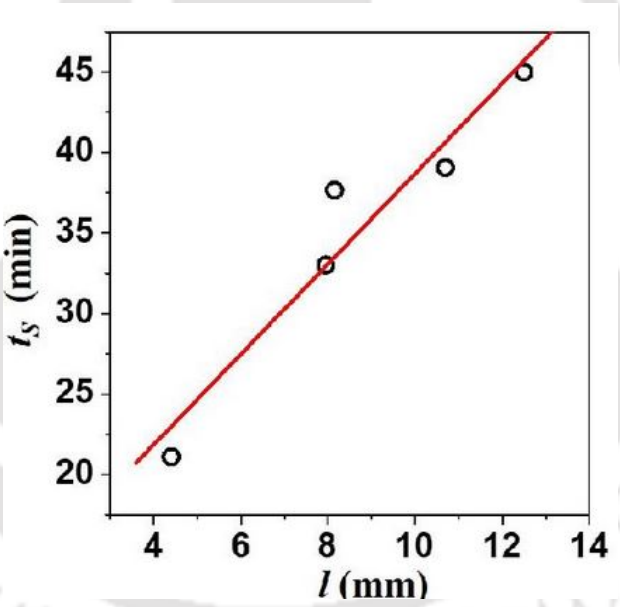

Figure 5.6: Variation of synchronization time (t_S) with increasing rotor distance (l) with obstacle size $d_1 = 1.8$ mm and $d_2 = 2.7$ mm.

We measured the time required for synchronization (t_S) by varying the distance between the rotors (l) [Fig. 5.6]. We carried out several experiments with exactly the same circular disks of diameters $d_1 = 1.8$ mm and $d_2 = 2.7$ mm. The trend of synchronization time with distance was linear. Some points are found to deviate a little from the straight line, which may be because of several factors, such as temperature fluctuations or air bubbles leading to slight local heterogeneities.

5.4 Numerical Model

We chose the generic Barkley model for carrying out our numerical experiments. This model is widely used for the study of spiral and scroll waves in reaction-

diffusion processes [26, 27]. The two-variable model is given as:

$$\frac{\partial u}{\partial t} = \frac{1}{\epsilon}\left[u(1-u)(u-\frac{v+b}{a})\right] + D_u\nabla^2 u \tag{5.2}$$

$$\frac{\partial v}{\partial t} = u - v + D_v\nabla^2 v \tag{5.3}$$

where the activator u and inhibitor v are related to the concentrations of bromous acid and the oxidized form of ferroin, respectively; $D_u = D_v = 1.0$ are the diffusion coefficients of u and v, respectively; and $a = 0.84$, $b = 0.07$, and $\epsilon = 0.02$ are chosen as the system parameters. The space is discretized into 300×300 grid points, and the system of equations is numerically integrated by using the fourth-order Runge-Kutta method and a nine-point Laplace stencil. Zero-flux boundary conditions are applied across all four walls of the system. With a time interval of $\Delta t = 0.012$ (arbitrary time units) and a step size $\Delta x = 0.35$ (arbitrary space units), this system can sustain rigidly rotating spiral waves having a core diameter of 1.8 space units, a wavelength of 18.2 space units, and a time period of 5.3 time units [28].

The numerical experiments are set up just like the BZ experiments. A plane wave is initiated between two unexcitable circular regions with diameters d_1 and d_2, placed at a distance l from each other. These act as pinning heterogeneities for the spiral waves. Throughout our simulations, we fix u and v within these circles at zero. A zero-flux boundary around these circular entities will not change the results of our simulations, except that the core size will be smaller in the latter case, leading to slightly reduced time periods. Initially, the variables u and v are taken to be zero across the entire space, except for a narrow region between the obstacles, where thin strips of altered values of the u and v variables are taken in a fashion so as to give directionality to the initial waveform [28]. With time, a pair of counterrotating spirals eventually forms. The values of d_1, d_2, and l are varied to explore the dynamics of interacting pinned spiral rotors. We have taken obstacle diameters of 2.45, 3.85, 4.55, 5.25, and 5.95 space units, each having individual time periods of 4.9, 6.0, 6.6, 7.4, and 7.9 time units, respectively (for $d_1 = d_2$). The spiral tip is identified as the intersection of the isoconcentration lines $u = 0.5$ and $v = a/2$ - $b = 0.35$. Its coordinates with respect to the center of the spiral core are again labeled (x_i, y_i).

5.5 Numerical Results and Discussion

5.5.1 In Phase Synchronization

Figure 5.7 shows the synchronization of spiral rotors pinned to two disks of diameters $d_1 = 5.25$ and $d_2 = 5.95$ space units (s.u.), placed $l = 40.95$ space units apart. Initially, the two rotors oscillate with their individual time periods, viz., 7.4 and 7.9 time units (t.u.), respectively. This is observable in Fig. 5.7(b), which also shows that the two oscillators are out of synchrony. After several rotations (over 40), the oscillators are seen to have synchronized perfectly in frequency. The time variation of the y-coordinates of the spiral tips [Fig. 5.7(f)] bears testimony to the same. The time periods of both rotors are now 7.4 time units, the same as the characteristic frequency of the smaller obstacle (diameter 5.25). We observe similar trends across all combinations of pinning heterogeneities. The faster rotor always takes over the slower one, and at the final stage, the frequencies of the two rotors are the same. Observations along the same lines have been made in earlier

studies of spiral waves [29, 30]. Having established this, we now move on to explore the phase dynamics of the frequency-synchronized rotors.

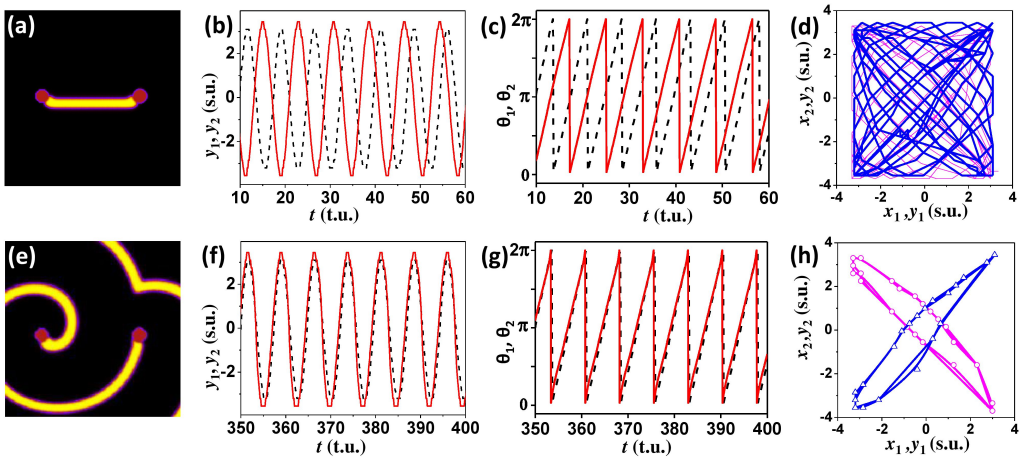

Figure 5.7: In-phase synchronization of two spiral rotors for $d_1 = 5.25$, $d_2 = 5.95$, and $l = 40.95$. Snapshot of the experiment at (a) $t = 0.24$ time units and (b) t= 360 time units. The area of each snapshot is 73×73 space units. Simulation results are for (a)−(d): the initial and (e)−(h): post synchronization stages of the study. (b) and (f): Variation of the vertical position y_i . (c) and (g): Phase angle variations with time. Black dashed lines are for rotor 1, and red solid lines are for rotor 2. (d) and (h): Phase plots of the two rotors. The y plots are blue curves with triangles, while the x plots are magenta curves with circles. A similar coloring scheme has been used in Fig. 8.

The phase angles θ_1 and θ_2 plotted in Fig. 5.7(c) show that initially, the rotors were not phase synchronized. The space-filling plot of y_1 versus y_2 [Fig. 5.7(d)] also confirms the asynchronous behavior of the two rotors in the early stages of the experiment. The exact overlap of θ_1 and θ_2 at later times in Fig. 5.7(g) confirms the in-phase locking synchronization of the two rotors. The phase portrait for y_1 versus y_2 (x_1 versus x_2) in Fig. 5.7(h) is a thin ellipse along the right (left) diagonal, which establishes that the two counterrotating spirals are synchronized in phase.

This kind of exact phase locking was not observed in our experiments with rotors of different initial frequencies. Additional simulations confirmed that such strong synchronization would only be possible for pinning sizes of comparable dimensions. Otherwise, the mismatch in size leads to the phase resetting phenomenon, which will not allow the y-positional coordinates to match exactly throughout one oscillation. More experiments have to be carried out with the BZ system with pinning disk sizes that vary about 10% in diameter in order to be able to observe complete phase synchrony.

5.5.2 Lag Synchronization

In Fig. 5.8, we show the synchronization of two rotors pinned around heterogeneities of extensively different diameters, viz., $d_1 = 2.45$ and $d_2 = 4.55$ space units. The initial data show the unsynchronized nature of the two oscillators [Figs. 5.8(a)−5.8(c)]. After frequency synchronization, the two rotors are seen to display unique dynamics in both position and angle. Here, the phase jump of the larger rotor (red solid lines) is evident in the plots of position as well as phase angle

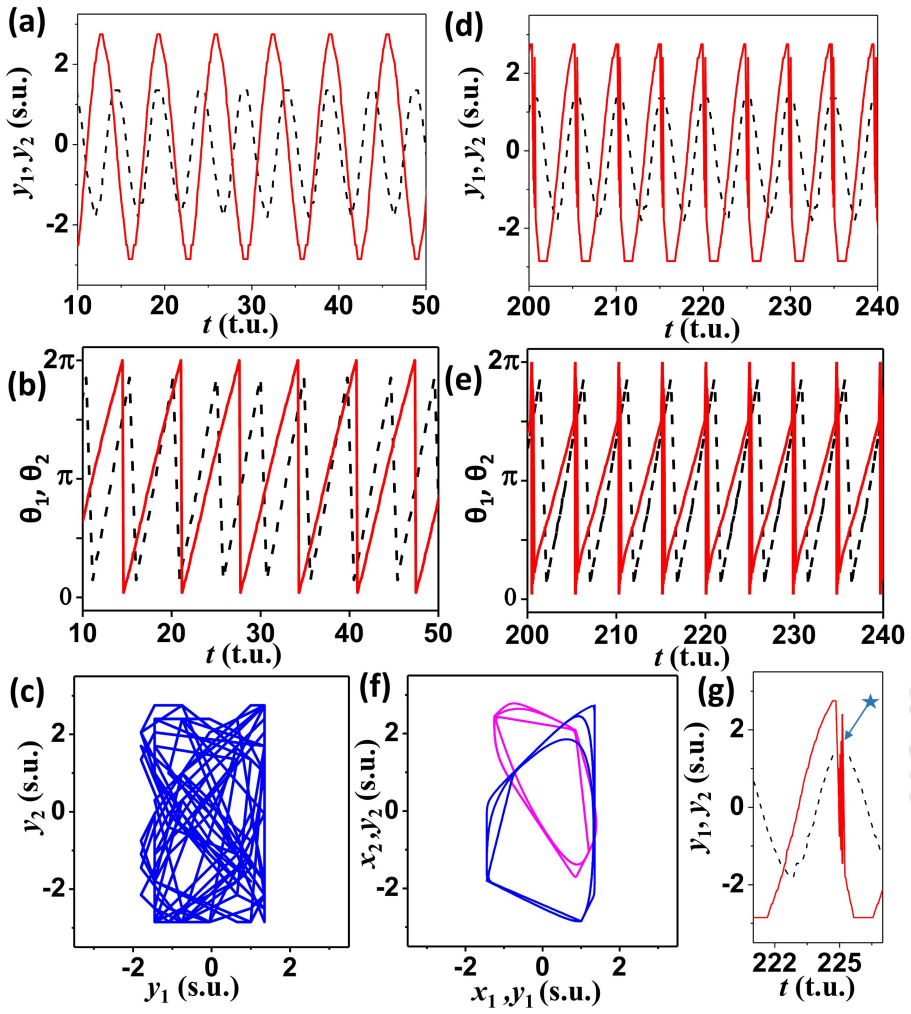

Figure 5.8: Simulation result demonstrated phase jump and lag synchronization for disk diameters of $d_1 = 2.45$ and $d_2 = 4.55$ and the distance between the center of the disks $l = 110.95$. (a)−(c): initial results and (d)−(g): later results. Shown are (a) and (d): the dynamics of positional coordinates; (b) and (e): the phase angles; and (c) and (f): phase portraits demonstrating the emergence of lag synchronization. (g) Close-up of (d), showing the presence of multiple spiral tips on the second rotor (red solid curve) during phase resetting. The position is marked with a star.

[Figs. 5.8(d) and 5.8(e)]. The plot of y_1 versus y_2 shows a wide elliptic profile, which is typical of two oscillators having equal frequencies and a constant phase shift [Fig. 5.8(f)]. Hence, we might call it a case of lag synchrony.

In Fig. 5.4, the experimental snapshots show the presence of three spiral tips on the larger obstacle for a very short time (compared to the time period). The signature of the new singularities is observable in the plot of the y-coordinate of the tip (y_2), as well as the corresponding phase angle (θ_2) plot [Figs. 5.8(d) and 5.8(e)]. A small portion of Fig. 5.8(d) is expanded at Fig. 5.8(g) for better visibility. At the instant of the overlap of the two tip positions [marked with a blue star around 225 time units in Fig. 5.8(g)], there is more than one spiral tip identified by our program. Subsequently, the phase position and angle are reset as a result of these intricate dynamics. The phase portraits at later times [Fig. 5.8(f)] have the flattened ellipse structure seen in Figs. 5.3 and 5.5.

5.5.3 Phase Diagram

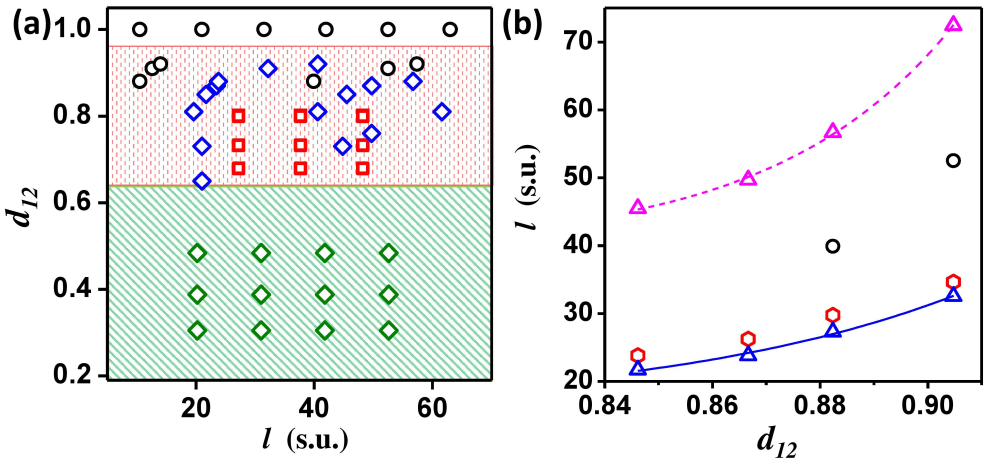

Figure 5.9: Nature of synchronization as a function of interrotor distance l. (a) The ratio of the two diameters d_{12} $(=d_1/d_2)$ is plotted as a function of l. The green shaded area with diamonds depicts phase-resetting dynamics, and the red shaded area with squares shows lag synchronization. Blue triangles are points of anti-synchronization (π-phase difference) and black circles denote points of complete synchronization (zero-phase difference). (b) Trend of in-phase and anti-phase synchronization for a few d_{12} values. The blue solid line with triangles depicts the first occurrence of antiphase locking, and the magenta dashed line with triangles denotes the second occurrence of antisynchronization, as l is increased. Black circles denote any inphase synchronized state between these two lines. The red hexagons stand for the wavelength of the faster spiral (λ_1).

A phase diagram for studying the nature of synchronization has been constructed. Figure 5.9 depicts the changing dynamics of the interacting rotors as a function of the ratio of obstacle diameter (d_{12}) and the space separating them, l. When the two obstacles are of widely differing dimensions ($d_{12} < 0.65$), we observe phase-resetting dynamics [Fig. 5.9(a)]. As the ratio increases, we move to a region of lag synchronization. Within this region, we come across some points of antiphase synchronization and fewer points of complete in-phase locking. A deeper analysis of these seemingly arbitrary points reveals that the first antiphase synchronization for a given ratio occurs at the value of $l \simeq \lambda_1 - d_s$, where λ_1 is the wavelength of the spiral wave arm near the smaller obstacle and d_s is the core diameter of a free spiral [Fig. 5.9(b)]. This is an interesting observation when seen in the context of interacting spiral waves. It has been established in a recent study on the interaction of free spirals that two spiral cores having the same frequency cannot modify the trajectory of one another when placed beyond a critical distance d_c, where $d_c = \lambda - d_s$ [28] (here λ is the characteristic wavelength of the spiral). This critical distance is close to the l value showing the first antiphase synchronization of non-identical rotors in Fig. 5.9(b). The second antiphase synchronization occurs after a larger distance. At ratios greater than 0.88, complete synchronization occurs at some specific values of l, which lie between the two antiphase synchronized states. At $d_{12} = 1.0$, or obstacles of equal diameter, in-phase synchronization is observed for all values of l. While in numerical simulations we are able to initiate waves

with the exact same phase of rotation, this is not always the case in experiments. There, the initial phases of the two spirals may be the same or different. In simulations with rotors of the same initial frequency (attached to identical circular disks) having different initial phases, we found that the spirals synchronize in phase as long as they are within one wavelength of each other. Beyond that distance ($l > \lambda_1$), the two rotors are locked with the initial phase lag. This can be explained on the basis of the fact that when the frequencies of both waves are equal, the wave arms touch each other somewhere between the heterogeneities, and if this distance is greater than the critical distance d_c, one spiral will not be able to modify the phase of the other [28].

5.5.4 Synchronization Time (t_S) vs. Distance (l)

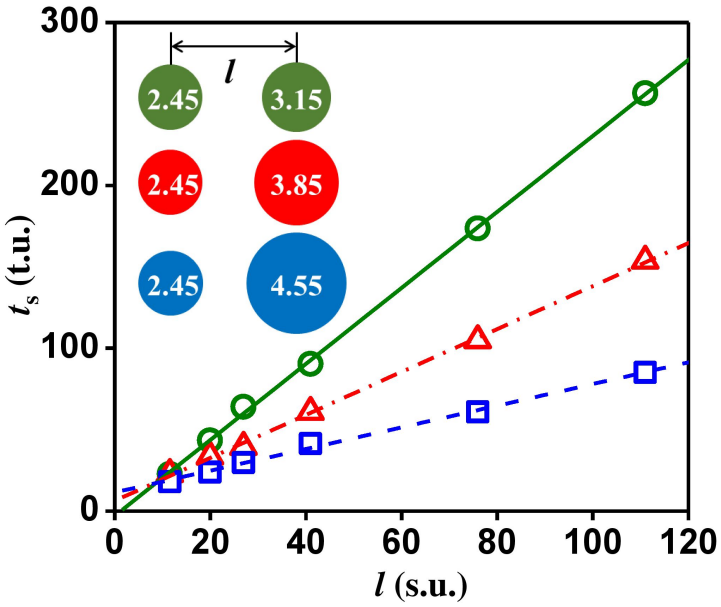

Figure 5.10: Variation of synchronization time t_S with increasing interrotor distances l, for three sets of obstacle sizes. $d_1 = 2.45$ space units across all simulations. The d_2 values are 3.15 (olive circles), 3.85 (red triangles), and 4.55 (blue squares) across the three graphs.

We also measured the time required for synchronization (t_S) for varying obstacle sizes and spacings. Figure 5.10 shows the variation of t_S as a function of the distance between the two rotors, l, for three sets of d_2 values. We have kept d_1 constant at 2.45 space units. We see that for a given d_2 value, t_S increases linearly with l. The velocity of the waves emanated by rotor 1 remains the same for all the experiments. As the distance between the two rotors increases, the time required for the waves to cover this path and reach the slower rotor increases, which is reflected in the positive slopes of the lines. However, with the increase in the value of d_2, the time of synchronization decreases. This happens because, as we increase the size of the heterogeneity (d_2), the rotor becomes slower. The number of waves it emits at any given time also decreases. Hence, the wave arm of the faster rotor has to overcome fewer collisions with the oncoming waves. This enables it to reach the second rotor within a shorter time duration, thus leading to smaller t_S values.

For a given l, t_S is the smallest for the largest d_2 value, except when $l < \lambda$, when all values of t_S are almost comparable. Within one wavelength, the wave arm of the faster rotor does not have to encounter any oncoming waves from its larger neighbor before reaching it. The slope of the graph for the smallest obstacle 2 size (d_2) is the highest, meaning that the farther apart the two beads are placed, the longer it will take for the waves from obstacle 1 to reach obstacle 2, and it also has to encounter more oncoming waves. So these two factors contribute to an increase in the slope of the line.

5.6 Conclusion

We have established that a system of pinned spiral waves can be considered a promising candidate for the study of rotational synchronization. It will be an addition to the already existing library of rotors such as Josephson junctions, mechanical rotors, and camphor boats used for such studies. We have shown with our experiments and simulations that spiral rotors pinned to unexcitable heterogeneities can indeed act as coupled oscillators that synchronize in frequency and phase. By pinning the spirals to disks of different dimensions, we were able to generate and sustain spirals of different characteristic frequencies while also ensuring that they do not translate in space. With that ensured, we carried out detailed observations of rotor position and phase angle to show how two initially unsynchronized rotors with different frequencies and sometimes phases can synchronize. Depending on several factors, such as a difference in obstacle size and the distance separating them, we observed in-phase locking, out-of-phase locking, lag synchronization, and phase resetting. The results of our numerical simulations have corroborated the different kinds of phenomena observed in our experiments while illustrating the nuances of phase resetting in the larger obstacle. Also, a linear trend in synchronization times with interrotor distance has been established. This may be explored in future investigations to obtain an estimate of the coupling strength of these pinned rotors.

The chirality of the two spiral rotors plays an important role in their interaction. It will be interesting to study experimentally the interaction of corotating pinned spiral waves. Future investigations could be carried out with lattices of spiral rotors. As established for free spirals [28], the nature of the interaction of pinned spirals may also change with an increased number of coupled rotors, which may give rise to a plethora of richer synchronization dynamics.

In the cardiac system, the pinning of free spiral waves is known to modify polymorphic ventricular tachycardia into a monomorphic one [4]. If there is more than one such pinned excitation wave, their interaction may change the nature of the graph obtained from an electrocardiogram (ECG), which is commonly used to monitor cardiac activity in patients. Studies of wave propagation dynamics in the cardiac system suggest that the activity of a high-frequency rotor can give rise to the fastest dominant frequency domain [31]. Hence, a better understanding of wave interaction and synchronization will be of vital importance in the correct diagnosis of heart conditions based on clinical procedures, such as the use of ECG.

Bibliography

[1] A. Pikovsky, M. Rosenblum, and J. Kurths, *Synchronization* (Cambridge University Press, Cambridge, 2003).

[2] B. Blasius, A. Huppert, and L. Stone, Nature (London) **399**, 354 (1999).

[3] V. Hakim and N. Brunel, Neural Comput. **11**, 1621 (1999).

[4] J. Jalife, M. Delmar, J. Anumonwo, O. Berenfeld, and J. Kalifa, *Basic Cardiac Electrophysiology for the Clinician*, 2nd ed. (Wiley-Blackwell, Oxford, 2009).

[5] M. Bier, B. M. Bakker, and H. V. Westerhoff, Biophys. J. **78**, 1087 (2000).

[6] A. Biswas, D. Das, and P. Parmananda, Phys. Rev. E **95**, 042202 (2017).

[7] R. Toth, A. F. Taylor, and M. R. Tinsley, J. Phys. Chem. B **110**, 10170 (2006).

[8] Y. Kuramoto, *Chemical Oscillations, Waves, and Turbulence* (Springer, Berlin, 1984).

[9] B. C. Daniels, S. T. M. Dissanayake, and B.R.Trees, Phys. Rev. E **67**, 026216 (2003).

[10] J. Sharma, I. Tiwari, D. Das, V. Pimienta, and P. Parmananda, Phys. Rev. E **101**, 052202 (2020).

[11] I. I. Blekhman, *Synchronization in Science and Technology* (ASME, New York, 1988).

[12] J. Schwarz-Linek, C. Valeriani, A. Cacciuto, M. E. Cates, D. Marenduzzo, A. N. Morozov, and W. C. K. Poon, Proc. Natl. Acad. Sci. U.S.A. **109**, 4052 (2012).

[13] R. Di Leonardo, A. Búzás, L. Kelemen, G. Vizsnyiczai, L. Oroszi, and P. Ormos, Phys. Rev. Lett. **109**, 034104 (2012).

[14] J. Sharma, I. Tiwari, D. Das, P. Parmananda, V. S. Akella, and V. Pimienta, Phys. Rev. E **99**, 012204 (2019).

[15] A. Prasad, Chaos Soliton. Fract. **43**, 42 (2010).

[16] J. Sharma, I. Tiwari, D. Das, and P. Parmananda, Phys. Rev. E **103**, 012214 (2021).

[17] O. Steinbock and S. C. Müller, Phys. Rev. E **47**, 1506 (1993).

[18] J. Jalife, R. A. Gray, G. E. Morley, and J. M. Davidenko, Chaos **8**, 79 (1998).

[19] F. Xie, Z. Qu, and A. Garfinkel, Phys. Rev. E **58**, 6355 (1998).

[20] D. Olmos, Phys. Rev. E **81**, 041924 (2010).

[21] W.-J. Rappel, Phys. Rev. E **105**, 014404 (2022).

[22] M. Sutthiopad, J. Luengviriya, P. Porjai, M. Phantu, J. Kanchanawarin, S. C. Müller, and C. Luengviriya, Phys. Rev. E **91**, 052912 (2015).

[23] F. M. Zanotto and O. Steinbock, Phys. Rev. E **103**, 022213 (2021).

[24] D. Mahanta, N. P. Das, and S. Dutta, Phys. Rev. E **97**, 022206 (2018).

[25] K. Czolczynski, P. Perlikowski, A. Stefanski, and T. Kapitaniak, Commun. Nonlinear Sci. Numer. Simulat. **17**, 3658 (2012).

[26] D. Barkley, M. Kness, and L. S. Tuckerman, Phys. Rev. A **42**, 2489 (1990).

[27] D. Barkley, Physica D 49, 61 (1991).

[28] H. Kalita and S. Dutta, Phys. Rev. E **105**, 054213 (2022).

[29] V. Krinsky and K. Agladze, Physica D 8, **50** (1983).

[30] U. Parlitz, A. Schlemmer, and S. Luther, Phys. Rev. E **83**, 057201 (2011).

[31] F. H. Samie and J. Jalife, Cardiovasc. Res. **50**, 242 (2001).

Chapter 6

Conclusion

In this thesis, we have explored some aspects of the interaction dynamics of spiral waves and various phenomena arising from those interactions, both experimentally and theoretically. The interaction of free spirals can either be attractive, which finally leads to annihilation, or repulsive, which pushes the spirals away from each other until a certain limiting distance. Throughout our investigation, we have found that the interaction of spiral waves mainly depends on the distance between the spirals, their relative chirality (corotating or counterrotating), and relative phases. It was observed that interaction between spirals can happen up to a certain limiting distance, beyond which they do not interact. When their distance from one another increases, the arms of the spirals have ample room to spread out and shield their spiral core from neighboring spiral arms. We define this limiting distance as the critical distance of interaction. Two counter-rotating spirals show attractive interaction when their separation is very low. With the increasing separation between them, this attractive interaction becomes repulsive. Up until the critical distance, repulsion persists. After the critical distance, the tips rotate around the initial core without interaction. For two counterrotating spirals, we see only repulsive interaction within critical distance, which is also true for two counterrotating spiral pairs at high phase angle differences. For two counterrotating spirals with an increasing phase angle difference between the spiral waves, the range of interaction, i.e., the critical distance, increases. In contrast, the trend is the opposite for a pair of corotating spirals. We have established a relationship between this critical distance to the properties of the spiral wave, its wavelength, and core diameter. We observed spontaneous symmetry-breaking instability for a network of interacting rotors. In our final study, we pinned the spiral waves with rubber cylinders of differing dimensions to modify their frequencies. Two spirals pinned to obstacles of different diameters have different frequencies. The higher-frequency rotor can produce more waves than the lower-frequency rotor. The wave arms produced by the higher frequency spiral gradually approach the lower frequency rotor by annihilating the waves of the lower frequency rotor. Finally, they hit the lower frequency rotor and make it rotate with the frequency of the higher frequency rotor, and that's how frequency synchronization happens. Phase synchronization takes several forms depending on how their respective characteristic frequencies differ. During the experiments, we observe synchronization that is both in-phase and out-of-phase, lag synchronization, and phase resetting. The amount of time required for the two spirals to synchronize depends on the distance between them and the respective sizes of the pinning barriers.

We are keen to test different spiral configurations (varying angle and chirality)

with more rotors to understand interaction dynamics better. Our modeling of phase-mismatched counterrotating spiral waves has demonstrated phase-resetting dynamics. It will be worthwhile to look into whether such phase-resetting dynamics lead to phase synchronization and chimera in the case of three or more rotor systems with different initial phase angles. The issue of symmetry-breaking is also intriguing. Throughout our systems, we have maintained a certain level of excitability. Observing how excitability affects the synchronization and interaction of spiral waves will be interesting. In the case of pinned rotors, it will be interesting to observe how the overall synchronization behavior gets affected in a system of more than two rotors and different combinations of angle and chirality.